Development of analytical methodologies for iodine species in gaseous and particulate phases of the coastal atmosphere

Dissertation zur Erlangung des Grades
„Doktor der Naturwissenschaften“

am Fachbereich Chemie, Pharmazie und Geowissenschaften
der Johannes Gutenberg-Universität Mainz

vorgelegt von
M.Sc. Hongwei Chen
geboren in Jiangmen (Guangdong), V.R. China

Mainz, 2005

Dekan:

1. Berichterstatter:

2. Berichterstatter:

Tag der mündlichen Prüfung:

Die praktischen Arbeiten wurden am Institute for Analyitcal Sciences (Institut für Spektrochemie und Angewandte Spektroskopie, ISAS) in Dortmund und am Institut für Anorganische & Analytische Chemie der Johannes Gutenberg-Universität Mainz durchgeführt.

人能弘道，非道弘人！

It is not truth that makes man great, but man that makes truth great!

—— *Confucius*

Development of analytical methodologies for iodine species in gaseous and particulate phases of the coastal atmosphere

Abstract

It has been demonstrated that iodine does have an important influence on atmospheric chemistry, especially the formation of new particles and the enrichment of iodine in marine aerosols. It has been pointed out that the most probable chemical species involved in the production or growth of these particles are iodine oxides, produced photochemically from biogenic halocarbon emissions and/or iodine emission from the sea surface. Recent chamber and model studies have confirmed those particle formations from I_2 or CH_2I_2 in the presence of ozone and UV light. However, the iodine chemistry from gaseous to particulate phase in the coastal atmosphere and the chemical nature of the condensing iodine species are still not understood. Therefore, sampling, identification and quantification of those iodine species have become necessary for the understanding of atmospheric iodine chemistry in the Marine Boundary Layer (MBL).

A Tenax / Carbotrap adsorption sampling technique and a thermo-desorption / cryo-trap / GC-MS system has been further developed and improved for the volatile organic iodine species in the gas phase. Several iodo-hydrocarbons such as CH_3I, C_2H_5I, CH_2ICl, CH_2IBr and CH_2I_2 etc., have been measured in samples from a calibration test gas source (standards), real air samples and samples from seaweeds / macro-algae emission experiments. A denuder sampling technique has been developed to characterise potential precursor compounds of coastal particle formation processes, such as molecular iodine in the gas phase. Starch, TMAH (TetraMethylAmmonium Hydroxide) and TBAH (TetraButylAmmonium Hydroxide) coated denuders were tested for their efficiencies to collect I_2 at the inner surface, followed by a TMAH extraction and ICP/MS determination, adding tellurium as an internal standard. The developed method has been proved to be an effective, accurate and suitable process for I_2 measurement in the field, with the estimated detection limit of ~0.10 $ng \cdot L^{-1}$ for a sampling volume of 15 L. An H_2O/TMAH-Extraction-ICP/MS method has been developed for the accurate and sensitive determination of iodine species in tropospheric aerosol particles. The particle samples were collected on cellulose-nitrate filters using conventional filter holders or on cellulose nitrate/tedlar-foils using a 5-stage Berner impactor for size-segregated particle analysis. The water soluble species as IO_3^- and I^- were separated by anion exchanging process after water extraction. Non-water soluble species including iodine oxide and organic iodine were digested and extracted by TMAH. Afterwards the triple samples were analysed by ICP/MS. The detection limit for particulate iodine was determined to be 0.10~0.20 $ng \cdot m^{-3}$ for sampling volumes of 40~100 m^3. The developed methods have been used in two field measurements in May 2002 and September 2003, at and around the Mace Head Atmospheric Research Station (MHARS) located at the west coast of Ireland.

Elemental iodine as a precursor or a by-product of the iodine chemistry in the coastal atmosphere, was determined in the gas phase at a seaweed hot-spot around the MHARS, showing I_2 concentrations were in the range of 0~1.6 $ng \cdot L^{-1}$ and indicating a positive correlation with the ozone concentration. A seaweed-chamber experiment performed at the field measurement station showed that the I_2 emission rate from macro-algae was in the range of 0.019~0.022 $ng \cdot min^{-1} \cdot kg^{-1}$. During these experiments, nanometer-particle concentrations

were obtained from the Scanning Mobility Particle Sizer (SMPS) measurements. Particle number concentrations were found to have a linear correlation with elemental iodine in the gas phase of the seaweeds chamber, showing that gaseous I_2 is one of the important precursors of the new particle formation in the coastal atmosphere.

Iodine contents in the particle phase were measured in both field campaigns at and around the field measurement station. Total iodine concentrations were found to be in the range of 1.0 ~ 21.0 $ng \cdot m^{-3}$ in the PM2.5 samples. A significant correlation between the total iodine concentrations and the nanometer-particle number concentrations was observed. The particulate iodine species analysis indicated that iodide contents are usually higher than those of iodate in all samples, with ratios in the range of 2~5:1. It is possible that those water soluble iodine species are transferred through the sea-air interface into the particle phase. The ratio of water soluble (iodate + iodide) and non-water soluble species (probably iodine oxide and organic iodine compounds) was observed to be in the range of 1:1 to 1:2. It appears that higher concentrated non-water soluble species, as the products of the photolysis from the gas phase into the particle phase, can be obtained in those samples while the nucleation events occur. That supports the idea that iodine chemistry in the coastal boundary layer is linked with new particle formation events. Furthermore, artificial aerosol particles were formed from gaseous iodine sources (e.g. CH_2I_2) using a laboratory reaction-chamber experiment, in which the reaction constant of the CH_2I_2 photolysis was calculated to be $k = 1.10 \sim 1.30 \times 10^{-3} s^{-1}$ based upon the first order reaction kinetic. During these experiments also the end products of iodine chemistry in the particle phase were identified and quantified.

In the future, to fully understand the whole mechanism for iodine-containing emission and their role in particle formation process, further laboratory experiments and field measurements are necessary. For instance, monitoring of some gaseous iodine species such as HI, HOI, in the field measurement and laboratory study might be important to discover more knowledge about the iodine chemistry in the MBL.

Table of Contents

1 Introduction

Atmospheric aerosol can affect the climate in a direct or an indirect way. Marine clouds originate from the formation of marine aerosol and cloud condensation nuclei, which depend ultimately on the availability of new, nanometer-scale particles in the marine boundary layer [O'dowd 2002b, 2005]. It has been approved that iodine-containing emissions from coastal and marine algae are not only suspected to be involved in tropospheric ozone degradation, but also in new particle formation processes. If this phenomenon occurs on a larger scale, it could have significant effects on global climate [Kolb 2002], due to marine aerosols and clouds scattering the incoming radiation and contributing a cooling effect to the Earth's radiation budget [Slingo 1990].

1.1 Iodine Species in the Marine Boundary Layer (MBL)

Iodine, as one of the elements of the VIIA group in the periodic table, is occurring in 6 oxidation states: -1, 0, +1, +3, +5 and +7. In the marine boundary layer, iodine species vary from inorganic (I^-, I_2, IO_3^-, iodide oxides and acids etc.) to organic (iodo-carbons) and particulate iodine. Those species are involved in at least 3 phases: sea water, gas phase and particle phase. Figure 1-1 summarizes the various iodine species in the MBL.

Iodine species in the sea water

Iodine species in the sea water are mainly dissolved inorganic iodide (I^-) and iodate (IO_3^-), whose concentrations are in the order of 0.7×10^{-7} mol·L^{-1} or 3×10^{-7} mol·L^{-1} respectively [Tsunogai 1971, Ullman 1990], as well as some nonvolatile dissolved organic iodine. It has been found that the iodate predominates in deep sea (> 250 m), while iodate are reduced to iodide by phytoplankton assumedly in near-surface water [Waite 2003], thus their concentrations become comparable or even more iodide in the sea-air interface[Schwehr 2002]. A complicated reaction-pack of iodide with oxygen [Miyake 1963] and ozone [Garland 1981] at the sea surface might produce some other inorganic iodine species like I_2, HOI [Garland 1981, Thompson 1983] and I_3^-.

Iodocarbons (also namely Volatile Organic Iodine, VOI) were observed in sea-surface water as well, such as CH_3I, CH_2I_2, CH_2ClI and C_3H_7I etc., with typical I concentrations in the order of 10^{-10} mol·L^{-1}. It was first suggested by Lovelock in 1975 that the marine algae were the source of those organohalogens [Lovelock 1975, Laturnus 2000, Moore 2003], although the precise mechanism is still not clear up till now [Vogt 1999b]. For instance, the mechanism for production of monohalogenated compounds involves a halide ion methyl transferase enzyme, found in both macroalgae (seaweeds) and microalgae (phytoplankton), whereas di- and tri-halogenated hydrocarbon production involves the haloperoxidase enzyme, present in a wide range of terrestrial and marine organisms [Wever 1991]. Halo-peroxidases catalyze the oxidation of halides by hydrogen peroxide, which is released as part of normal cell metabolism and during defense reactions [Küpper 2002]. The resulting reactive electrophilic halogenating species can react with available organic material within the cell apoplast via the iodoform reaction to form volatile organohalogens that are released to the surrounding seawater or air. Under conditions of oxidative stress, H_2O_2 would otherwise build up to high levels, and thus the mechanism is essential for the health of the organism [Küpper 1998]. As a

result, the sea water near the interface to the atmosphere becomes locally super-saturated with those iodo-hydrocarbons, thus causing a flux from the aqueous into the gas phase [Singh 1983].

Iodine species in the gas phase

It is believed that the ocean is the main source of gas-phase iodine species. Those volatile iodine species are emitted from algae and getting saturated in the sea surface, causing the sea-air flux to the gas phase [Carpenter 2002]. Measurements of iodine species in the atmosphere were made several decades ago, which indicated that volatilization of organic iodides from the ocean provides the main source of atmospheric iodine [Vogt 1999a]. It was estimated previously that more than 5×10^{11} g of iodine is involved in the atmospheric cycle over the globe annually [Miyake 1963], including 6 to 12 $\times10^{10}$ g of elemental iodine (I_2) [Garland 1981]. However, recent studies obviously indicate that the iodine species in the gas phase are more complicated than ever before. Molecular iodine [Saiz-Lopez 2004 b, Gaebler 1993a], iodine oxide radicals such as IO [Saiz-Lopez 2004 b, Alicke 1999], OIO [Saiz-Lopez 2004 b, Allan 2001], and acids like HI, HOI [Gaebler 1993a] were observed recently in the troposphere of several different coastal areas.

Iodine species in the aerosol particle

Particulate iodine species includes nearly all of its oxidation states. In the MBL, there exist direct sea-salt aerosols, in which the dissolved inorganic (I^-, IO_3^-) and organic iodine are involved by the uptake of the seawater. The higher iodine oxides in the particles such as I_2O_4 or I_2O_5 are considered as the products from the photolysis of iodocarbons or molecular iodine in the presence of UV radiation and ozone, which cause the substantial bursts of the new particles in the marine atmosphere [Hoffmann 2001, O'Dowd 1999, 2002a].

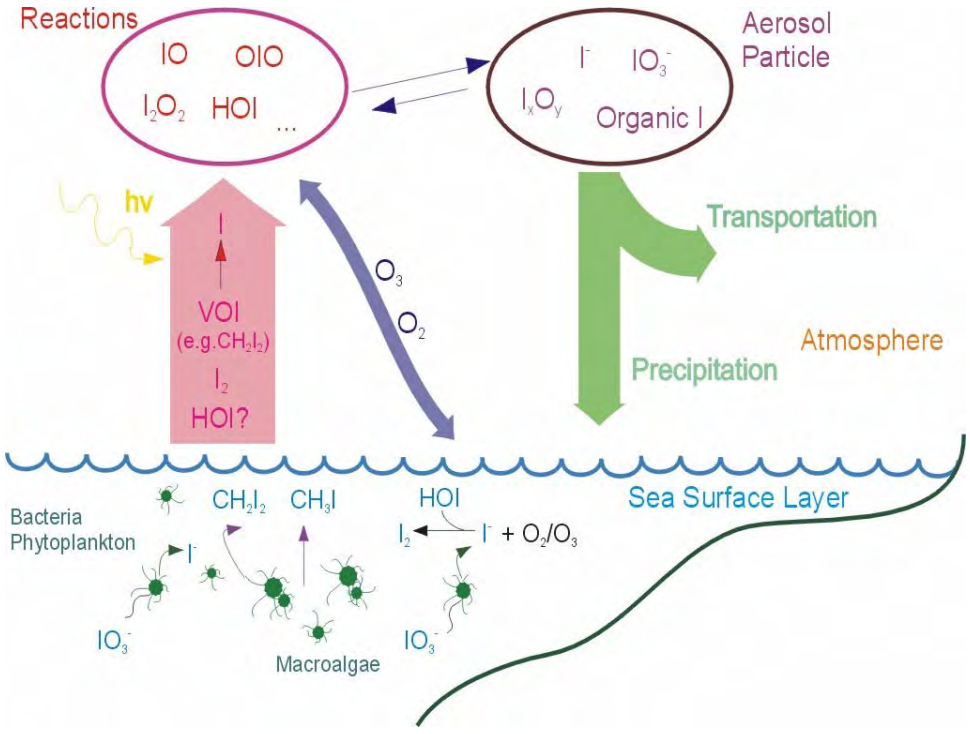

Figure 1-1 Iodine species in the Marine Boundary Layer (MBL)

1.2 Iodine chemistry in the MBL

Over the past few years, there has been demonstrated that iodine does have an important influence on atmospheric chemistry [Adams 2002, Carpenter 2003a], at least for several reason including the influence of iodine oxides on the oxidizing capacity of the troposphere, the formation of new particles, and the enrichment of iodine in marine aerosols and the transport of this essential dietary element to the continents [Saiz-Lopez 2004 b]. Probably the hottest issue in the research about iodine chemistry in the atmosphere is the role of the iodine species in the formation of new particles in the MBL.

Photolysis of iodine species

The current understanding of the main features of gas- and particle-phase iodine photochemistry is shown in Figure 1-2. The cycle is initiated by photolysis of organic iodines with lifetimes ranging from several days (CH_3I, C_2H_5I, C_3H_7I)), several hours (CH_2ICl), an hour or less (CH_2IBr), to about 5 min at midday (CH_2I_2) [Carpenter 2003 a]. More recently it was discovered that elemental iodine (I_2) has a lifetime of 5-10 seconds for overhead sun, where a maximum absorption cross-section in the actinic wavelength range of σ =(4.24±0.50)×10^{-18} cm^2 ·$molecule^{-1}$ at λ =533.0 nm was reported [Saiz-Lopez 2004 a]. Although the lifetimes of the polyhalomethanes are controlled almost entirely by photodissociation, OH^- and Cl^- initiated attack could account for 10-20% of the removal of CH_3I and compete with photolysis for removal of the propyl iodides [Cotter 2001]. An analysis of the secondary chemistry arising from OH or Cl abstraction of a hydrogen bonded to the same carbon as iodine shows that iodine atom release occurs with greater than 90% yield for CH_3I and slightly lower for the higher alkyl iodides [Cotter 2001].

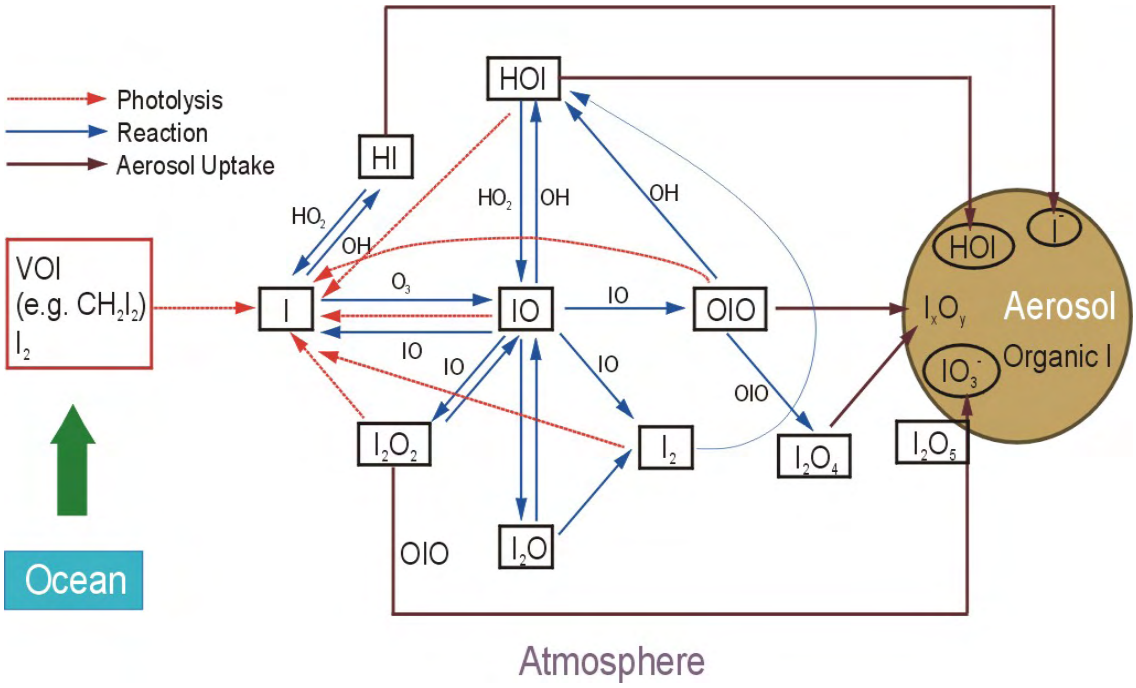

Figure 1-2 Chemical pathways from gaseous iodine to aerosol production, based on the current knowledge of atmospheric chemistry and photochemistry.

Iodocarbons with two chromophores, e.g. CH_2I_2, CH_2ICl, and CH_2IBr, have been shown to be the most important iodine atom precursors in some environments [Carpenter 1999]. The following reactions show the photolysis of CH_2IX (X=Cl, Br, I):

$$CH_2IX + h\nu \rightarrow CH_2I + X$$
$$CH_2I + h\nu \rightarrow CH_2 + I$$

According to Cotter's experiments [Cotter 2001], it seems there is a fairly rapid release of both iodine atoms in the case of CH_2I_2.

Gas-phase processes

Unlike chlorine and bromine atoms, which react with a range of organic molecules, iodine atoms do not react with either saturated or unsaturated organic compounds. Reacting with O_3, forming the iodine monoxide (IO) radical, is their major fate. Regeneration of iodine atoms through photolysis of IO is rapid; therefore, a daytime steady state exists between I and IO (collectively termed IO_x). This cycle has no net effect on IO_x or O_3 chemistry, as shown below.

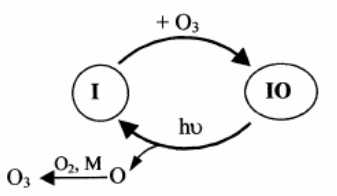

Although this reaction cycle is the predominant pathway for I-to-IO inter-conversion, a number of temporary inorganic reservoir products are formed via IO_x radical termination reactions with HO_2, NO_x, and IO. Only cycles which regenerate I atoms without concomitant O atom formation can lead to catalytic O_3 loss. The reaction of IO with HO_2, forming hypoiodous acid, HOI, is an important example:

$$I + O_3 \rightarrow IO + O_2$$
$$IO + HO_2 \rightarrow HOI + O_2$$
$$HOI + h\nu \rightarrow OH + I$$
$$\overline{O_3 + HO_2 \rightarrow OH + 2O_2}$$

HOI is believed to be the major component of inorganic iodine in the gaseous phase [Jenkin 1992] and an important route to the aerosol phase. This cycle has also been suggested as the dominant O_3 loss cycle at NO_x levels below about 500 pptv [Stutz 1999]. For typical conditions at Mace Head, Ireland, Stutz et al. calculated 0.3 ppb h^{-1} O_3 loss at 100 pptv of NO_x from the HOI cycle, where the NO_x is not playing important role in the iodine chemistry.

Finally, the relative rates of the branching channels of the self-reaction of IO radicals and the lifetimes of their products are important in determining both the gas and particulate chemistry of iodine. Early modeling studies assumed that the dimer of IO, I_2O_2, was the main product and also the major carrier of iodine to aerosol [Davis 1996, Vogt 1999b, Jenkin 1992]. Cox et al. identified reaction, forming iodine dioxide (OIO), as an additional channel, with a yield of ~40% [Cox 1999, Rowley 2001, Bloss 2001].

$$IO + IO \rightarrow I + OIO$$

The photolysis pathway of OIO is critical in determining its ozone destruction potential; only this channel will result in net loss of O_3:

$$OIO + h\nu \rightarrow I + O_2$$
$$OIO + h\nu \rightarrow IO + O(^3P)$$

Quantum calculations indicate the upper reaction dominates in the visible region and that the photolysis lifetime of OIO is about 1s, which would suggest that detectable OIO concentrations should be present only at night. This is contrast to the work of Cox et al. and an independent computational study [Misra 1998] that indicated a high photochemical stability for OIO. Apart from photolysis, the fate of OIO is uncertain, but it is assumed the uptake to aerosol and surfaces.

Aerosol uptake and recycling

The net transfer of iodine from the gas to the condensed phase is reflected by the factor of 100- to 1000-fold enrichment of I in fine fraction marine aerosol by comparison to the I/Na ratio in seawater [Baker 2000]. Some of the condensed iodine is, however, recycled back to the gas phase; the exact rates and mechanisms involved are key parameters for the prediction of the atmospheric impact of iodine. As shown in Figure 1-2, HI, HOI, OIO and I_2O_2 are the major species taken up by aerosols from the gas phase: the uptake of HI forms iodide (I^-) in the particle, HOI are directly taken up from gas to particle [Holmes 2001], while the irreversible accumulation of OIO and I_2O_2 has been assumed as the main cause of iodate (IO_3^-) enrichment of marine aerosol [Cox 1999]. Also a self-reaction of OIO was proposed to form low-volatility iodine oxides, such as I_2O_4 (or $[IO]^+[IO_3]^-$). This might finally lead to stable chainlike structures from further collisions with OIO [Hoffmann 2001, Mäkelä 2002]. However, more recent work [Ashworth 2002] suggests that self-reactions of OIO are unlikely to be an important mechanism for new particle formation, due to its short photolysis lifetime. And it was found that the reactive uptake of HOI in the MBL can liberate Cl atoms from sea-salt aerosol at a significant rate [Mcfiggans 2002]. Therefore, the iodine chemistry from gaseous to particulate phase in the coastal atmosphere, the whole chain of events including the chemical nature of the condensing iodine species, are not completely understood so far.

Modeling of reactive iodine species

Several modeling approaches were performed recently by several research groups. An observationally constrained photochemical box model was developed to investigate the atmospheric chemistry of iodine in the MBL in 2000 [McFiggans 2000] for instance. Using a model calculation, nucleation from the photolysis of CF_3I or CH_2I_2 in the presence of ozone and UV, demonstrates that IO and OIO concentrations reported in recent field measurements are not sufficient to account for significant aerosol production either in the coastal or open ocean marine boundary layer using the mechanism presented [Carpenter 2001]. Instead, it was demonstrated that inhomogeneous sources of iodine oxides, i.e. “hot spots” with elevated iodine species emissions, could account for the aerosol production bursts observed in the coastal region near Mace Head, Ireland [Burkholder 2003]. And more recently, using a newly measured molecular iodine photolysis rate, it was shown that, if atomic iodine is involved in the observed particle bursts, it is of the order of at least 1000 times more likely to result from molecular iodine photolysis than diiodomethane photolysis. A hypothesis for the molecular iodine release from intertidal macroalgae and the potential importance of macroalgal iodine particles in their contribution to cloud condensation nuclei (CCN) and global radiative forcing was presented by Mcfiggans [McFiggans 2004]. Again, discussed as earlier, the total mechanism causing gaseous iodine species enrich in aerosol is not clear yet.

1.3 Determination of iodine species in the atmosphere

The first iodine observation in the air can be dated back to the mid- 19th century, when Chatin (1850) measured total iodine from the air in Paris where he found 0.002 mg iodine in 4000 L air sample [Hofmann 1924, Rosenfeld 2000]. Due to the importance of the iodine chemistry cycle in the MBL, during the past 50 years various analytical techniques, including wet chemical analysis, NAA (Neutron Activation Analysis), or Gas Chromatography and Mass Spectrometry (GC/MS) have been applied and much more has been discovered about inorganic, organic, particulate iodine species in the atmosphere. Many observations of iodine species in the gas phase of the MBL have been made during past 10 years, as well as the iodine compounds in the marine particle phase. Besides the DOAS (Differential Optical Absorption Spectroscopy), NAA and ICP/MS (Inductively Coupled Plasma Mass Spectrometry) are all techniques in common use to detect iodine in the laboratory [4]. The determination of iodine species in the atmosphere involves currently at least in two phases, the gas and the particle phase, as discussed below.

Gaseous iodine species

Analytically VOIs, as a main part of organic iodine in the gas phase, are treated and determined in the same way as the other volatile organic compounds (VOCs). Several different instrumental methods have been applied for these compounds during the past decades, such as in-situ GC/MS [Carpenter 1999] or Tenax/Carbotrap adsorption off-site TD (Thermo Desorption)-GC-MS, purge-and-trap GC-ECD (Electron Capture Detector) [Schall 1997], HG/LT (Hydride Generation/Low Temperature)-GC/ICP-MS [Grüter 2000] and GC-ECD-ICP/MS [Schwarz 2000]. Many volatile iodinated hydrocarbons (for example methyl iodides) were measured in different locations especially at the Atlantic coast [Carpenter 1999, 2000] as well as the Arctic [Schall 1993] and the Western Pacific [Yokouchi 1997] coastal atmosphere. Table 1-1 summarizes some atmospheric mixing ratios of organoiodines. Note that there are some measurements, e.g. CH_2I_2 concentrations are only approximately 1/1000 of that of CH_3I (i.e. below the detection limit of current instrumentation).

Elemental iodine (I_2) was just recently measured at Mace Head by DOAS, indicating that the I_2 concentration range varied from the instrumental detection limit of about 3 pptv to maximum levels of 93 pptv at night and 25 ppt during daytime [Saiz-Lopez 2004b]. Iodine oxides (like IO, OIO) as the important inter-products in the gas phase of MBL iodine chemistry, were also observed by DOAS at and around Mace Head, western coast, Ireland, with IO maximum up to 8 ppt under sunlight at midday, and OIO maximum mixing ratio of 3 ppt after sunset [Allan 2001, Saiz-Lopez 2004b]. For comparison, in the Antarctica coastal atmosphere IO mixing ratios were between 5 and 10 ppt in summer [Frieß 2001]. However, due to its long absorption path (i.e. 8.4 km, and about 20 m above the sea) [Saiz-Lopez 2004b], the DOAS measurements are obviously too rough to determine the source of iodine emission. Therefore, to identify the exact biogenic emission source (especially for the identification of hot-spots) or ocean surface sources of selective gaseous iodine compounds, more intensive monitoring methods including sampling and detecting techniques are required in the further research work.

Table 1-1 Atmospheric mixing ratios of organoiodines measured in different locations

Compounds	Region	Concentration (pptv)		Reference
		Mean	Range	
CH_3I	W.Ireland (Spring)	0.43	0.12~1.47	Carpenter et al. 1999
	W.Ireland (Summer)	3.78	1.30~12.03	Carpenter et al. 2000
	W.Ireland (Summer)	3.40	1.9~8.7	Bassford et al. 1999
	Spritzbergen, Arctic	1.04	<0.004~2.12	Schall & Heumann 1993
	Asian Seas	0.63	0.24~2.0	Yokouchi et al. 1997
	W.Pacific	0.87	0.05~5.0	Yokouchi et al. 1997
	Okinawa, Japan	1.20	0.5~2.0	Li et al. 1999
C_2H_5I	W.Ireland (Spring)	0.06	<0.02~0.21	Carpenter et al. 1999
	W.Ireland (Summer)	0.16	<0.02~0.50	Carpenter et al. 2000
	Asian Seas	0.09	0.03~0.31	Yokouchi et al. 1997
	Spritzbergen, Arctic	0.20	<0.02~2.28	Schall & Heumann 1993
	Spritzbergen, Arctic	2.00	<0.02~5.98	Schall & Heumann 1993
CH_2ICl	W.Ireland (Spring)	0.11	<0.02~0.21	Carpenter et al. 1999
	W.Ireland (Summer)	0.16	<0.02~0.50	Carpenter et al. 2000
	Spritzbergen, Arctic	0.07	<0.004~0.18	Schall & Heumann 1993
	Alert	0.01	<0.01~0.05	Yokouchi et al. 1996
CH_2IBr	W.Ireland (Spring)	0.08	<0.02~0.32	Carpenter et al. 1999
	W.Ireland (Summer)	0.06	<0.02~0.30	Carpenter et al. 2000
CH_2I_2	W.Ireland (Spring)	0.05	<0.02~0.36	Carpenter et al. 1999
	W.Ireland (Summer)	0.10	<0.02~0.46	Carpenter et al. 2000
	Spritzbergen, Arctic	0.46	<0.08~1.02	Schall & Heumann 1993

cited from [Carpenter 2003a]

Table 1-2 Atmospheric iodine species fractions in different locations

Location	Total Iodine / $ng \cdot m^{-3}$	Species fractions / %			
		Particulate	HI/I_2	HOI	Organic
Regensburg (De)	11.80	26	3.5	6.5	64
North Sea	11.16	25	12	16	47
Antarctica	1.42~2.58	15~17	24~49	13~22	24~38
Japan	--	8~27	3~5 (as I_2)	3.4~10	59~82
Japanese Coast	9.7~25.6	8~12	13~15 (as inorganic)		73~77

cited from [Gäbler 1993a]

For instance, a system was developed by Heumann et al. (1993) to determine four different atmospheric iodine species by preparing glass microfibre filters, which were arranged in consecutive order, where particulate iodine was collected by a particle filter, HI and I_2 by a NaOH impregnated filter, HOI was adsorbed on a TBAH impregnated filter and organoiodine was adsorbed on a filter loaded with activated charcoal. Samples in those filters were then analyzed by using isotope dilution mass spectrometry (IDMS) for quantification [Gäbler 1993a]. Using FTIR (Fourier Transform Infrared Spectroscopy), HOI was also observed in laboratory chamber experiments [Barnes 1992]. Groups from Japan have developed some separation systems for gaseous iodine species [Noguchi 1988, Yoshida 1995]. The total iodine

concentrations and the relative contribution of the iodine species measured are shown in Table 1-2. As can be seen, the fractions of the investigated iodine species are in a wide and uncertain range, although the gaseous organic fractions are dominant in all the measurements.

Particulate iodine species

The sampling of particulate iodine is in principle simpler than the sampling for the different gaseous iodine species. Filtration and impaction sampling techniques are the most commonly used methods. Filtration is a simple, versatile, and economical technique for the collection of aerosol samples. However, size fractionated sampling is not possible with the filter technique. For size fractionated particle collection, multiple stage-impactors are suitable sampler, in which the particles of different sizes can be separated. Particle sample are then extracted by different solvents (e.g. water or organic solvents) and pre-treatments depending on the iodine species of interest, followed by a sensitive detection method such as NAA and ICP/MS.

Table 1-3 Measurements of "total iodine" / iodine species in the aerosol particles

Sort	Locations	"Total Iodine" / $ng \cdot m^{-3}$	Iodine Species / $ng \cdot m^{-3}$			References
			Iodide (I^-)	Iodate (IO_3^-)	Other iodine	
Coastal / Marine	Atlantic Ocean	0.2~2.4	0.05~0.46	N.D.~1.9	--	Baker 2004
	English Coast	0.7~2.8	0.7~3.8		--	Baker 2000
	South Atlantic	~2.05	~0.35	~1.70	--	Wimsch. 1995
	Japanese Coast	9.7~25.6	--	--	--	Yoshida 1995
	North Sea	2.83	--	--	--	Gäbler 1993
	Gulf of Guinea	4.0	--	--	--	Kritz 1980
	Bermuda	3.8	--	--	--	Rahn 1977
	Pacific Ocean	5.3~17.7	--	--	--	Brauer 1974
	Atlantic Ocean	1.9~5.7	--	--	--	Brauer 1974
	Hawaii	1.4~5.2	--	--	--	Moyers 1972
Continental	Regensburg (De)	1.99~7.79	0.39~0.91	1.60~6.88	--	Wimsch. 1995
	Regensburg (De)	3.06	--	--	--	Gäbler 1993
	Bonn (De)	2.0 ± 1.9	--	--	--	Wershof. 1989
	Colorado	1.7~3.7	--	--	--	Voill. 1979
	New York City	<1.0	--	--	--	Rahn 1977
	Washington	0.6~3.0	--	--	--	Brauer 1974

The first observation of iodine in the particulate phase of the atmosphere can be dated back to early 1970's, when the physical behavior of radioactive contaminants in the atmosphere was concerned, where particulate iodine were found to exist in the continental atmosphere [Brauer 1974]. Later on, some measurements have been performed by several groups at locations varying from continental to coastal and marine areas all over the world. Table 1-3 shows some representative results of the particulate iodine measurements in the last 30 years. It is obvious that the concentrations of particulate iodine from coastal/marine atmosphere are usually higher than those from continental areas. And as can be seen, there was no iodine species separation and determination for the particulate iodine until 1995. More and more techniques, such as laser ionization mass spectrometry [Murphy 1997, Middlebrook 1998] have been used to quantify the iodine species of the marine particles. However, the iodine species measured in the previous work, are mainly inorganic (water-soluble) iodine species, and no other species data were reported. Therefore, some "total iodine" values in Table 1-3 are calculated only from I^- and IO_3^- values. Although it was pointed out that the enrichment of

iodine in the marine aerosol of different size-fractions was in a large range, for example particles smaller than 1 µm enrich much more iodine than those greater than 1.5 µm [Baker 2000], there are no advanced analytically reliable data set about the concentration of other iodine species.

Additionally, there are several new instrumental methods for the chemical characterization of aerosol particles. For instance, AMS (Aerosol Mass Spectrometry) and ATOFMS (Aerosol Time-Of-Flight Mass Spectrometry) are the newly developed instrumental, online and in situ methods for the qualification and quantification of chemical composition for individual aerosol particles. Raman spectroscopy and its Surface Enhanced Raman Spectroscopy (SERS) version have rather unexplored potentials in the field of individual aerosol particle analysis as well. Unfortunately, up to now, there's no application for the purpose of particulate iodine species using those new techniques.

1.4 QUEST Campaign

Part of this work was contribution to the international European Union (EU)-Project named "Quantification of Aerosol Nucleation in the European Boundary Layer" (QUEST). The main objective of this project was to quantify the number of new secondary aerosol particles formed through homogeneous nucleation in the European boundary layer and the relative contributions of natural and anthropogenic sources. Three typical boundary layers were selected in this research project: Boreal area, coastal area and an anthropogenically influenced area in Southern Europe. The measurement campaign at the western coast of Ireland was the second campaign of the project. It was performed from the end of May to early Jun in 2002. All measurements were taken at the Mace Head Atmospheric Research Station (MHARS, 53°20'N, 9°54'W, Figure 1-3 shows the location), located about 100 m from the tidal zone and surrounded by rocky area.

Figure 1-3 Location of the Mace Head Atmospheric Research Station:
Carna, Co. Galway, Ireland (53.3° N, 9.9° W)

The campaign focused on the flux of iodine species, their contribution to aerosol production, and the resultant flux of aerosols from the coastal zone. Additionally, airborne measurements spatially mapped the homogeneity of these coastal events and the relative source strength of the field station region compared to the rest of the coastline. Other quantities were measured in addition to the continuously measured variables, such as pulse height CPC (Condensation Particle Counter) -size distribution, ultrafine particle hygroscopicity, vertical aerosol fluxes, the complete aerosol size distribution and condensation sink with size distribution measurements up to 20 microns using an Aerodynamic Particle Sizer etc., performed by different research groups involved in the whole project. Relevant parameters including temperature, pressure, relative humidity, wind speed and direction, NO_x and O_3 concentration were also measured continuously at the station during the field campaign.

1.5 BIOFLUX Campaign

The MHARS is located directly at the shoreline. However in certain areas around this station, the sea weed density is much higher than at the rocky area around the station itself. As a result, it is believed that *hot spot*s nearby, such as Mwneesh area, should have greater potential in terms of particle formation. This hypothesis was proved to be true during QUEST airborne measurements. In April 2002, airborne particle concentration measurements using condensation particle counters (CPCs) with different size cut-offs, performed by the Group of O'Dowd from the National University of Ireland Galway, showed that nanometer-particles were formed over Mwneesh and Roundstone area, Co. Galway, while the Mace Head station showed no particle formation. These *hot-spots* are likely to have a significant regional impact on the aerosol population. After the use of a research aircraft to identify the so-called *hot-spots*, it was proposed to conduct a study BIOFLUX at a particularly strong *hot-spot* site to examine the relationship between the flux of biogenic iodine gases into the boundary layer and the resulting flux of particles [Yoon 2004]. A field campaign BIOFLUX was conducted in Carna, Galway Ireland, in September 2003 to identify the particle formation and biogenic gas fluxes from marine algae.

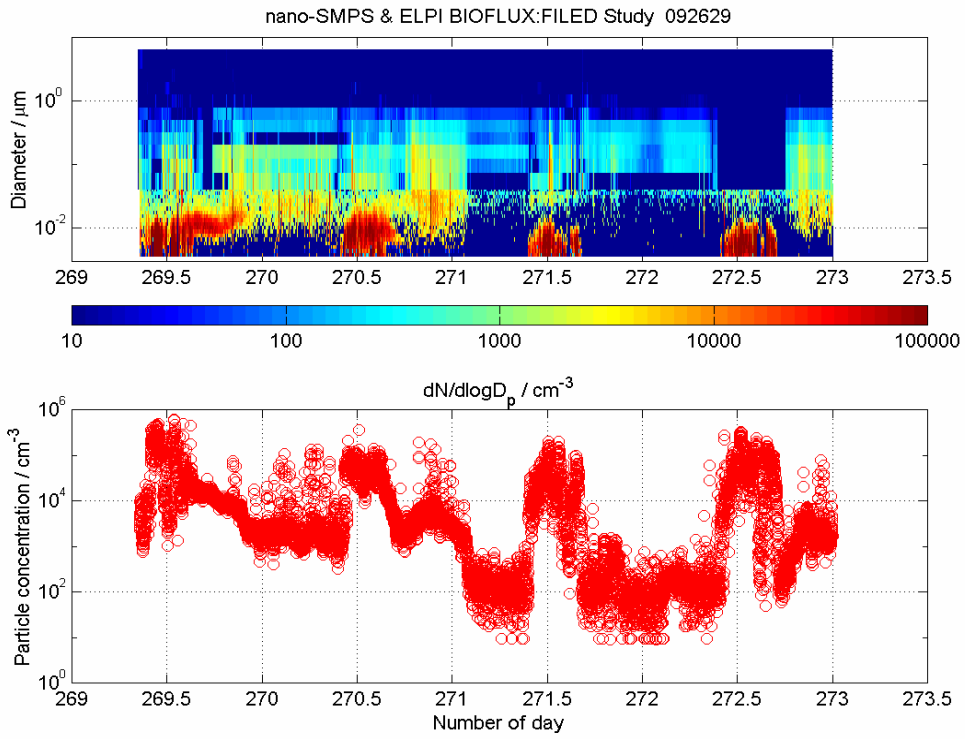

Figure 1-4 Aerosol size distribution and total concentration from *hot-spots* measurements – Mwneesh area: The surface plot represents the aerosol size distribution measured with SMPS systems and the lower concentration graph represents total particle concentration from the integration of the surface plot [Yoon 2004].

For *hot-spot* measurements, a Scanning Mobility Particle Sizer for nano-particles (nano-SMPS) was installed into a mobile lab, by the group of Prof. Pirjola from Helsinki Polytechnic, Department of Technology Finland. The nano-SMPS was set to measure particle sizes from 3.5 nm to 50 nm with a time resolution of 30 seconds. The laboratory is also equipped with Electric Low Pressure Impactor (ELPI) which measured particle size

distribution from 7 nm to 10 μm. The ELPI was operated with 12 stages and detecting time resolution of 30 seconds. Figure 1-4 shows a typical new particle formation process (so called nucleation event) in the coastal atmosphere during the campaign, indicated by the sudden burst of the nanometer-particle numbers.

A seaweed-chamber experiment was performed to test the hypothesis that biogenic gas emissions during low tide explain new particle bursts at the coastal environment, during the campaign. The chamber was in the dimension of 2m × 1m × 1m, and made from Perspex (PMMA, Poly-Methyl-Meth-Acrylate) of which UV radiation transmittance is about 50 %. The chamber was filled with varied amount of sea weeds collected near the Mace Head Atmospheric Research Station. Three combinations of sea weeds were tested: Laminaria, Fucus, and mixture of these two species. These two species are widely found at the Mace Head tidal area. A filter was applied to the inlet, and particle size distributions were measured by deploying nano-SMPS and ELPI. To identify the gaseous molecular iodine composition and VOC, chamber air was sampled and measured using the developed methods for iodine species analysis.

1.6 Objectives of this work

In this work, there were several objectives to be obtained and gaps in the understanding of the atmospheric chemistry of iodine compounds to be filled.

Firstly, to develop and improve the analytical methodology to identify the volatile organic iodine (VOI) species in the gas phase of the coastal atmosphere. The Tenax / Carbotrap adsorption sampling technique was selected to be applied, and the Thermo-Desorption / Cryo-Trap / GC-MS system to be used for the identification and quantification of VOI.

Secondly, to develop the sampling and determination methods for the *in situ* measurement of elemental iodine in the gas phase of the coastal atmosphere, so as to fill the gap of *in situ* observation of this iodine species in ambient air. A cylindrical diffusion denuder sampling technique, in which the inner surface is coated with chemisorption materials such as starch/amylose, was finally chosen to be developed as a sampling method, and Tetra-Methyl-Ammonium Hydroxide (TMAH) extraction, followed by a sensitive ICP-MS technique for detection.

Thirdly, to develop and improve the analytical methodologies for the identification and quantification of iodine species and total iodine in the particulate phase, including PM2.5 (Particles smaller than 2.5 μm in diameter) and size-fractionated particles of the coastal atmosphere. Particle samples would be collected at filters in a conventional filter holder (using a pre-separator for PM2.5) or foils in a 5-stage impactor (for size-fractionated particles). A water / TMAH extraction and anion-exchange separation procedure would be applied for the sample pre-treatment in order to separate the iodine species in the solution, followed by the ICP-MS detection.

Furthermore, to carry out the measurements of iodine species in the coastal atmosphere during the two field measurement campaigns at and around Mace Head Ireland, using all the developed analytical methods; VOI and elemental iodine in the gas phase to be monitored in the seaweed-chamber experiment as well. And to perform a laboratory reaction-chamber experiment, to identify the iodine species in the artificial aerosol particle, formed from the photolysis and ozonolysis of volatile iodine species (e.g. CH_2I_2), in the presence of ozone and

simulated sunlight, so that the iodine species in which would be compared with those from the real samples in the coastal atmosphere.

And finally, based upon the observations and data obtained from those laboratory experiments and field measurements, some statements and explanations would be concluded on the roles of iodine species in the marine boundary layer. Moreover, several undone issues and outlook about this theme would be laid out for the future studies.

2 Analytical Methods for the Measurement of Iodine Species in the Gas Phase

The iodine species in the gaseous phase in the MBL include organic and inorganic iodine compounds. As described in Chapter 1, volatile organic iodine compounds (VOIs) are believed to be the most important precursors of the new marine particles. A recent study found that elemental iodine is another potential initiator to form particles. Furthermore, the intermediate products of iodine in the complicated process, such as HI, HOI and iodine oxides are pivotal to clarify the whole mechanism from gas phase to particle phase in the coastal atmosphere. In this Chapter, the development and application of a Tenax/Carbotrap adsorption sampling technique and a Thermo-Desorption /Cryo-Trap-Focusing/GC-MS detection will be described for the VOI analysis, as well as a cylindrical diffusion denuder sampling technique combining ICP-MS for the in-situ measurement of gas elemental iodine.

2.1 Determination of volatile organic iodine

The VOIs can be treated and determined as biogenic volatile organic compounds (BVOCs) in ambient air. Due to the fact that research about BVOCs are performed since several decades, there exist several analytical methods for the measurement of the target compounds, such as *in-situ* GC-MS, purge-and-trap GC-ECD and GC-ECD-MS etc. [Giese 1999]. Among these techniques, the most common and widely used one is the adsorptive enrichment on solid adsorbents followed by thermal desorption and capillary gas chromatographic analysis, so called Adsorptive Sampling / Thermo-Desorption / Cryo-Trap-Focussing / GC-MS method. This technique provides several advantages, such as pre-concentration of the analytes during the adsorption sampling procedure, a high selectivity for specific VOCs and an extremely low determination limit for the trace analysis of VOCs in the atmosphere.

2.1.1 Tenax/Carbotrap sampling

For the sampling of biogenic VOCs, several different techniques can be used, such as whole air sampling with stainless canisters or telfon (PTFE) bags. Adsorption on solid adsorbents such as Tenax, Carbotrap or Carbosieve is the most widespread technique in use [Komenda 2001].

Adsorption materials

There are a number of different adsorption materials commercially available for the quantitative determination of gaseous BVOCs as well as VOIs. Two major classes of adsorbents are commonly used for the enrichment of VOCs [Dettmer 2000]:

- Carbon based adsorbents, such as graphitized carbon blacks or carbon molecular sieves.
- Synthetic polymers such as Tenax.

Table 2-1 shows the material properties of Tenax TA and Carbotrap, as the two adsorbents applied in this work. As can be seen in the table, the specific surface area of Tenax TA is only about 1/3 of the surface area of Carbotrap. Therefore Tenax is most suited to the less volatile compounds, while Carbotrap can collect also smaller molecules. Due to the week UV-

resistance of Tenax TA, the adsorption material in the tube has to be kept in darkness before, during and after the sampling, being covered by Aluminium-foil.

Table 2-1 Material properties of the absorption materials

Items	Tenax TA	Carbotrap
Substance	Poly-2,6-diphenyl-p-phenylenoxide	Graphitized Carbon Blacks
Specific surface area	35 $m^2 \cdot g^{-1}$	100 $m^2 \cdot g^{-1}$
Pore volume	2.4 $cm^3 \cdot g^{-1}$	
Average pore size	0.2 nm	
Density	0.2 $g \cdot cm^{-3}$	
Thermal stability	up to 350 °C	up to 400 °C
UV- resistance	bad	good
Adsorbable substances	monoterpene, alcohol, ketone, aldehyde etc.	mid- and less volatile organic compounds
Particle diameter	0.18 – 0.25 mm	0.4 – 0.8 mm
Mesh size	60/80	20/40

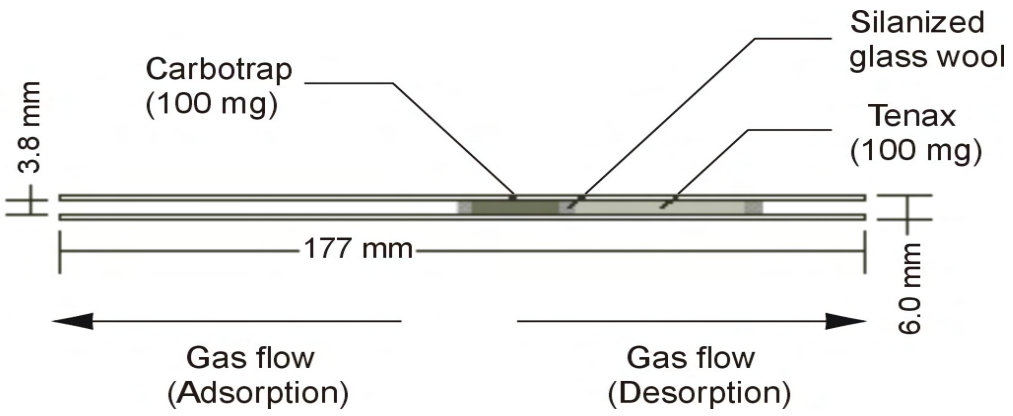

Figure 2-1 Schematic diagram of the adsorption tube for VOI sampling
(Glass tube filled with 100 mg Tenax TA and 100 mg Carbotrap)

Preparation of the adsorption tube

Silanized glass tubes (($Ø_i$ 3.8 mm × $Ø_o$ 6 mm × L 177 mm, $Ø_i$ = inner diameter, $Ø_o$ = outer diameter and L = length), filled with adsorption material were applied as adsorption tubes (Figure 2-1). The preparation process of the adsorption materials and tubes is listed as follows [Spanke 2002]:

- For the purpose of silanization, the glass tubes were kept at a moderate temperature at 120 °C in a drying furnace and immersed into a measuring cylinder, which was filled with 5 % (vol.) Dimethyl-dichlor-silane in n-hexane. After ca. 5 min, tubes were then placed into a measuring cylinder with methanol to replace the remaining Cl-atoms at the glass surface by methoxy group. Subsequently, the tube dried again at 120 °C.
- The adsorbents Carbotrap and Tenax TA were purified with methanol for about 18 hours in a Soxhlet-Extractor.

- The adsorbents (100 mg Tenax TA and 100 mg Carbotrap) were finally filled into the glass tubes, using silanized glass wool to fix and separate the two materials (see Figure 2-1).
- The filled adsorption tubes were then additionally cleaned with methanol for 12 hours using Soxhlet-Extraction.
- Finally, the tubes were treated further by a gas flow of ca. 30 mL·min N_2, for 12 hours at 275 °C in a GC oven. Before entering the oven, the gas flow of N_2 was purified by passing a liquid nitrogen trap. Afterwards, the adsorption tubes were closed with Swagelok blind-plugs, and ready for sampling.

Adsorption tube sampling

A convenient sampling unit was built up for the purpose of VOI sampling (Figure 2-2). A small membrane pump (ASF Thomas, 12 V/DC) was applied for the pumping unit, and a needle valve was used to control the sampling flow rate, with the indication of a mass flow meter (Aalborg Instrument & Controls Inc.). The sampling flow rate was adjusted to 200 $mL \cdot min^{-1}$ for VOI sampling. All tubings in use were made of PTFE (Poly-Tetra-Floro-Ethylene, Teflon®).

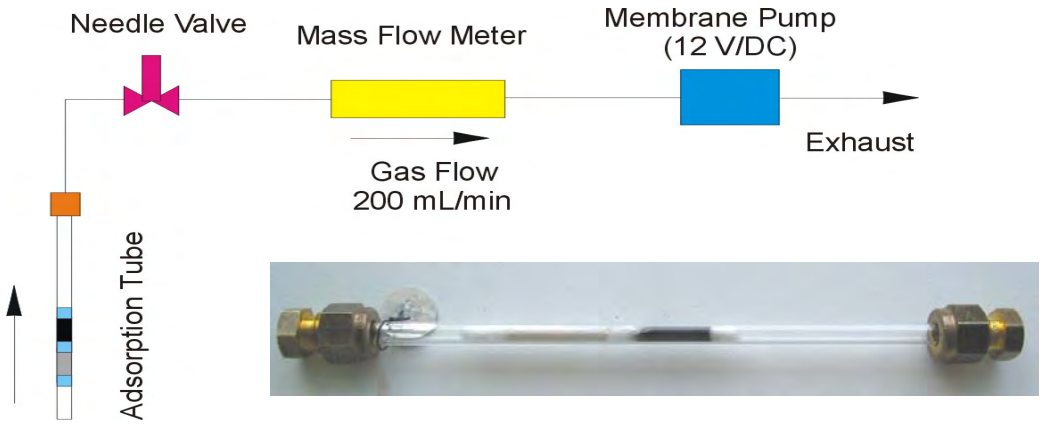

Figure 2-2 Schematic diagram of the self-made VOI sampling unit and picture of an adsorption tube

UV-light or any sunlight has to be avoided during the sampling, due to the VOI photo-sensitivity and the week UV-resistance of the Tenax TA adsorption materials. Care has to be taken for the direction of sampling and desorption flows using the two-adsorbent tubes. This is because the less volatile organic compounds should be first in contact with the Tenax TA (with a relative small specific surface area), while the other higher volatile compounds will be adsorbed by the Carbotrap (with much greater specific surface area). For the desorption process, the flow of the desorbing gas has to be in the opposite direction to avoid that the less volatile components are forced to travel over Carbotrap packing.

The test gas source

In order to test the analytical methods and to calibrate the measurements for the VOIs, a test gas source was built up in the laboratory. For that purpose, a test gas source based on controlled evaporation of the compounds of interest was used. The evaporation of a volatile organic compound depends primarily on the temperature, which affects the vapor pressure of the compound. Therefore, using a thermostat, one can easily chose a defined temperature in

order to adjust the VOI concentration in the carrier gas (N_2 4.6). This exact VOI concentration can be calculated from the weight loss of the VOI, the flow-rate of the carrier gas and the duration of the evaporation. Figure 2-3 shows the set-up of the test gas source. A temperature of 20 °C was selected for the thermostat. To reduce the VOIs' concentrations to the lower levels which match more realistic atmospheric conditions, de-activated capillaries (FD-Methyl-Sil-Desaktive 0.53 mm ID, CS-Chromatographie Sevice GmbH) were installed at the top of vials containing the VOIs. The VOI output from these vials is then limited by diffusion and therefore depends also upon the length and the diameter of the capillaries. Hence different lengths of the capillary have been tested to control the VOI concentrations. The flow rate of the carrier gas has no significant effect on the VOI output in the gas source. A flow rate of 200 mL·min^{-1} was selected.

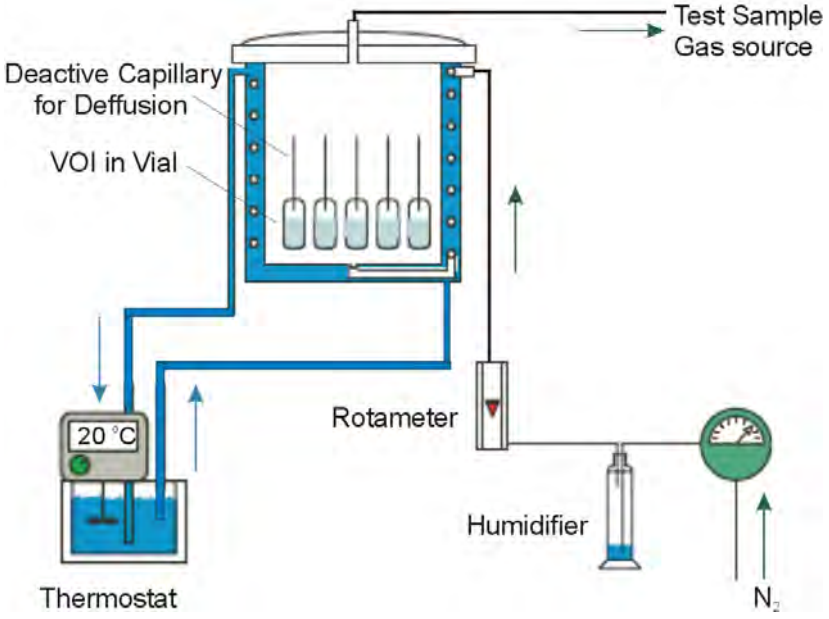

Figure 2-3 Schematic diagram of the test gas source for VOIs in the laboratory

Table 2-2 Calibration of the test gas source for VOIs

VOIs	Molecule Weight	Boiling point / °C (1 atm)	Vapor Pressure / hPa (20 °C)	Capillary Length / cm	Concentrations in the gas source / μg·min^{-1}
CH_3I	141.94	42~43	438	3	13.33[1]
				5	9.29[1]
				10	5.48
C_2H_5I	155.97	71~72	143	3	4.03[1]
				5	2.33[1]
				10	1.13[1]
CH_2ICl	176.38	107~109	31.4	10	2.98[2]
CH_2IBr	220.84	138~141	8.02	5	1.06[2]
CH_2I_2	267.84	181	1.23	5	0.139[1]
				10	0.0717[1]

Note: [1]With the exposed surface area of 0.08 cm^2 (small vial, 0.25 mL);
[2]With the exposed surface area of 0.78 cm^2 (bigger vial, 1.5 mL).

Five VOIs of interest for the calibration have been used, i.e. CH_3I, CH_2I_2, C_2H_5I, CH_2ICl ($\geq 99.5\%$, Fluka Chemie GmbH) and CH_2IBr (Sigma-Aldrich Chemie GmbH). Due to the photo-sensitivity of these compounds, the whole system was strictly in the darkness to avoid any UV or visible light. Some physical properties and the calibration details of these iodo-hydrocarbons used in this work are listed in Table 2-2.

2.1.2 Thermo-Desorption and GC/MS detection

The substances adsorbed in the sampling tubes were analyzed by a Thermo-Desorption and Gas Chromatography / Mass Spectrometry (TD-GC/MS) system. The TD-GC/MS system is shown in Figure 2-4. The operation and technical details of the instrumental system are described as follows.

Thermo-desorption and cryo-trap focussing

Liquid nitrogen was used for the carrier gas cleaning. Impurities such as water or other substances were frozen out when the helium carrier gas passed the liquid nitrogen. Firstly, the liquid nitrogen was also used to cool the cryo-trap as low as at least - 80 °C, via a cold nitrogen gas injection into the cryo-trap. After the maximal cryo-trap temperature was reached (temperature lower than – 80°C), the adsorption tube was installed into the desorption oven. Then, to start the thermo desorption process, the desorption oven was heated up to 275 °C at a heating rate of about 50 °C/min. During this time the split valve was open so that the purified carrier gas could pass through the sample tubing to elute the adsorbed substances away from the adsorbents and into the cryo-trap. The thermo desorption step lasted for ca. 10 minutes.

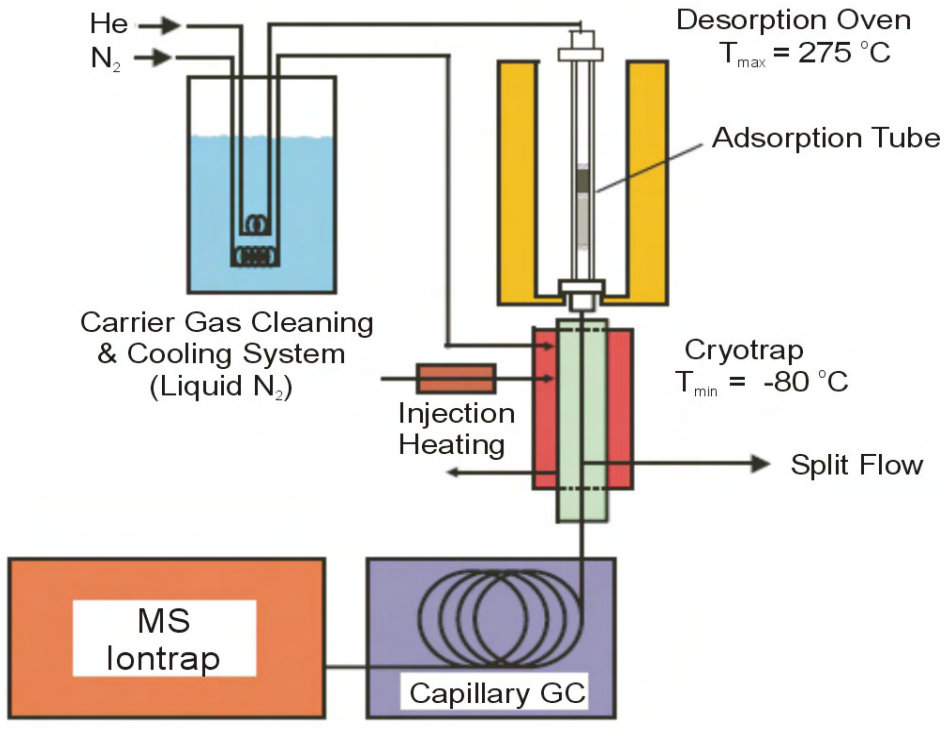

Figure 2-4 Schematic diagram of the Thermo-Desorption / Cryo-Trap / GC-MS system [Spanke 2002]

Cryo-trap purge and injection

After the thermo desorption step, the substances of interest were frozen and focused in the cryo-trap at about -80 to -100 °C. Then the split valve was closed. Afterwards the cryo-trap was heated up rapidly (at about 30 °C /s) to 250 °C, and purged by the carrier gas at the same time, so that the analytes in the trap zone were injected directly into the capillary column of the GC.

Separation of the substances by GC

Since there are hundreds of different substances in the sample, generally a separation process before the detection is necessary. The capillary Gas Chromatograph (GC) is the usual and robot technique for the purpose of separating the volatile hydrocarbons. Based on their similar chemical and physical characteristics, to separate the certain class of substances, a suitable capillary column has to be chosen. There a number of different capillary columns commercially available, which differ in column diameters, length, polarity type and thickness of the stationary phase. In order to improve the separative power, the advancement of the different column types is a constant development [Eiceman 1998]. The selection of the capillary column is mainly based on the polarity, the vapour pressure and the quantity of the analytes to be separated. For the VOIs separation, a non-polar capillary column was chosen. The temperature program of the GC capillary oven is another helpful way to improve the separation performance.

Technical details for GC:

- *Gas Chromatograph:* Type DANI 6500 GC (Dani GmbH, Mainz-Kastel)
- *GC capillary:* Type 50QC2/BPX5 1.0, Non-polar, 50 m length, film thickness of stationary phase 1 µm, inner diameter 0.32 mm (Fa. SGE, Weiterstadt).
- *Carrier gas*: Helium 5.0 at minimum press of 3.5 bar.
- *Temperature program of the GC:*

  Start at 50 °C and keep for 2 min;
  Heating at the rate of 8 °C/min to 200 °C;
  Heating at the rate of 10 °C/min to 220 °C, and keep for 18 min;
  The complete time of the temperature program is about 40 min.

Detection by ion trap Mass Spectrometry

After the separation by GC, VOCs like hydrocarbons can be detected by several instrumental methods, such as FID (Flame Ionization Detector), EFID (Electrolyzer-power Flame Ionization Detector), PFPD (Pulsed-Flame Photometer Detector) [Jing 1997], ECD (Electron Capture Detector). However, those techniques are not suitable for qualification of the analytes, which have to identify the substances according to the exact retention time of the standards for reference. For qualification and quantification at the same time, mass spectrometry or ICP-MS [Schwarz 2000] are widely used nowadays [Richardson 2004], especially for unknown analytes. In this work ion trap detection system (ITDS, see Figure 2-5) was applied. The MS was directly coupling to the GC system, via a transfer line at 200 °C.

Technical details for MS

- *Ion Trap Mass Spectrometry:* Type ITD 700 (Fa. Finnigan, Bremen);
- *Ionization:* Electron-impact Ionization (EI), 70 eV, transfer-line temperature 200 °C;
- *Ion trap:* Multiplier voltage 1400 V;
- *Data acquisition:* mass spectrum record at every 0.5 s, m/z range 46-280, Filament / Multiplier delay 180 s, data acquisition for 40 min.

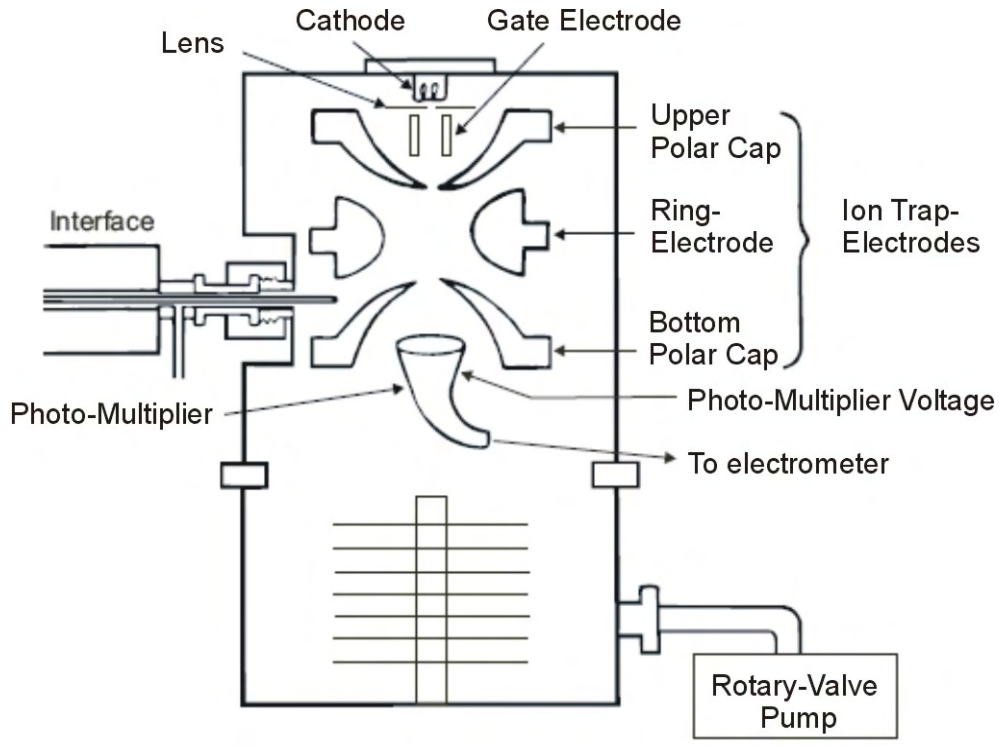

Figure 2-5 Schematic diagram of the ion trap detection system (Finnigan ITD 700)

Ionization by Electron Impact (EI)

The use of EI for ionization dates back to the infancy of mass spectrometry in the early 20th century. Ionization is effected by shooting energetic electrons onto a neutral molecule that have been transferred into the gas phase before. EI is definitely the mostly used approach to ionize analytes in organic mass spectrometry, and still represents an important technique for the analysis of low- to medium-polarity, non-ionic or organic compounds in the range of molecular weights up to $M = 1000$ [Gross 2004].

Electrons are produced by heating a metal filament, usually formed from a fine wire or ribbon of tungsten or rhenium. These electrons are accelerated by a potential difference between the filament and the ion source box, pass through entrance and exit apertures in the box, and are collected by a trap electrode. Voltage is applied to a repeller electrode within the box that accelerates ions toward the ion exit aperture. A collimating magnetic field is applied parallel to the electron beam axis, and the field strength is chosen to provide high transmission of the electrons with minimal perturbation of the ion beam. A field on the order of 100 G is typically

used. The electron current is stabilized by monitoring either the total emission current or the current to the trap with feedback to the filament heater power supply to maintain a constant current. Samples are introduced directly into the ion source box, and for most analytical applications, the vapor input rate and the orifices in the source box must be chosen so that the probability of ion-molecule reactions is minimal [Vestal 2001].

For analytical applications, electron energy of 70 eV has been adopted as the standard. That is reasonable for [Gross 2004]:

- There is no atom or molecule that cannot be ionized at 70 eV, whereas at 15 eV gases such as He, Ne, Ar, H_2, and N_2 would not.
- The plateau of the ionization efficiency curve around 70 eV makes small variations in electron energy negligible; in practice EI woks equally well at 60-80 eV.
- This assures better reproducibility of spectra, and therefore allows comparison of spectra obtained from different mass spectrometers or from mass spectral database.

Ion trap detection

As can be seen in Figure 2-5, the ion trap consists essentially of three oddly shaped electrodes: Two end-cap electrodes (Upper and Bottom Polar Caps) and the Ring Electrode. When an appropriate high frequency voltage is applied to the ion trap electrodes, these generate a three-dimensional electrical field, in which ions in aperiodic oscillations can be held within the electrode dimensions. The ions can be removed then by an additional direct current potential between the two polar caps, with the rising m/z relationship from the ion trap. Afterwards, these ions will be magnified by the photomultiplier and the resulting electronic signal detected by the following electro-meter [March 1997].

The complete principle and theory of the ion trap was founded in late 1980's. Many of the developments in quadrupole / ion-trap mass spectrometry of the mid-1980s to early 1990s, such as mass range extension by resonance ejection (to roughly *m*/*z* 70 000), high resolution via slow scanning (to as high as 107 at *m*/*z* 600), MS^n (with *n* as high as 10), the use of tailored waveforms for ion manipulation, etc., are currently available, to varying degrees, in commercial instruments [McLuckey 2001].

Identification and quantification of the VOIs

To identify the substances from the gas chromatograph of the air sample, one can simply judge by the retention time the components of interest, since the retention time a VOI is always the same if using the same GC operating conditions. However, it is necessary to have a "standard" chromatogram for all the substances of interest. Such a chromatogram can be obtained from the sample of the test gas source containing different VOIs. But VOIs can also be identified by the mass spectrum. Comparing the mass spectrum of a peak to the reference mass spectrum from the NIST library (software and database from National Institute of Standards and Technology, USA), the components can be identified if the separation of the GC is satisfying. Fo quantification, usually a calibration curve based on the peak area integration of each substance is applied. Internal standards are also helpful to improve reproduceability. However, in this work for the quantification of VOIs in ambient air, the comparison of peak heights was used.

2.1.3 VOI test gas source

Samples from the test gas source and sefl-made emission chambers have been taken and measured by the method described above. Figure 2-6 shows the Total Ion Current (TIC) of the test gas sample, containing the 5 iodo-hydrocarbons. CH_2Br_2 was also identified, probably an impurity of CH_2IBr. As can be seen in the chromatogram, the separation of the components is satisfactory. The reference mass spectra of the iodo-hydrocarbons can be found in Appendix I.

The retention time and absolute amount of each compound in this sample are listed as follow: CH_3I: 3.34 min, 3820 ng; C_2H_5I: 4.19 min, 2530 ng; CH_2ICl: 5.99 min, 248 ng; CH_2IBr: 7.84 min, 88.3 ng; CH_2I_2: 10.47 min, 11.6 ng.

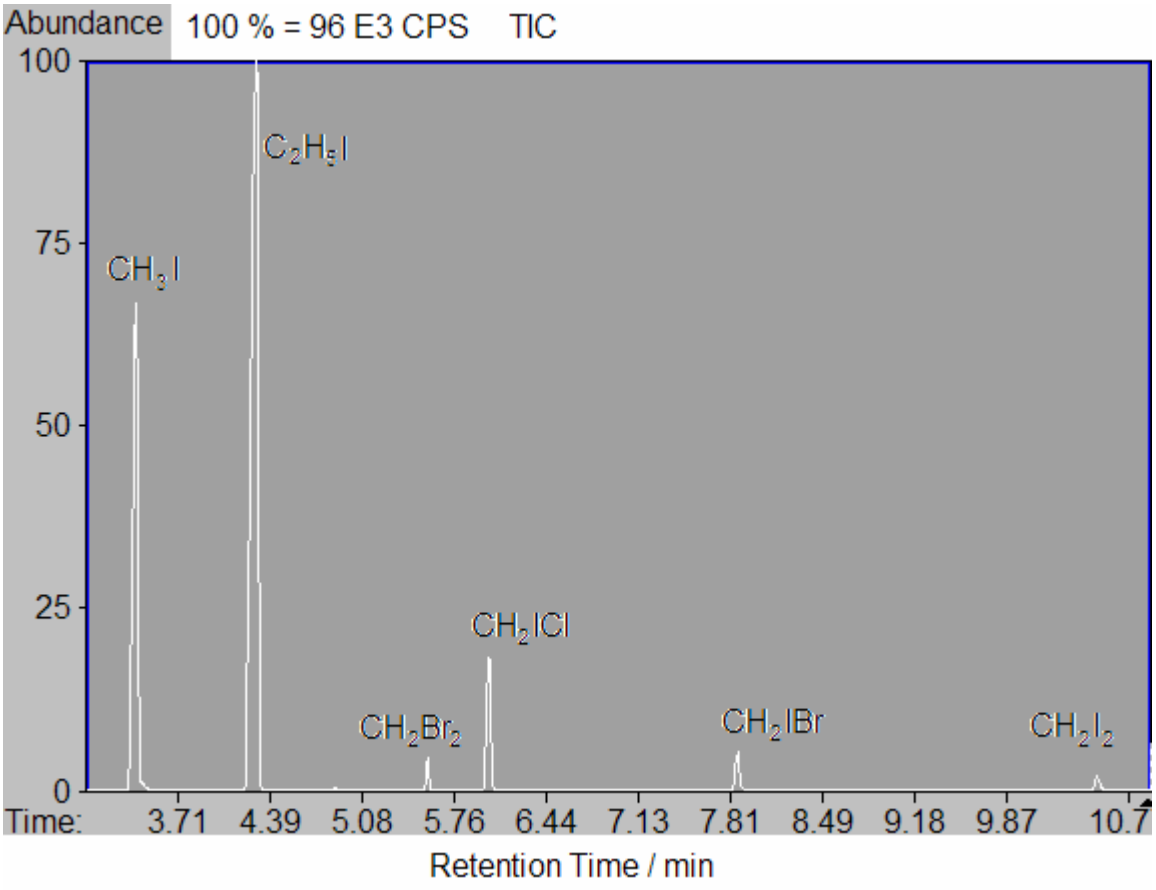

Figure 2-6 Total Ion Chromatograph (TIC) of a sample from the test gas source

The emission from a dry macro-algae sample (Laminaria, about 30 g) was used as a real air sample to test the developed method. The algae was contained in a beaker, and put into a glass chamber (~ 5 L) which was flushed with pure nitrogen at a flow rate about 200 $mL \cdot min^{-1}$. After allowing the system 30 min to equilibrate, the air sample was taken from the chamber outlet with a sampling time of 20~40 min.

Figure 2-7 shows the Selected Ion Current (SIC, *m/z* 127) of the real air sample emitted from the dry macro-algae. More than 6 iodo-hydrocarbons can be identified from the emission, including CH_3I, C_2H_5I, 1-C_3H_7I, 2-C_4H_9I, the 3 other homologs of C_4H_9I (in one peak, difficult to be separated by the GC column) and CH_2I_2 (more detail in Table 2-3). The other halogen species like CH_2ICl or CH_2IBr were not found in this sample. The quantification of

the test measurements indicate that the emission rates for some VOIs from the macro-algae are estimated as: CH_3I: ~ 0.29 ng·min^{-1}; C_2H_5I: ~ 0.080 ng·min^{-1}; CH_2I_2: ~0.020 ng·min^{-1}. It was found that iodo-methane is the most important VOIs emitted from this macro-algae sample, which agrees well with the former results [Adams 1998, Laturnus 2001, Carpenter 2003a, b].

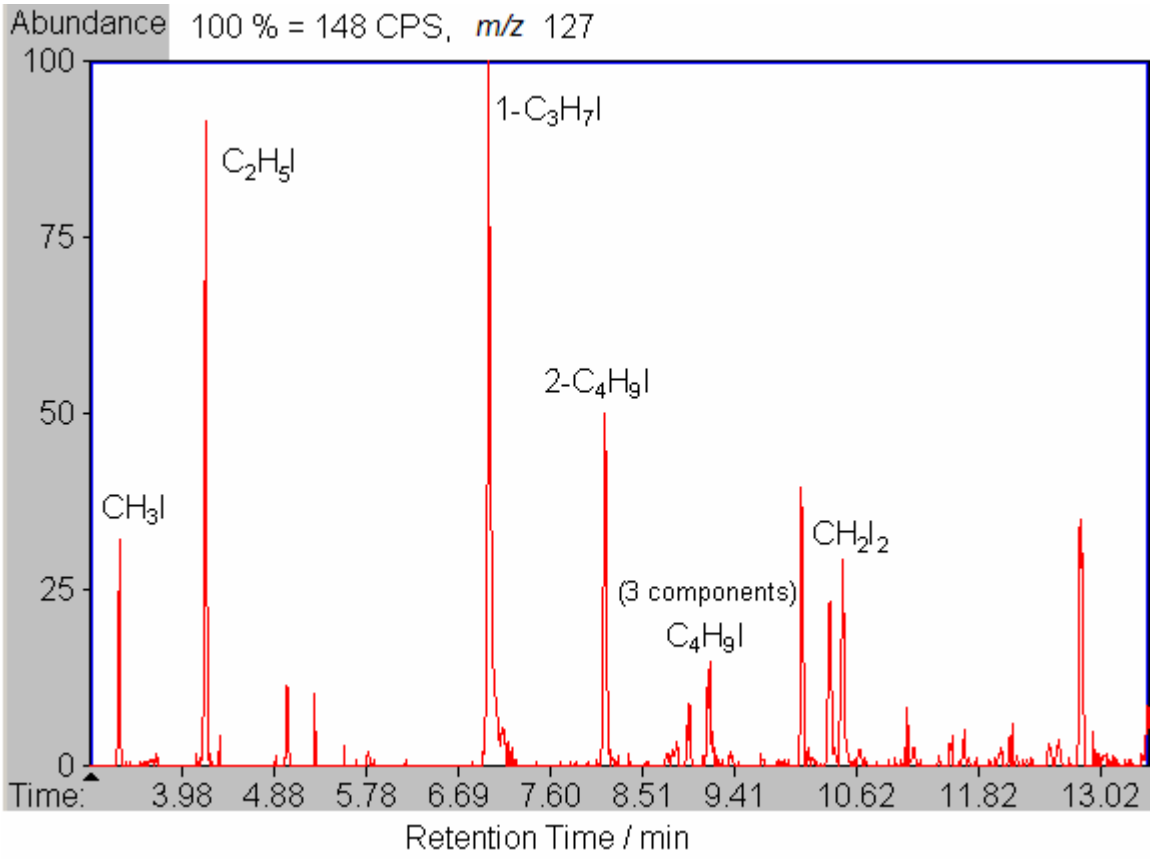

Figure 2-7 Selected Ion Current (SIC, *m/z* 127) of an air sample with iodo-containing emission from a dry (dead) macro-algae

Table 2-3 Test measurement of the emission from a dry Laminiria sample

VOIs found	Molecule Weight	Retention Time / min	Absolute amount found[1] / ng
CH_3I	142	3.34	2.33~9.42
C_2H_5I	156	4.19	0.55~1.58
1-C_3H_7I	170	6.99	--
2-C_4H_9I	184	8.14	--
C_4H_9I (3 components)	184	9.11~9.23	--
CH_2I_2	268	10.47	0.27~0.88

Note: Absolute amounts are calculated by the comparison of peak areas and heights of the substances in the real sample and the test gas source.

2.2 Determination of elemental iodine

Already several decades ago, gaseous elemental iodine was believed to be one the iodine-contain emissions from the ocean surface several [Miyake 1963, Garland 1981]. However, up to now there have not been any quantitative data available from the field measurements. Just recently there were modeling studies [Mcfiggans 2004] and observations of elemental iodine in the coastal atmosphere using DOAS [Saiz-Lopez 2004 b]. In this section, using a diffusion denuder sampling technique, followed by a TMAH extraction and ICP/MS detection, an analytical method has been developed for the *in situ* measurement for elemental iodine in the coastal atmosphere.

2.2.1 Diffusion denuder sampling technique

Principle of denuder sampling technique

Denudation techniques have been widely applied for the determination of trace components in air. At laminar air flow conditions, the diffusion coefficient of a gas molecule is at least 100 times bigger than those of particles larger than 10 nm diameter [Mader 2001]. According to the Gormley-Kennedy Equation (1949), gas molecules can diffuse to the walls of an open channel much more rapidly than the particles. Consequently, gas molecules can be separated from the particles in the ambient air. Figure 2-8 shows the process in a cylindrical denuder in which the separation of gaseous molecules from particles occurs.

The phenomenon of denudation involves movement of molecules and/or particles being a result of two forces [Kloskowski 2002]:

- a force vectored in the same direction as the gas stream, resulting from the forced flow of gas,
- a force perpendicular to the longitudinal axis of the denuder (and its walls), resulting from the radial diffusion.

Under such conditions, the combined process of isolation and enrichment of analytes can proceed directly from the primary (original) matrix: analytes present in the gaseous phase are retained by the sorption medium, due to their high diffusion coefficients, while solid particles can pass the tube practically avoiding any contact with the walls of the device.

Theory of cylindrical denuder

The separation of gaseous molecules from particles by denudation is based on their different diffusion behavior. Diffusion of gaseous molecules and aerosol particles, obey the *Fick's first law of diffusion*:

$$J = -D\frac{dn}{dx}$$

where, D is the diffusion coefficient. The larger the value of D, the more vigorous the Brownian motion and the more rapid the mass transfer in a concentration gradient. Table 2-4 compares the diffusion coefficients of I_2 gas molecules versus particles of different diameter (smaller than 1 μm) in air. Figure 2-9 shows the log-log plot of the particle diameter and their diffusion coefficient, indicating that smaller particles have bigger value of diffusion coefficients and diffusion coefficients of gas molecules are much bigger than the diffusion coefficient of particles. The gaseous elemental iodine has a diffusion coefficient about 170 times larger than that of 10-nm particle.

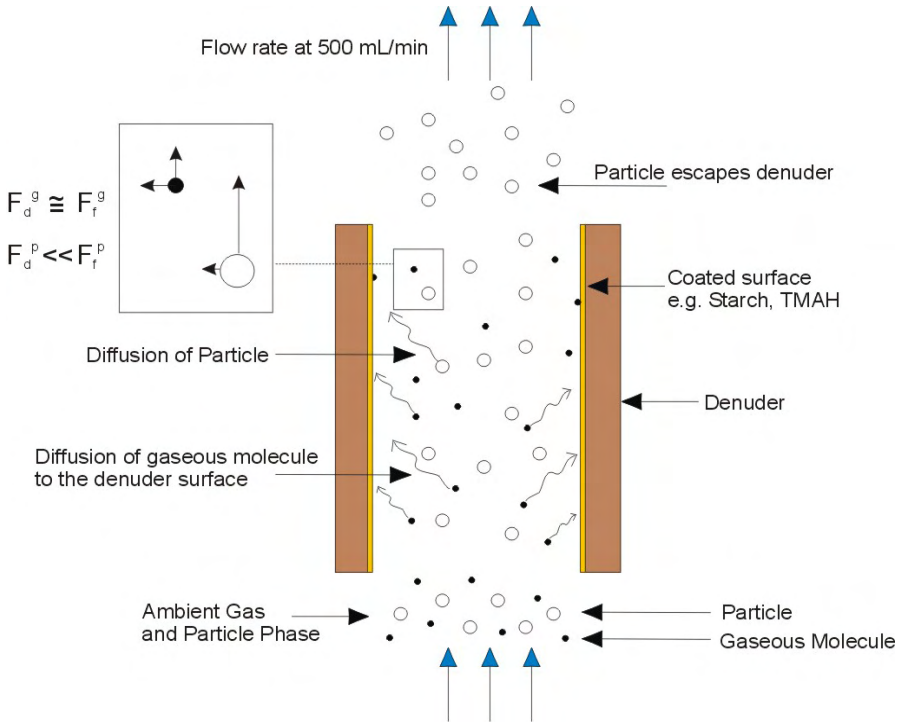

Figure 2-8 The principle of separation of gaseous molecules from particles in a cylindrical denuder. (F-Force, g-gas, p-particulate matter, d-diffusion, f-air flow)

Table 2-4 Diffusion coefficients of gaseous molecules and particles in the air at Standard Conditions (calculated for standard density spheres at 293 K (20°C) and 101 kPa (1 atm))

Items	Diameter d/μm	Diffusion Coefficient D/$cm^2 \cdot s^{-1}$
"air molecule"	~ 0.00037	2.0×10^{-1}
I_2 (Gas) molecule[a]	~ 0.0005	9.22×10^{-2}
Airborne Particles	0.001	5.32×10^{-2}
	0.002	1.33×10^{-2}
	0.005	2.15×10^{-3}
	0.01	5.45×10^{-4}
	0.02	1.40×10^{-4}
	0.03	6.39×10^{-5}
	0.05	2.43×10^{-5}
	0.1	6.94×10^{-6}
	0.2	2.23×10^{-6}
	0.5	6.24×10^{-7}
	1	2.74×10^{-7}

From [Hinds 1999] and [Seinfeld 1998]

Note: [a]Diffusion coefficient of gaseous elemental iodine was estimated using the **FSG** method [Lyman 1990]. The Fuller, Schettler and Giddings (FSG) method is based on the regression formula:

$$D_{air} = 0.001T^{1.75}M_r^{1/2} / P(V_A^{1/3} + V_B^{1/3})^2$$

where:

D is the diffusion coefficient in $cm^2 \cdot s^{-1}$;

T is the temperature in K, e.g. room temperature, 293 K;

M_r is the following function of molecular weight: $M_r = \frac{M_A + M_B}{M_A M_B}$,

where M_A is the molecular weight of air, approximately 28.97 g·mol^{-1};
and M_B is the molecular weight of the compound of interest, e.g. for I_2: 253.81 g·mol^{-1};
V_A is the molar volume of air, approximately 20.1 cm^3·mol^{-1};
V_B is the molar volume of the compound of interest, e.g. for I_2: 60.4 cm^3·mol^{-1};
P is the pressure in atm, e.g. 1 atm.

Calculated at 20°C, 1 atm, for I_2 gaseous molecule, $D \approx 0.0922 cm^2 \cdot s^{-1}$
[also from US EPA online tools: http://www.epa.gov/athens/learn2model/part-two/onsite/estdiffusion.htm]

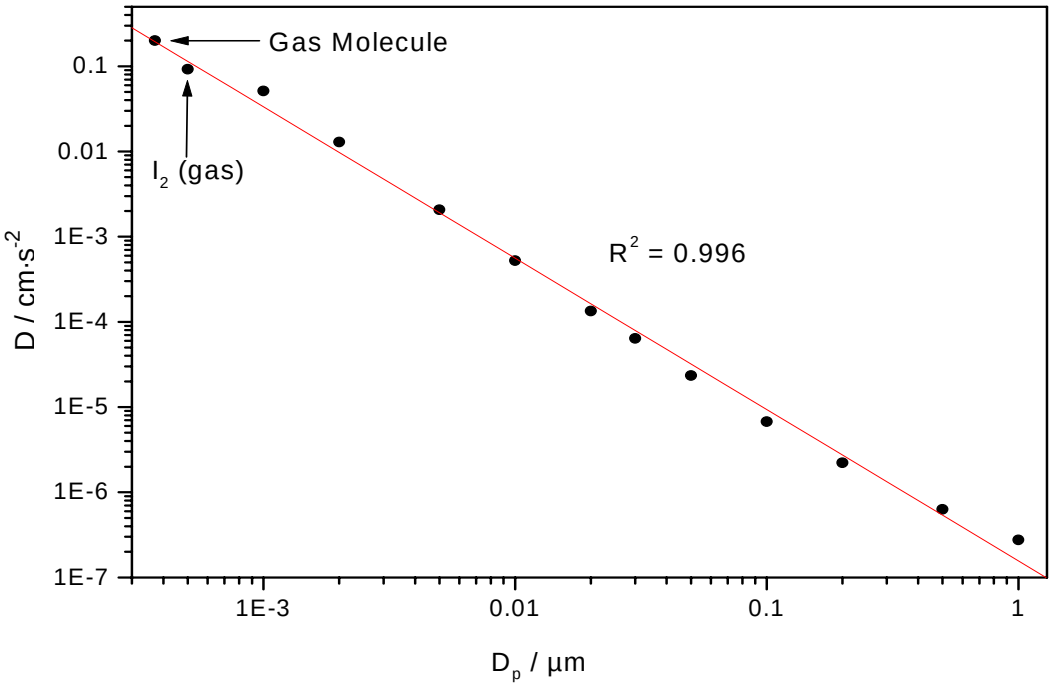

Figure 2-9 Correlation between particle diameter and their diffusion coefficient

If c_A denotes concentration of component A in air [mol·cm^{-3}], then one can write that:

$$c_A = f(t, x, r),$$

where: t is time [s],
x is longitudinal coordinate [cm],
r is distance from the longitudinal axis of the cylinder [cm].

In a general case, the balance of component A in the denuder (Figure 2-10) is given by the following differential equation [Katsanos 1995]:

$$\frac{\partial c_A}{\partial t} = -\upsilon \frac{\partial c_A}{\partial x} + D_A \frac{\partial^2 c_A}{\partial x^2} + D_A \left(\frac{\partial^2 c_A}{\partial r^2} + \frac{1}{r} \frac{\partial c_A}{\partial r} \right) - r_A \qquad \text{(a)}$$

where:
υ – actual linear velocity of air flow [cm·s^{-1}], for laminar flow given by equation:

$$\upsilon = 2\upsilon_{av}(1 - r^2/R^2);$$

υ_{av} – linear velocity of air flow [cm·s^{-1}];
R – internal radius of the denuder [cm];
D_A – diffusion coefficient of component A in air [cm·s^{-1}];
r_A – component A gas-phase reaction rate [mol·cm^{-3}·s^{-1}].

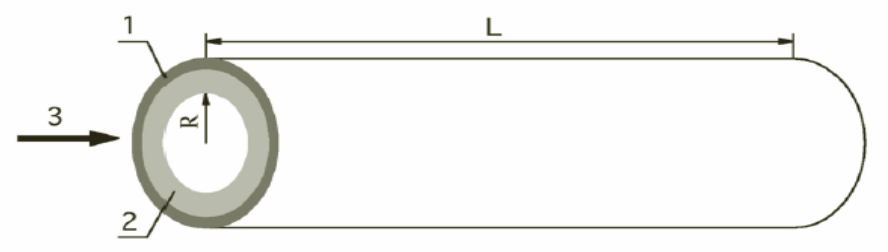

Figure 2-10 A schematic view of a cylindrical denuder:
1 – cylindrical walls, 2 – retaining medium, 3 – air flow, R – radius, L – length

Equation (a) describes the rate of change in the concentration of component A in the cylinder, resulting from: the forced movement of the air along the denuder (first term), longitudinal diffusion (second term), radial diffusion (third term), and a homogenous chemical reaction (fourth term).

It is obvious that the solution of the equation depends on the assumed initial conditions ($t = 0$) and boundary conditions with respect to x (from $x = 0$ to $x = L$, where L is the cylinder length) and r (from $r = 0$ to $r = R$). It should be noticed, that the case of $r = R$ should include any heterogenous chemical reaction between component A and the stationary phase material.

Besides the boundary conditions, additional assumptions [Katsanos 1995] have to be made to solve Eq(a) The first, and the most commonly used one, is the assumption that composition of the air does not change during its flow along the denuder, i.e. $\partial c_A / \partial x = 0$. Subsequently, one can omit, with satisfactory approximation, the second term of the equation, $D_A(\partial^2 c_A / \partial x^2)$, due to the fact that linear velocity of molecules of component A resulting from longitudinal diffusion is negligible compared with linear velocity of the air stream pumped through the denuder $\upsilon(\partial c_A / \partial x)$. Such a situation exists when the Peclet number, $2R\upsilon / D_A$, is greater than 10. The last approximation lies in assuming that no homogenous reactions occur in the denuder (the analytes neither are formed, nor they disappear), $r_A = 0$. Introducing these assumptions permits simplification of Eq.a to the form:

$$\frac{\partial c_A}{\partial t} = D_A\left(\frac{\partial^2 c_A}{\partial r^2} + \frac{1}{r}\frac{\partial c_A}{\partial r}\right) \qquad \text{(b)}$$

Further assumptions, such as component A is present in trace concentrations, the flow is laminar, the temperature is constant, and the amount of retained component A is mall when compared with the capacity of the stationary phase, lead to the best known Gormley-Kennedy (GK) solution [Gormley 1949]:

$$\frac{c_{av}}{c_0} = 0.819\exp(-14.63\Delta) + 0.0976\exp(-89.22\Delta) + 0.0325\exp(-227.8\Delta) + \cdots \qquad \text{(c)}$$

where:

c_{av} – average concentration of analyte A in the gas stream leaving the denuder;

c_0 – concentration of analyte A in the gas stream at denuder inlet;

Δ – equivalent length (dimensionless) given by equation:

$$\Delta = \frac{\pi}{4} \times \frac{D_A L}{V} \qquad \text{(d)}$$

where:

L – length of the cylinder [cm];

V – volume air flow rate [$cm^3 \cdot s^{-1}$] through the denuder, accounting for the actual conditions in the device.

Relations of equation (c) and (d) indicate that the effectiveness of a cylindrical denuder ($1-c_{av}/c_0$) increases with an increase in the length of the denuder and the diffusion coefficient of the compound in question and with a decrease in the gas flow rate.

Actually, equation c can be further simplified. Equation e is the approximation of the GK equation for gas molecules and particles smaller than 2 nm.

$$\frac{c_{av}}{c_0} = 0.819\exp(-14.63\Delta) + 0.0976\exp(-89.22\Delta) + 0.01896\exp(-212\Delta) \quad \text{(e)}$$

And for the larger particle (ca. > 0.2μm), the GK equation can be written:

$$\frac{c_{av}}{c_0} = 1 - 2.56\Delta^{2/3} + 1.2\Delta + 0.177\Delta^{4/3} \quad \text{(f)}$$

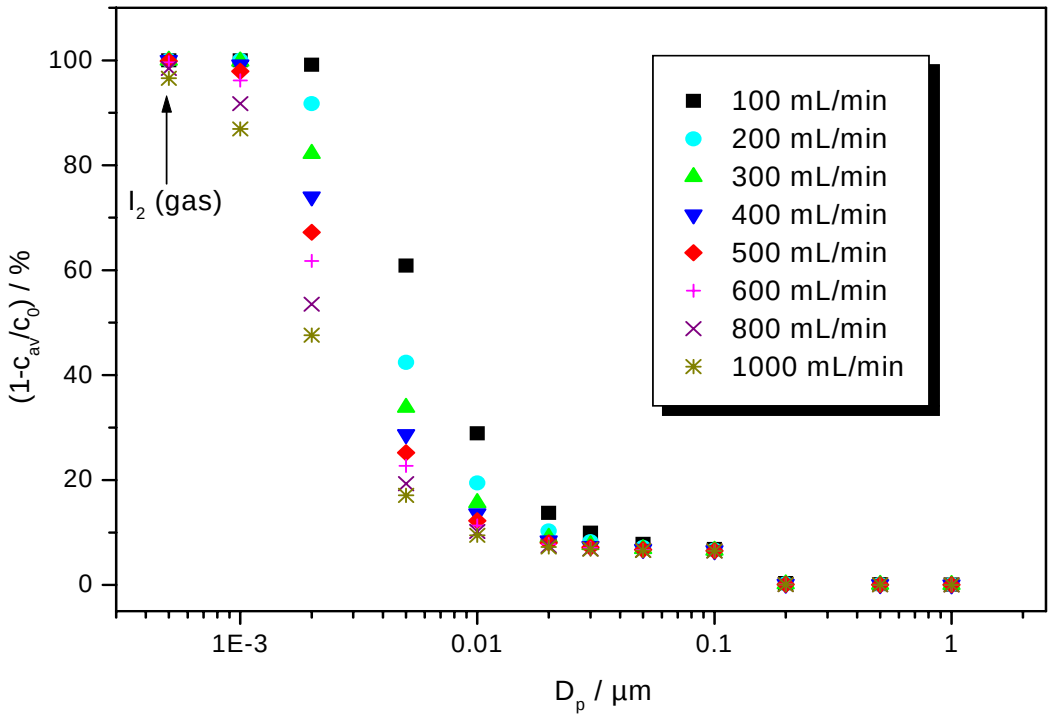

Figure 2-11 The collecting efficiency of a cylindrical denuder sampler ($Ø_i$ 6 mm × 50 cm) for gaseous I_2 and particles of different sizes at different sampling flow rate, based on the calculation of the Gormley-Kennedy equation (e and f).

To optimize the denuder sampling conditions, one can easily control the gas flow rate for a denuder of given inner diameter and length. For the sampling of gaseous elemental iodine, using a denuder with dimension of $Ø_i$ 6 mm × $Ø_o$ 9 mm × 50 cm, the effectiveness of the cylindrical denuder ($1-c_{av}/c_0$) is shown in Figure 2-11. Figure 2-11 indicates the efficiency of the gaseous separation from the particles of different sizes as well. As can be seen, at the listed sampling flow rate, nearly 100% of gaseous elemental iodine (as a sub-nanometer particle) can be collected to the inner-surface of the denuder, and more than 90 % of the particles greater than 10 nm can pass through the denuder without contacting to the denuder wall, while nearly 100% of particle bigger than 100 nm will freely escape from the denuder. Obviously, it is difficult to separate the gaseous molecules from nanometer-particles. To

optimize the sampling condition, 500 mL·min^{-1} was selected for the sampling flow rate for the denuder sampling in this work.

Starch/amylose used as chemisorption material

Based on the physical-chemical properties of the gaseous compounds of interest, denuder samplers have been designed widely [Kloskowski 2002] and efficiently [Fan 1996] for several different gaseous inorganic species, such as HNO_2 [Simon 1995], HNO_3 [Simon 1995, Taira 1993], NH_3 [Sioutas 1996, Slanina 2001], SO_2 [Simon 1993, Guo 2003, Rosman 2001], as well as volatile organic compounds like alcohols and ketones [Peskova 2001] and mono-terpene [Sklenska 2002] and semi-volatile organic compounds [Swartz 2003].

The specific reaction between iodine and starch, forming amylose-iodine (AI) or starch-iodine (SI) complex, has been known for more than a century [Hollemann 2001]. Recently, it was found that the AI complex can be synthesized without adding KI to the solution and its formation does not involve absorption of iodide ions. The dissociation mechanism provides additional support for the absence of iodide or polyiodide ion involvement with the complex. A minimum of 12 AGUs is needed to enclose the I_6 ($3I_2$) chromophore unit within the amylose helix cavity [Calabrese 1999, Rendleman 2003]. The structures of starch-amylose and AI complex are shown in Figure 2-12.

$$A + 3I_2 \Leftrightarrow AI - Complex$$

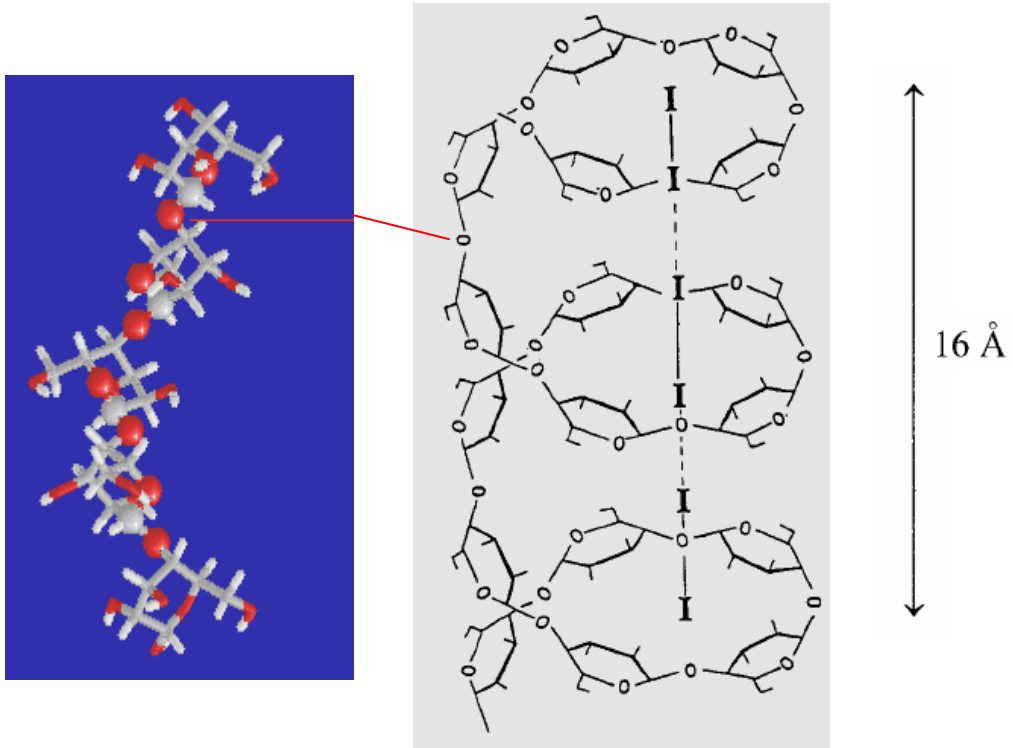

Figure 2-12 The schematic structure of starch-amylose (left) [Ophardt 2003] and AI complex (right) Left-handed amylose helix enclosing the chromophore of six iodine atoms ($3I_2$) within the cavity [Calabrese 1999]

Based on this specific reaction, starch/amylase can be use as the chemisorption material for the collection of elemental iodine at the inner surface of the cylindrical denuder sampler. That is, amylose coated at the inner wall of the denuder can rapidly react with I_2 forming the AI

complex, when elemental iodine diffuse and contact the coated surface of the denuder. However, it is novel and the first time to combine the denuder technique with this reaction for the determination of gaseous elemental iodine, therefore it is necessary to test the complete procedure of the methods such as the efficiency of collection.

Denuder preparation and sampling unit

Brown glass tubes ($Ø_i$ 6 mm × $Ø_o$ 9 mm × L 50 cm) used as denuders, were soaked in 5 % HNO_3 (Acros Organics) for 24 hours and washed with MilliQ water, then dried by pure nitrogen flushing through the denuders. Starch / ethanol solution of 2 mg·mL^{-1} was prepared from starch (in fine powder, Fluka) mixing with ethanol (99.8%, p.a., Carl Roth), for coating the inner surfaces of the denuders. In order to coat the starch powder uniformly to the inner-denuder walls, four times 0.5 mL coating-solution were slowly instilled onto the rotating denuder, simultaneously with N_2 flush at a flow rate of 0.5 L·min^{-1} for drying. TMAH ($\geq 95\%$, Fluka) and TBAH ($\geq 99\%$, Fluka) alcoholic solutions (2 mg·mL^{-1}) were also used as a test coating solution respectively. All prepared denuders were sealed with end PP-caps (Poly-Propene vessels, 1.5 mL, Roth) and ready for sampling.

The sampling unit for the denuder was built-up similarly as the one for VOIs (Figure 2-2), but with an additional filter to protect the membrane pump. The sampling flow rate was adjusted to 500 mL·min^{-1}.

2.2.2 Sample extraction and ICP/MS detection

Sample pretreatments

The iodine-amylose complex at the denuder inner walls was eluted and extracted with 4 mL of a TMAH-solution (aq. 5 % by weight) at 90 °C for 3 hours [Knapp 1998, Haldimann 2000]. TMAH is applied as the solvent not only for the extraction, but also for the purpose of reducing the memory effect of the measurement of iodine by ICP-MS [Al-Ammar 2001]. Howevre, due to the high matrix loading of TMAH which may produce carbon-black when oxidized in the plasma and to avoid blocking of any parts of the plasma sampling channel with the matrix, all samples were diluted to 1 % TMAH before introduced into the nebulizer and plasma. Tellurium (^{126}Te, 200 ng·mL^{-1} in the final sample solution, original standard solution from Merck KGaA, Darmstadt Germany) was added as internal standard for the ICP-MS measurements.

ICP-MS detection

ICP-MS is one of the few methods which are suitable and sensitive to detect trace amounts of iodine. It has been widely used for the trace analysis of iodine in food and biological samples [Gélinas 1998, Leiterer 2001]. Iodine measurements in the atmosphere, both in gaseous [Schwarz 2000] and particulate [Wimschneider 1995, Gaebler 1993] phase, applied the ICP-MS technique as well, such as IDMS (Isotope Dilution Mass Spectrometry).

Figure 2-13 shows an ICP-MS instrumental system, which was used in this work. Argon (4.6) is usually used as carrier gas and plasma gas. Liquid sample is first pumped and carried into the nebulizer, where the liquid is nebulized to aerosol and enters the spray chamber, then into the plasma torch. Ionization takes place when the sample goes through the plasma. Afterwards, ions are sampled into the vacuum chamber via the sampler and skimmer and finally separated and detected by the quadrupole mass spectrometer.

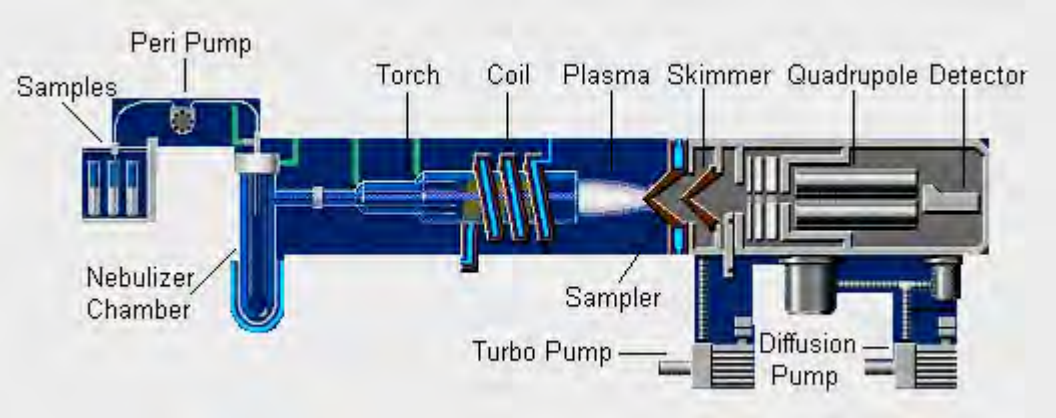

Figure 2-13 Schematic diagram of the ICP-MS system

Inductively Coupled Plasma

Inductively Coupled Plasma (ICP) source was originally developed as a superior excitation source for elemental analysis of solutions by atomic emission spectroscopy (AES) [Vestal 2001]. The plasma is sustained by RF (Radio Frequency) energy applied to the load coil. The electromagnetic field transfers energy from the coil to the plasma. Most of the energy is added to the outer, annular portion of the plasma inside the load coil. The sample traverses only the axial channel, which is heated by energy transferred from the outer, induction region. The physical separation of the sample from the region where the energy is added has important analytical implications. The sample composition can change substantially and have little effect on the electrical processes that sustain the plasma. Also, the absence of electrodes in physical contact with the ICP prevents contamination by sputtered electrode material.

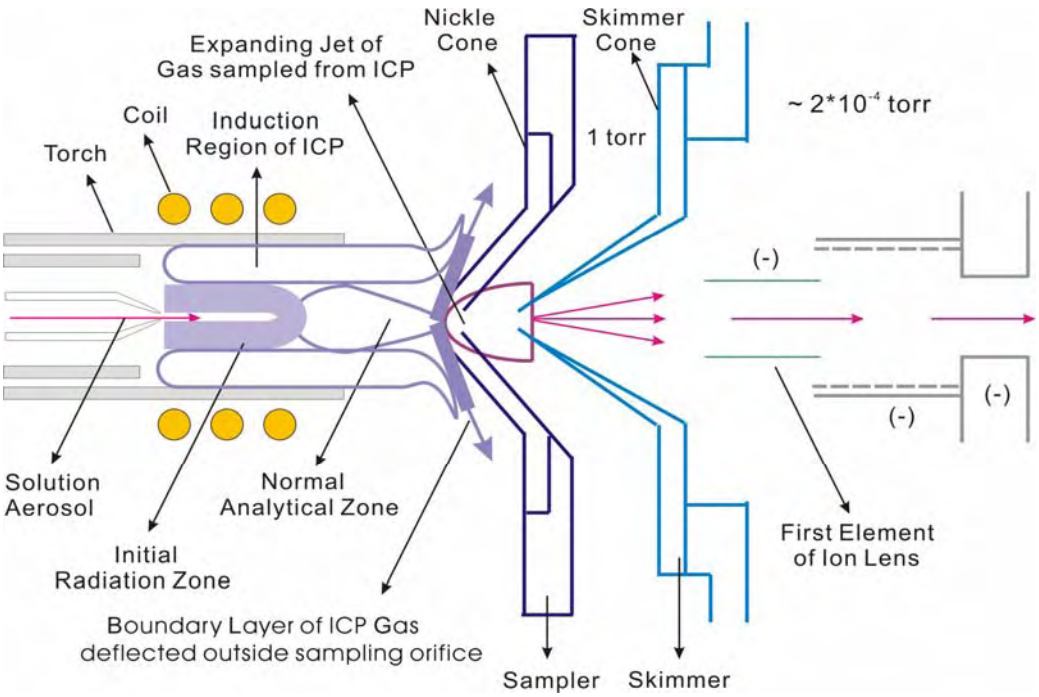

Figure 2-14 Schematic diagram of ICP ion source and sampling interface to a Quadrupole Mass Spectrometer [Houk1986, Vestal 2001]

The challenge with ICP-MS is to efficiently transfer ions from the plasma at atmospheric pressure and ca. 5000 K into the vacuum of the mass spectrometer. As shown in Figure 2-14, the plasma flows around the tip of a water-cooled metal cone. This cone has a circular orifice of ca. 0.5-1 mm in diameter at its tip. Gas from the ICP enters this orifice from a cross section of the axial channel which is approximately three times the orifice diameter; thus, a large fraction of the gas in the axial channel is sampled. The central orifice of a conical skimmer is located beyond the sampler at an appropriate distance to transmit as much of the sampled beam as possible into a second vacuum chamber without overloading the second vacuum system. The pressure here is low enough (ca. 10^{-5} Torr or less) so that ion lenses can be used to collect, focus, and transmit the ions to the mass analyzer with minimal losses by scattering.

ICP is a very efficient source for producing singly charged elemental ions. Positive ions have been detected for all of the naturally occurring elements except F, Ne, and He, all with ionization potentials greater than Ar used to form the plasma [Vestal 2001]. On theoretical grounds, some 54 elements are expected to be ionized with efficiencies of 90% or more, as well as for the halogens, especially for iodine.

Technical detail of ICP-MS operations

Two ICP-MS (PQ2 Turbo Plus, VG elemental, UK; and HP 4500, Agilent USA) instruments have been applied in this work. The operation conditions of the ICP-MS instruments are listed in Table 2-4.

Table 2-4 ICP-MS operating conditions

Instruments	Items	PQ2 Turbo Plus VG Elemental	HP 4500
Plasma	Forward Power	1350 W	1200 W
	Reflected Power	5 W	--
	Cool Gas Flow	14 L·min^{-1}	20 L·min^{-1}
	Auxiliary Gas Flow	2.0 L·min^{-1}	1.3 L·min^{-1}
	Nebulizer Gas Flow	0.96 L·min^{-1}	1.02 L·min^{-1}
Nebulization System	Nebulizer	Meinhard, Type A (Quartz)	Babington (Quartz)
	Spray Chamber	Cooled Double-pass Spray Chamber (Quartz) at 5°C	Cooled Double-pass Spray Chamber (Quartz) at 2 °C
	Peristaltic Pump	Gilson Minipuls 3	HP/Agilent
	Sample Uptake Rate	0.7 mL·min^{-1}	Peristaltic pump (0.2 rps)
Ion Sampling	Sampler	Ni, 1.0 mm	Ni, 1.0 mm
	Skimmer	Ni, 0.7 mm	Ni, 0.7 mm
	Sampling Depth	13 mm	7 mm
Acquisition Parameters	Masses	I 127, Te 126 as Internal Standard	I 127, Te 126 as Internal Standard
	Mode	Peak jumping	Peak jumping
	Points/Peak	3	3
	Dwell Time	40.96 ms, 10.24 ms	--
	Detection Mode	PC	PC/Spectrum
	Acquisition Time	10 s	3.73 s
	Replicates	5	5
Ion Lens Settings		Optimised on ^{127}I in 1% TMAH	Auto tuning

Standard solutions of iodine (0.1 % and 1 µg·mL^{-1} [I] aqueous solutions for store) were prepared from KIO_3 ($\geq 99.5\%$, p.a., Fluka, dried at 90 °C for 5 hours and stored in an exsiccator). Calibration curve range for the full quantification in use depends on the estimated iodine concentrations of the samples in interest, with the linear range of 0~8 ng·mL^{-1} in most cases but up to 50 ng·mL^{-1} for this work. All iodine standard solutions were prepared in 1 % TMAH, the same as for the sample solutions. Figure 2-15 shows an example for the calibration curve of the iodine analysis by ICP-MS.

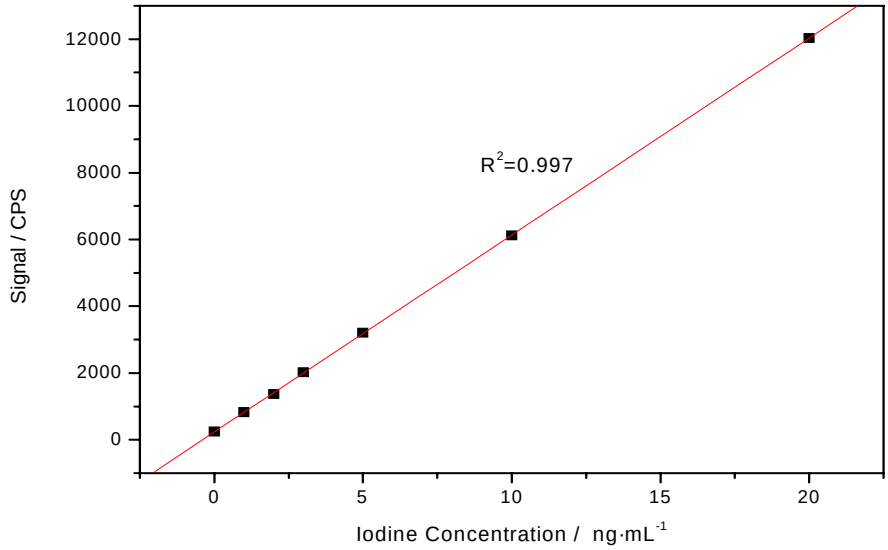

Figure 2-15 A calibration curve of iodine measurement by ICP-MS

The detection limit of iodine for the ICP-MS measurement was calculated from the standard deviations (10s) of the blank samples, in which 10 blank samples (1% TMAH aqueous solution with matrix) were measured. The detection limits of iodine using the developed method for the VG-PQ2 and HP-4500 instruments are respectively 0.077 ng·mL^{-1} (ppb) and 0.025 ng·mL^{-1} (ppb).

2.2.3 Results from the I_2 test gas

To test the denuder sampling technique, a gas source of I_2 was set up to be used as model air sample in the laboratory, which is similar to the test gas source of VOIs (Figure 2-3). Sublimation of solid iodine is influenced strongly by temperature. Using a thermostat and capillary diffusion reducer, nitrogen stream (0.5 L·min^{-1}) carrying vapor iodine with the mixing ratio of 480 ng·L^{-1} (~ 45 ppbv) was controlled at 20 °C. Iodine-containing gas was then sampled by the uncoated- and coated-denuders at the flow rate of 0.5 L·min^{-1} for 1~2 minutes.

In order to test the efficiency of the I_2 denuder sampling, a breakthrough experiment using a two-stage denuder (coupled denuders) was performed, shown in Figure 2-16. Uncoated denuders, Starch-, TMAH-, TBAH- coated denuders were applied in the experiments. Results are shown in Figure 2-17. As can be seen in Figure 2-17 a, more than 90 % molecular iodine can be absorbed or adsorbed by the starch, TMAH and TBAH coated denuders in the first denuder, while molecular iodine can not be collected by the uncoated denuders. For the starch-denuders the breakthrough of the I_2 into the second denuder is not more than 15 %,

hence a single denuder is efficient enough for the trace analysis of iodine in the atmosphere where the iodine concentrations are much smaller than those of the test gas source in the laboratory.

TMAH-denuders can collect CH_2I_2 with 95 % efficiency of the first denuder (Figure 2-17 b). In this case, TMAH or TBAH is not specific for sampling the molecular iodine, but collecting other iodine-containing species as well. The mechanism of the absorption or adsorption by TMAH and TBAH is not only due to their strong alkaline properties, but also the ability to form organic nitrogen-compounds with iodine, in which the large cation R_4N^+ can be polymeric with polyiodide (I_x^{n-1}) [Hon 1979]. Therefore, TMAH-coated denuders might be able to be used for total iodine sampling in the gas phase in the future. However, further experimental test has to be done for other iodine species.

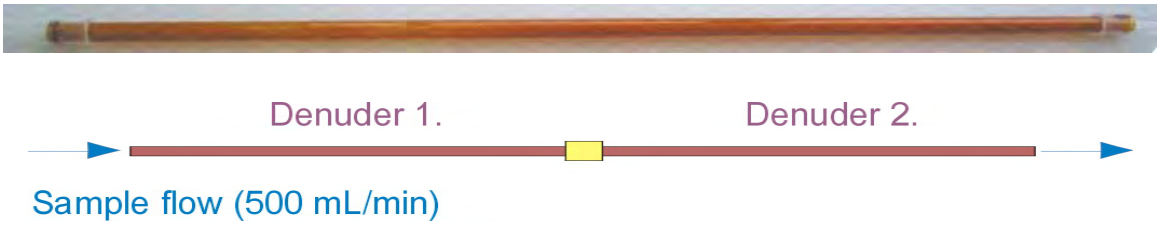

Figure 2-16 Breakthrough experiment for I_2, using 2-stage denuder sampling (bottom) and picture of a real denuder (above)

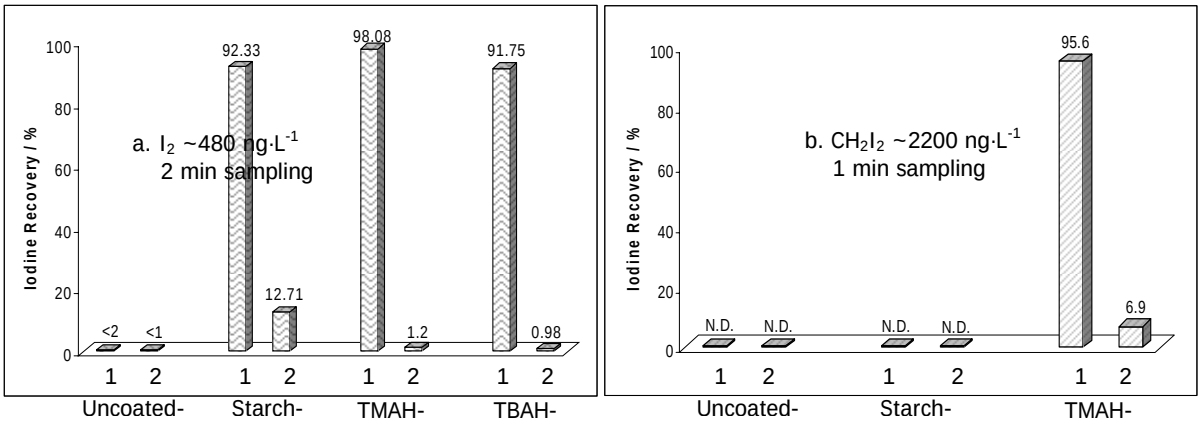

Figure 2-17 Recoveries of iodine sampling from I_2 (a.) and CH_2I_2 (b.) test gas source using different coating denuders at sampling flow of 500 mL·min^{-1} (N.D.=Not Detected)

For the sampling volume used for ambient air measurements (15 L), the determination limit (10 s) of gaseous elemental iodine using the sampling and detecting methods described above was estimated to be ~0.14 ng·L^{-1} (~12 pptv) for the VG-PQ2 instrument, and ~0.05 ng·L^{-1} (~4 pptv) for the HP-4500 instrument.

The adsorption tube sampling and TD-GC/MS measurements for the VOIs analysis in the gas phase of the coastal atmosphere has been used in both measurement campaigns at and around Mace Head Atmospheric Research Station (western coast Ireland). The denuder technique and ICP-MS detection method for the gaseous elemental iodine was applied only in the campaign in the “hotspot” area around Mace Head, i.e. BIOFLUX campaign in 2003. Results from the campaigns will be presented and discussed in Chapter 4.

3 Analytical Methods for the Measurement of Iodine Species in the Particle Phase

The iodine species in the particulate phase, as the end products of the process, are essentially important to understand the whole chain of iodine involved in the new particle formation in the coastal atmosphere. In this chapter, the analytical methodologies for the qualification and quantification of iodine species and total iodine in the particulate phase, was developed and improved, including PM2.5 (Particles smaller than 2.5 μm in diameter) and size-fractionated particles of the coastal atmosphere. Particle samples were collected at filters in a conventional filter holder (using a pre-separator for PM2.5) or foils in a 5-stage impactor (for size-fractionated particles). A water / TMAH extraction and anion-exchange separation procedure was applied for the sample pre-treatment in order to separate the iodine species in the solution, followed by the ICP-MS detection.

3.1 Sampling

The ability to collect representative samples for the analysis is an essential element in the study of aerosols. These samples must accurately reflect the airborne particles in concentration, size distribution, and the chemical composition. Filtration and impaction are the most commonly used sampling techniques.

3.1.1 Filter sampling for PM2.5

The capture of aerosol particles by filtration is the most common method of aerosol sampling. Filtration is a simple, versatile, convenient and economical way for collecting samples of aerosol particles. At low dust concentrations, fibrous filters are the most useful means for achieving high-efficiency of collection of sub-micrometer particles. The processing of the filtration is complicated and although general principles are well known there is still a gap between theory and experiment [Hinds 1999].

Mechanism and efficiency of filter sampling

The most important types of filters for aerosol sampling are fibrous and porous membrane filters. The membrane filters come in pore sizes of 0.01 – 10 μm, pore densities of 10^4 – 10^6 / mm^2, and solidities of 0.15 – 0.30. Figure 3-1 shows a structure of a porous membrane filter. The gas flow through the filter follows an irregular path through the complex pore structure. Particles are lost from the gas stream as they deposit on the structural elements that form the pores. Membrane filters have high efficiency and a greater resistance to air flow, pressure drop, than do other types of filters. But the mechanisms of collection and their region of application are the same as fibrous filters with the same properties. The high collection efficiency of porous membrane filters extends to aerosol particles much smaller than the manufacture's stated pore size. The most common material for such filters is cellulose ester, but other materials, such as polyvinyl chloride, nylon, PTFE, and sintered metals, also are commercially available.

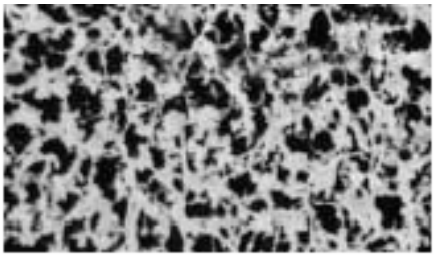

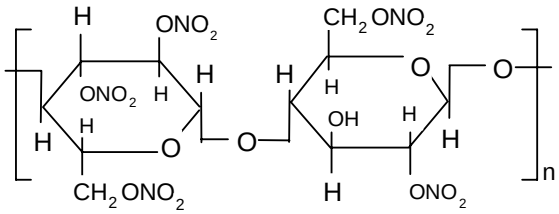

Figure 3-1 Scanning electron microscope photograph of a cellulose-nitrate membrane filter (ester) with a pore size of 0.45 µm (Sartorius AG, Goettingen Germany)

Here's an example for a fibrous filter to explain the mechanism and efficiencies of the filter sampling. There are five basic mechanisms by which an aerosol particle can be deposited onto a fiber in a filter [Hinds 1999]:

1. Interception
2. Inertial impaction
3. Diffusion
4. Gravitational settling
5. Electrostatic attraction

Collection by *interception* occurs when a particle follows a gas streamline that happens to come within one particle radius of the surface of a fiber. The particle hits the fiber and is captured because of its finite size. Thus, for a given size particle, certain streamlines will result in capture of the particle while other streamlines will not. For pure interception, it is assumed that the particles follow the streamlines perfectly; that is, they have negligible inertia, settling, and Brownian motion. Interception is the only mechanism that is not a result of a particle departing from its original gas streamline.

Inertial impaction of a particle on a fiber occurs when the particle, because of its inertia, is unable to adjust quickly enough to the abruptly changing streamlines near the fiber and crosses those streamlines to hit the fiber. The Brownian motion of small particles is sufficient to greatly enhance the probability of their hitting a fiber while traveling past t on non-intercepting streamline. This is a special case of *diffusion* to a surface, but important for the aerosol particle collection.

The *gravitational settling* is that the deposition due to the gravity, which is less important than impaction when the velocity of the air at the face of the filter (*face velocity*, U_0) is greater than 0.1 $m \cdot s^{-1}$. The remaining deposition mechanism, *electrostatic deposition*, can be extremely important, but is difficult to quantify because it requires knowing the charge on the particles and on the filter. Charged particles are attracted to oppositely charged fibers by coulombic attraction. A neutral particle can also be attracted to a charged fiber: the electric field created by the charged fiber induces a dipole, or charge separation, in the particle. And a charged particle can be attracted to a neutral fiber at close range by image forces.

The overall efficiency of a filter can be determinated by the following equation:

$$E = 1 - \exp\left(\frac{-4\alpha E_{\Sigma} t}{\pi d_f}\right)$$

Where:

E, is the overall efficiency of a filter;

α, is the volume fraction of fibers, so called packing density or solidity, $\alpha = 1 - porosity$, typically between 0.01 and 0.3;

t, is the thickness of the filter;

d_f, is the fiber diameter;

E_Σ, is the total single-fiber efficiency, which can be correctly combined by

$$E_\Sigma = 1 - (1 - E_R)(1 - E_I)(1 - E_D)(1 - E_{DR})(1 - E_G),$$

or approximately by $E_\Sigma \approx E_R + E_I + E_D + E_{DR} + E_G$;

where, E_R, E_I, E_D, E_{DR}, E_G are the single-fiber efficiencies for the mechanisms of particle capture: Interception, Impaction, Diffusion, Interception of Diffusion particles and Gravitational settling. There are some difficulties to calculate those efficiencies respectively due to the complicated and different mechanism. Actually, they are usually given by the empirical formulas obtained from the experiments.

Table 3-1 gives the single-fiber efficiency for each collection mechanism, for a filter having a thickness of 1 mm, a solidity α of 0.05, and a fiber diameter of 2 μm, operating at a face velocity of 0.1 m·s^{-1}. Figure 3-2 shows the total filter efficiency and the efficiency due to each of single-fiber mechanisms from Table 3-1. For this filter and face velocity, interception and impaction are negligible for small particles, but increase rapidly for particles larger than 0.3 μm. Diffusion is the only important mechanism for particle below 0.2 μm, but is of decreasing importance for particles above that size. For all particle sizes, gravity settling is small compared with other mechanisms. The collection of particles larger than 0.5 μm is governed by mechanisms that depend on the particle's aerodynamic diameter, but for particles smaller than 0.5 μm, collection is governed by mechanisms that depend on physical diameter.

Table 3-1 Single-fiber and total Efficiency for a filter having $t = 1mm$, $\alpha = 0.05$, $d_f = 2\mu m$, and $U_0 = 0.1m \cdot s^{-1}$

Particle Diameter / μm	Single-Fiber Efficiency						Overall Filter Efficiency / %
	E_R	E_I	E_D	E_{DR}	E_G	E_Σ	
0.01	0.000	0.000	0.840	0.020	0.000	0.861	100.0
0.02	0.000	0.000	0.339	0.016	0.000	0.356	100.0
0.05	0.001	0.000	0.106	0.013	0.000	0.119	97.7
0.1	0.003	0.000	0.046	0.011	0.000	0.059	84.9
0.2	0.010	0.002	0.021	0.010	0.000	0.043	74.3
0.5	0.055	0.034	0.009	0.009	0.000	0.108	96.8
1.0	0.183	0.238	0.005	0.010	0.001	0.437	100.0
2.0	0.550	0.887	0.003	0.011	0.003	1.454	100.0
5.0	1.965	3.500	0.002	0.012	0.027	3.500	100.0
10.0	4.585	6.000	0.001	0.014	0.183	6.000	100.0

Note: data are cited from [Hinds 1999]

The velocity of the air at the face of a filter, just before the air enters, is called the *face velocity*, U_0.

$$U_0 = \frac{Q}{A}$$

where Q is the volumetric flow rate through the filter and A is the cross-sectional area of the filter exposed to entering air-stream.

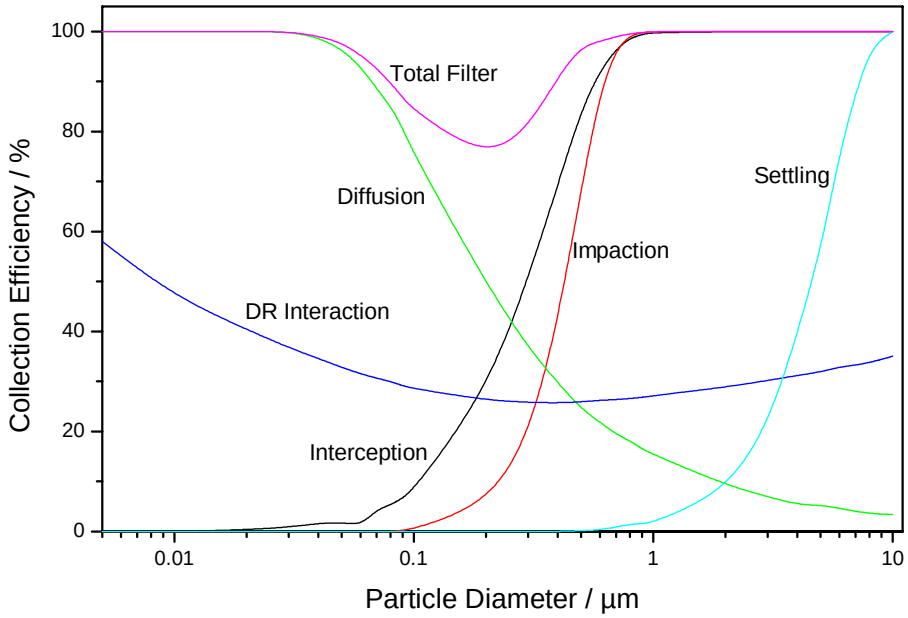

Figure 3-2 Filter efficiency for individual single-fiber mechanisms and total efficiency ($t = 1mm, \alpha = 0.05, d_f = 2\mu m$)

Figure 3-3 shows the effect of face velocity on filter efficiency as a function of particle size. Generally, decreasing face velocity increases efficiency for particle sizes close to the minimum efficiency. The particle size that gives the minimum efficiency, about 0.2 µm in Figure 3-2 and 3-3, is an in-between size that is too large for diffusion to be effective and too small for impaction or interception to be effective. Because these competing mechanisms are most effective in different size ranges, all filters have a particle size that gives minimum efficiency, usually in the range of 0.05 to 0.5 µm.

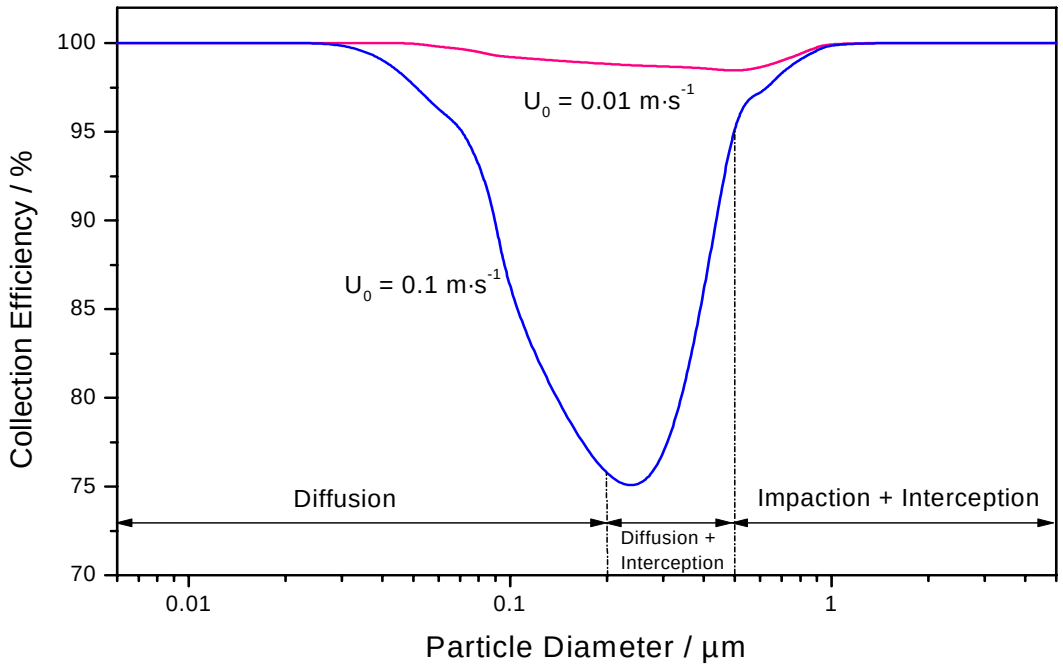

Figure 3-3 Filter efficiency versus particle size for a face velocities of 0.01 and 0.1 m·s^{-1} ($t = 1mm, \alpha = 0.05, d_f = 2\mu m$)

Cellulose nitrate is a standard material for membrane filters and offers a wide range of pore sizes from 8 µm to 0.45 µm. The cellulose-nitrate filters (membrane, pore size 0.45 µm, thickness 130 µm, ϕ = 37 mm and 70 mm, Sartorius AG, Goettingen, Germany) were selected to apply for the PM2.5 particle sampling in this work.

The filter holder sampler for PM2.5

The self-made sampling system is shown in Figure 3-4. In order to cut off the particles greater than 2.5 µm, a pre-separator was installed between the air inlet and the filter holder for the PM2.5 sampler. The pre-separator for PM2.5 was operated on the principle of impaction, which is discussed in section 3.1.2. All module units of the system were cleaned by HNO_3 (5 %) - ethanol (5 %) - water solution in a supersonic bath before brought to the sampling site for measurement sampling.

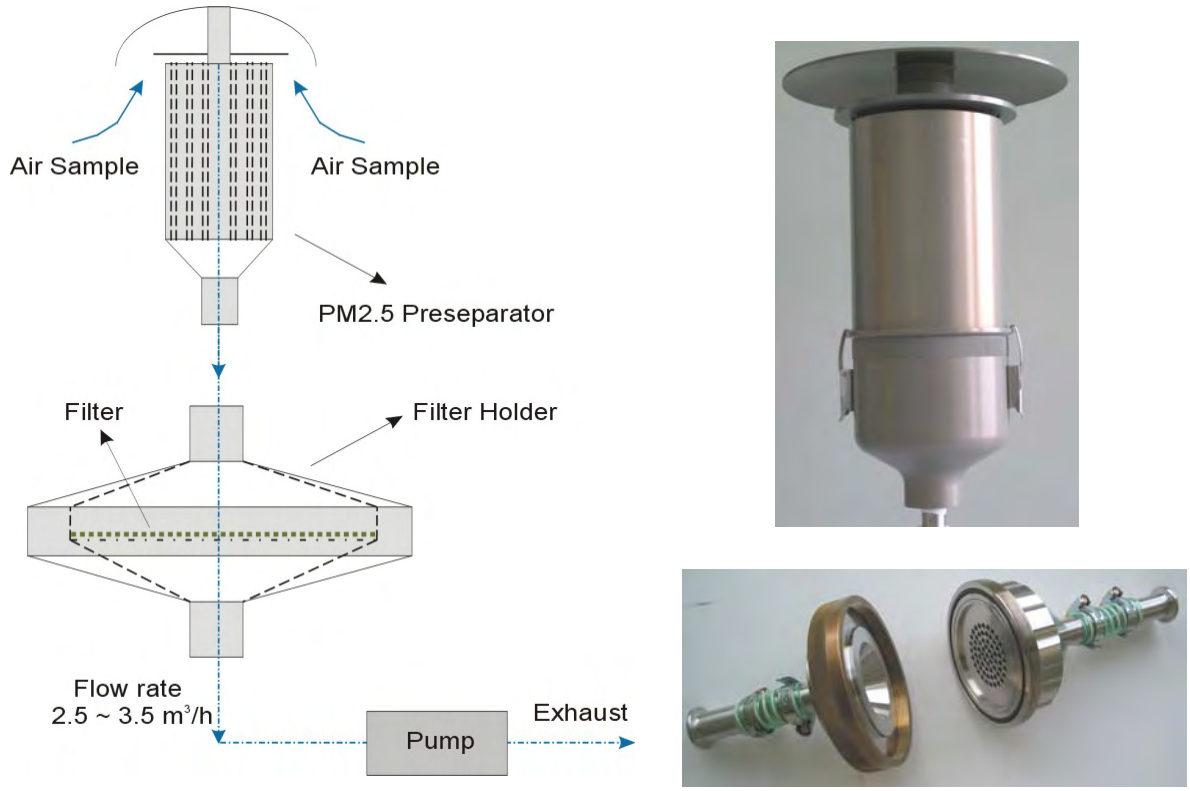

Figure 3-4 Schematic diagram of the PM2.5 filter sampler and picture of the components

By using a vacuum pump (Type TLV 15/12, 150 mbar, 0.58 kW) and split valve, the volumetric flow rate was adjusted to $Q \approx 2.5 \sim 3.5 m^3 \cdot h^{-1}$, with the cross-sectional area of the filter exposed to entering air-stream $A \approx 12 cm^2$, that is $U_0 \approx 0.58 \sim 0.81 m \cdot s^{-1}$.

3.1.2 Impactor for size-fractionated particle sampling

Impaction is a special case of curvilinear motion of aerosol particles that finds extensive application in the collection and measurement of airborne particles. Because of its importance, impaction has been investigated, theoretically and experimentally, more thoroughly than any other aerosol separation process. Therefore, many different types of impaction samplers (namely impactor) are widely used for in aerosol research.

Principle of impaction sampling

All inertial impactors operate on the same principle. As shown in Figure 3-5, an aerosol is passed through a nozzle and the output stream (jet) directed against a flat plate. The flat plate, called an impaction plate, deflects the flow to form an abrupt 90 ° bend in the streamlines. Particles whose inertia exceeds a certain value are unable to follow the streamlines and collide (impact) on the flat plate, assuming that particles stick to the surface if they hit it. Smaller particles can follow the streamlines and avoid hitting the impaction plate. They remain airborne and flow out of the impactor or into the next stage of the impactor where the impaction separates the smaller particle (so called cascade impactor). Thus, an impactor separates aerosol particles into two or more size ranges; particles larger than a certain aerodynamic size are removed from the air-stream, and those smaller than that size remain airborne and pass through the impactor.

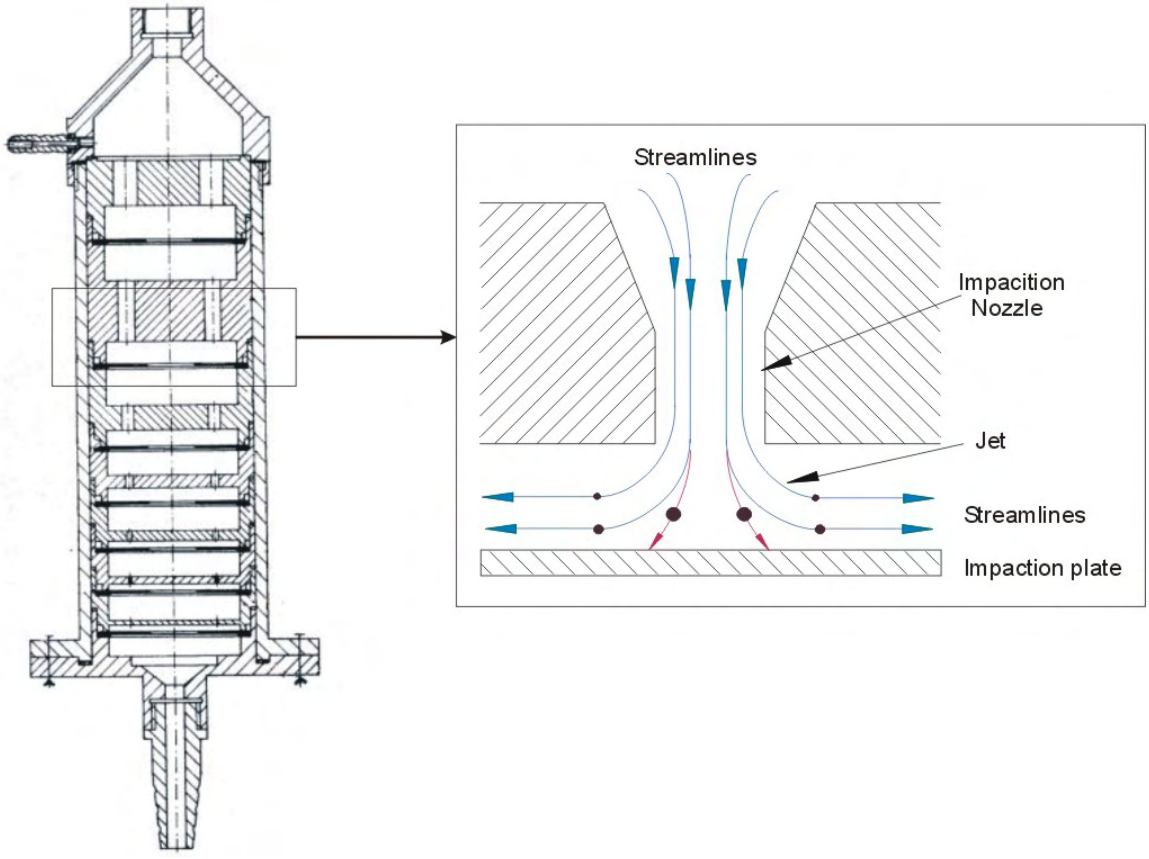

Figure 3-5 Schematic diagram of a cascade (stage)-impactor and the cross-sectional view of the single stage of the impaction

For most impactors, a complete curve of collection efficiency versus particle size is not necessary. Impactors that have a “sharp cutoff” curve approach the ideal (from the standpoint of particle size classification) step-function efficiency curve, in which all particles greater than a certain aerodynamic size are collected and all particles less than that size pass through. The size in question is called the *cutoff size*, *cutoff diameter* or d_{50}. As a practical matter, most well-designed impactor can be assumed to be ideal and their efficiency curves characterized by a single number Stk_{50}, the Stokes number that gives 50% collection efficiency [Hinds 1999].

Cascade impactors

The use of several impactors in parallel is, however, not common, because of the complexity of controlling multiple flow rates. The more common approach is to operate several impactors in series, arranged in order of decreasing cutoff size with the largest cutoff size first. This configuration is called a cascade impactor. Each separate impactor is called an impactor stage, as shown in Figure 3-5. The cutoff size is reduced at each stage by decreasing the nozzle size. Since the same volume of gas flows through each stage, only one flow needs to be controlled. Each stage is fitted with a removable impaction plate for gravimetric or chemical characterisation of the collected particles. The last stage in a cascade impactor is usually followed by a filter that captures all particles less than the cutoff size of that stage.

In its operation, each stage is assumed to capture all particles reaching it that are larger than its cutoff size. Because the aerosol flows in sequence through successive stages, the particles captured on the impaction plate of a given stage represent all particles smaller than the cutoff size of the previous stage and larger than the cutoff size of the given stage. The sequential separation divides the entire distribution of particles into a series of contiguous groups according to their aerodynamic diameters. From the gravimetric measurements of each stage, the fraction of the total mass in each aerodynamic size range can be determined.

The berner impactor

A 5-stage cascade impactor, namely berner-impactor (Firma Dr. Eberhard Steinweg, Grebenhain, Germany), with fractionated sizes: 0.085 ~ 0.25, 0.25 ~ 0.71, 0.71 ~ 2.0, 2.0 ~ 5.9, 5.9 ~ 10.0 µm (D_{50} /µm: 10.0, 5.9, 2.0, 0.71, 0.25, 0.085), was used for the size-fractionated particle sampling in the field campaign of this work. Figure 3-6 shows the picture of the berner-impactor (made of steel). All subassemblies of the impactor were cleaned by HNO_3 (5 %) - ethanol (5 %) -water solution in a supersonic bath before brought to the sampling site for measurement sampling. The sampling flow rate of the berner-impactor was fixed to 4.2 ~ 4.5 $m^3 \cdot h^{-1}$ by using the vacuum pump (AEG, Type AM 90 LX4, 1.25 kW, Busch GmbH, Germany).

Figure 3-6 Picture of the 5-stage berner-impactor

PVF Tedlar®-foils (PolyVinyl Fluoride, Firma Dr. Eberhard Steinweg, Grebenhain, Germany) and cellulose-nitrate-filter foils (self-cut from the original filters $\phi = 120mm$, Sartorius AG, Goettingen, Germany) were used as the impaction plate for each stage. The annular foils (size: $\phi_o = 78mm$, $\phi_i = 40mm$) were placed in each impaction stage, on which particles were collected for the iodine measurements.

3.2 Sample pretreatments

3.2.1 Total iodine

The treatment of aerosol impacted filters and tedlar-foils is schematically shown in Figure 3-7, including the total iodine and iodine species. For total iodine or non-water soluble iodine species, TMAH was applied for the extraction process [Rädlinger 1998, Fecher 1998, Knapp 1998, Haldimann 2000]. TMAH and its aqueous solution is a strong alkaline reagent. For the preparation of analytical samples it is very effective for trace analysis of elements that are liable to become volatile with acid-digestion. In addition, compared to conventional alkaline digestions using NaOH or KOH, the use of TMAH enables more accurate determination due to its smaller matrix effects.

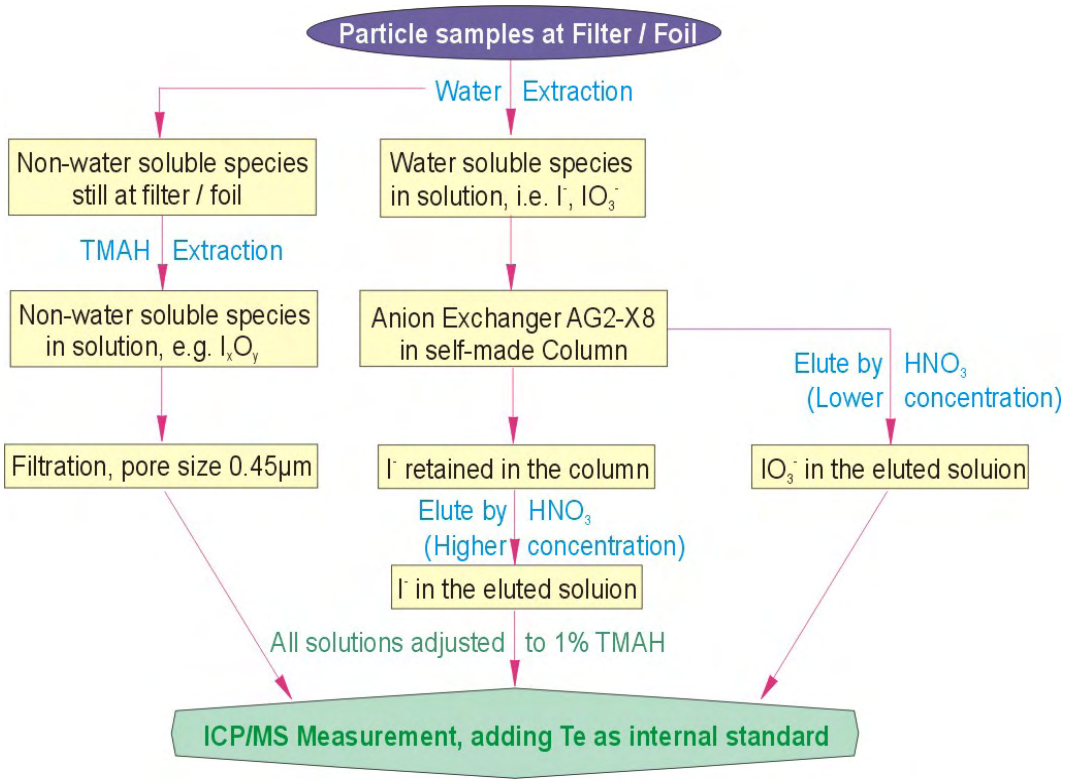

Figure 3-7 Sample treatment procedure for iodine and its species in the aerosol sample

Optimization experiments of the extraction conditions, such as TMAH concentration, extraction time and temperature, have been done, i.e. the orthogonal test (Results are presented in the following section 3.4.1). Following the optimized extraction conditions, 2 mL TMAH aqueous solution (10 % by weight) was added to the filter or foil sample contained in

a 50 mL poly-propene vial. Then the vial was put into an oven at a temperature of 90 °C. The extraction regularly lasted for 3 hours.

The cellulose-nitrate filters are decomposed in the TMAH solution during the extraction process, which avoids any loss of iodine species due to a non-ideal extraction step. Since the tedlar foils are not decomposed, thus to avoid the loss of analytes, a shaking procedure was necessary. However, an additional filtration step is necessary to remove remaining particles in the sample after the TMAH extraction, especially for the cellulose-nitrate-filter samples, in order to avoid any blocking of the channels of the detection instruments, such as ICP torch, sampler and skimmer. Two types of membrane-filters (pore size 5 µm and 0.45 µm, ϕ = 26 mm, filtration area 5.3 cm^2; Minisart®, Sartorius AG, Goettingen, Germany) were used for two-step particle filtration before the ICP-MS measurements. Finally, all the sample solutions were diluted to 1 % TMAH and Tellurium (^{126}Te, 200 $ng \cdot mL^{-1}$, also see section 2.2.2) added as internal standard for the ICP-MS measurements.

3.2.2 Iodine species

For the analysis of water soluble iodine species, an ion exchange technique [Wimschneider 1995, Hou 1999] was used to separate iodate (IO_3^-) and iodide (I^-), followed by the ICP-MS, as shown in Figure 3-7 as well.

Ion exchange reaction

Ion exchange is a reversible chemical reaction wherein an ion from solution is exchanged for a similarly charged ion attached to an immobile solid particle. These solid ion exchange particles are either naturally occurring inorganic zeolites or synthetically produced organic resins. The synthetic organic resins are the predominant type used nowadays because their characteristics can be tailored to specific applications. An organic ion exchange resin is composed of high-molecular-weight polyelectrolytes that can exchange their mobile ions for ions of similar charge from the surrounding medium. The following reaction shows an example for a cation-exchange process.

$$nR - SO_3^- H^+ + M^{n+} \Leftrightarrow (R - SO_3^-)_n M^{n+} + nH^+$$

R denotes the organic portion of the resin and SO_3^- is the immobile portion of the ion active group. M^{n+} is a metal ion with +n charges. As shown, the ion exchanger reaction is reversible. The degree the reaction proceeds to the right will depend on the resins preference, or selectivity for the metal ions compared with its preference for hydrogen ions. The selectivity of a resin for a given ion is measured by the selectivity coefficient K, which in its simplest from for the reaction:

$$R - A^+ + B^+ \Leftrightarrow R - B^+ + A^+$$

is expressed as:

$$K = \frac{[B^+]_{Resin}}{[A^+]_{Resin}} \times \frac{[A^+]_{Solution}}{[B^+]_{Solution}}$$

The selectivity coefficient expresses the relative distribution of the ions when a resin in the A^+ form is placed in a solution containing B^+ ions. It should be pointed out that the selectivity coefficient is not constant but varies with changes in the solution conditions. It does provide a means of determining what to expect when various ions are involved.

The anion-exchange resin

Ion exchange resins are classified as cation exchangers, which have positively charged mobile ions available for exchange and anion exchangers, whose exchangeable ions are negatively charged. Both anion and cation resins are produced from the same basic organic polymers. They differ in the ionizable group attached to the hydrocarbon network. It is this functional group that determines the chemical behavior of the resin. Each resin has a distinct number of mobile ion sites that set the maximum quantity of exchanges per unit of resin. Resins can be broadly classified as strong or weak acid cation exchangers or strong or weak base anion exchangers.

Table 3-2 Technical details of the AG1 and AG2 resins

Resin Type	Active Group	Thermal Stability	Solvent Stability	Resistance to Oxidizing Agents
AG1	$R\text{-}CH_2N^+(CH_3)_3$	OH^- form, fair to 50 °C; Cl^- and other forms, good to 150 °C	Very good	Slow sultion in hot 15 % HNO_3 or conc. H_2O_2
AG2	$R\text{-}CH_2N^+(CH_3)_2C_2H_4OH$	OH^- form, fair to 30 °C; Cl^- form, good to 150 °C	Very good	Slow sultion in hot 15 % HNO_3 or conc. H_2O_2

From *AG® 1, AG MP-1 and AG 2 Strong Anion Exchange Resin Instruction Manual* [1]

Two types of resin have been tested for the separation of iodate and iodide in this work. AG1-X4 and AG2-X8 resins (both in chloride form, Bio-Rad Laboratories, CA, USA) were selected to apply. AG1 and AG2 resins are strongly basic anion exchangers with quaternary ammonium functional groups attached to the styrene divinylbenzene copolymer lattice (Table 3-2 shows some technical details.). The amount of resin crosslinkage determines the bead pore size. A resin with a lower percentage of crosslinkage has a more open structure permeable to higher molecular weight substances than a highly crosslinked resin. It also has a lower physical resistance to shrinking and swelling, so that it absorbs more water and swells to a larger wet diameter than a highly crosslinked resin of equivalent dry diameter. For example, the lower crosslinked resins, particularly AG1-X2 2% crosslinked resin, are useful for the sorption and fractionation of relatively high molecular weight substances such as peptides, ribo- and deoxyribonucleotides and uranium. The higher crosslinked resins, particularly AG1-X8 8% crosslinked resin, are used for sorption, exchange, and separation of low molecular weight inorganic anions [1].

In the chloride form of AG1 and AG2 resin, the counter-ion on the resin is Cl^-. A resin can be converted from one ionic form to another. Usually the resin is used in an ionic form with a lower selectivity for the functional group than the sample ions to be exchanged. The sample ions are then exchanged onto the resin when introduced and can be eluted by introducing an ion with higher affinity for the resin or a high concentration of an ion with equivalent or lower affinity. Table 3-3 shows the relative selectivity of various counterions. In general, the lower the selectivity of the counterion, the more readily it exchanges for another ion of like charge. The order of selectivity can also be used to estimate the effectiveness for different ions as eluants, with the most highly selective being the most efficient. Finally, the order of

selectivity can be used to estimate the difficulty of converting the resin from one form to another. Conversion from a highly selected to a less highly selected form requires an excess of the new ion.

Table 3-3 Relative selectivity of various counter-ions [1]

Counter-ion	Relative Selectivity for AG1 Resin	Relative Selectivity for AG2 Resin
OH^-	1.0	1.0
Benzene Sulfonate	500	75
Salicylate	450	75
Citrate	220	23
I^-	175	17
Phenate	110	27
HSO_4^-	85	15
ClO_3^-	74	12
NO_3^-	65	8
Br^-	50	6
CN^-	28	3
HSO_3^-	27	3
BrO_3^-	27	3
NO_2^-	24	3
Cl^-	22	2.3
HCO_3^-	6.0	1.2
IO_3^-	5.5	0.5
HPO_4^-	5.0	0.5
Formate	4.6	0.5
Acetate	3.2	0.5
Propionate	2.6	0.3
F^-	1.6	0.3

Due to the big difference of the relative selectivities of iodide and iodate in the resin ($I^- / IO_3^- > 30$), there is a high possibility to separate the two ions using these AG resins. For instance, firstly, AG2-X8 in Cl^- form can be easily converted to NO_3^- form using 0.1 ~ 1 M HNO_3:

$$R-CH_2N^+(CH_3)_2C_2H_4OH-Cl^- + NO_3^- \rightarrow R-CH_2N^+(CH_3)_2C_2H_4OH-NO_3^- + Cl^-.$$

Then, when the aqueous solution containing iodate and iodide elute through the resin particles, they will be bounded to the function group:

$$R-CH_2N^+(CH_3)_2C_2H_4OH-NO_3^- + I^- \rightarrow R-CH_2N^+(CH_3)_2C_2H_4OH-I^- + NO_3^-$$

$$R-CH_2N^+(CH_3)_2C_2H_4OH-NO_3^- + IO_3^- \rightarrow R-CH_2N^+(CH_3)_2C_2H_4OH-IO_3^- + NO_3^-$$

Afterwards, when an excess of new NO_3^- ions elute the resin, the bounded IO_3^- would be eluted by less concentrated HNO_3 (e.g. 0.005 M) and I^- would be eluted by a higher concentrated NO_3^- (e.g. 0.3 M).That is the process that might be able to separate iodate and iodide in the aqueous solution after the water extraction of the particle samples.

Column method of anion exchanger

Column method involves pouring a column with the resin and passing the sample through to achieve the separation. Particle size will determinate the flow rate, which will affect the separation. The resin should be in the correct ionic form and equilibrated prior to the adding of the sample. For the separation of trace amounts of iodide and iodate in this work, flow rate of 1.0~1.5 mL/min was chosen [Bio-Rad and Hou 2000]. Some properties of the resin in use are shown in Table 3-4.

Table 3-4 Properties of the resin applied for the column separation

Resin	Ionic Form	Dry Mesh Size	Particle Diameter / μm	Capacity / meq/mL	Density / gm/mL
AG1-X4	Chloride	100~200	106~250	1.0	0.70
AG2-X8	Chloride	100~200	90~250	1.2	0.75

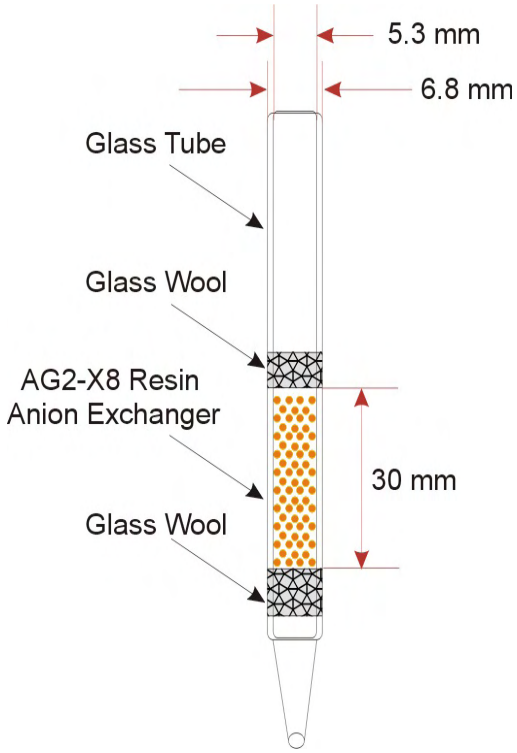

Figure 3-8 Schematic diagram of the anion exchanger column

A certain amount of AG1-X4 or AG2-X8 resin was soaked in de-ionized water for 24 hours and the resin slurry was packed in a glass column of i.d. 5.3 mm and 30 mm length and fixed by glass wool plugs (Figure 3-8) [Hou 2000]. To purify the resin in the self-made column, 15 mL de-ionized water was used to wash the packed column, followed by 10 mL HNO_3 (1 M) and 15 mL de-ionized water. The iodate / iodide separation procedure is shown in Figure 3-7. 10 mL HNO_3 of low concentration (e.g. 0.008 M) was used to elute the iodate bound to the resin in the column, and 15 mL HNO_3 of higher concentration (e.g. 0.3 M) was used for iodide. TMAH was added to all samples after the separation procedure, in order to reduce the memory effect iodine in the ICP-MS system. In order to reduce the matrix effects for the ICP-MS measurement, pH values were adjusted to 10~12 in all samples, that is about 1 % TMAH

in the final solutions. 200 ppb (equal to "ng·mL^{-1}" in aqueous solution) Tellurium (^{126}Te) was added as the internal standard for the ICP-MS measurements. Optimization of the elution conditions will be discussed in the following section.

3.3 ICP/MS detection

The prepared sample solutions were measured by the ICP/MS instrumentation. All the operation details of the ICP/MS detection for particulate iodine species were exactly the same as for the gaseous elemental iodine measurements following the denuder sampling technique. All technical details are described as Table 2-4 in section 2.2.2 Chapter 2.

3.4 Results of the test measurements

3.4.1 Iodine blank of the sampling materials

First of all, the iodine blanks of all the sampling materials, including cellulose-nitrate filters and foils as well as Tedlar®-foils were checked, in order to confirm that they are clean enough and suitable for iodine measurements of the particulate phase.

For the cellulose-nitrate materials, less than 1 ng iodine was found in each unit by using the TMAH and water extraction procedure as described in the previous section 3.2.1. This indicates that the cellulose-nitrate filters or foils can be securely applied for the particle sampling in combination with the iodine measurements. However, aiming at the more accurate results for the trace analysis, subtraction of the blank from the filter and the sampling system is always strongly recommended. Additionally, analytical results of 10 random cellulose-nitrate filters blank samples showed that the standard deviation (s) was 0.00769 ng·mL^{-1}, hence the detection limit of iodine using the VG PQ2 ICP-MS system can be estimated as 0.077 ng·mL^{-1} (10 times of s).

Tedlar®-foil was found to be not an ideal sampling material for size resolved iodine measurement in atmospheric particles [Chen 2003]. Tedlar®-foils without any particle sample were put in the 50 mL poly-propene vial, and extracted by 2 mL TMAH (10% by weight) for 3 hours at 90 °C in the oven. The amount of the iodine found in a single foil was observed by ICP-MS to be in the range of 16.6 ~ 28.9 ng, from the random 8 foils blank samples, with the average amount of about 22.0 ng. Moreover it was found that more iodine was extracted by TMAH when the extraction temperature was increased (e.g. 100 °C, up to 120 °C), indicating that the iodine can be extracted from the PVF material in which iodine species might be involved during manufacturing. However, there was not any iodine found in the Tedlar®-Foil by the TMAH extraction at lower temperatures (e.g. room temperature) or after water extraction. Hence, Tedlar®-Foils can still be used for impactor particle sampling with the purpose of measuring the water-soluble iodine species when water is used for the extraction at low temperatures. For the total iodine measurements in the fractionated particles in the Berner-impactor, cellulose-nitrate foils could be the ideal material. Tedlar®-Foils were still used in both field measuring campaign but only with the extraction at low temperature. Cellulose-nitrate foils were used only in the BIOFLUX campaign for the total iodine extraction at higher temperatures.

3.4.2 Optimization of the TMAH extraction

In order to optimise the extraction conditions, including the TMAH concentration (10%, 15%, 20% and 25%), extraction temperature (70°C, 80°C, 90°C and 100°C) and time (2h, 3h, 4h and 5h), a 3-factor-4-level ($L_{16}(4^3)$) orthogonal test was carried out. Orthogonal tests are commonly used methods for the optimization for scientific operation conditions. Lacking of reference standard samples for particulate iodine, 100 ng I (in KIO_3, aqueous solution) was added to the cellulose-nitrate filters to produce test samples.

Table 3-4 $L_{16}(4^3)$ orthogonal test table for the TMAH extraction optimisation

Exp.No.		c(TMAH) / %	Temp.(Ex.) / °C	Time(Ex.) / h	Iodine found / ng	Recovery / %
1		10	70	2	93.08	93.08
2		10	80	3	93.46	93.46
3		10	90	4	92.78	92.78
4		10	100	5	93.34	93.34
5		15	70	3	93.84	93.84
6		15	80	2	90.00	90.00
7		15	90	5	96.96	96.96
8		15	100	4	75.27	75.27
9		20	70	4	93.80	93.80
10		20	80	5	66.64	66.64
11		20	90	2	93.52	93.52
12		20	100	3	74.36	74.36
13		25	70	5	94.25	94.25
14		25	80	4	93.25	93.25
15		25	90	3	89.90	89.90
16		25	100	2	94.10	94.10
Data Analysis	L_1	93.16	93.74	92.68	Calculation example for L_i: L_1 (c(TMAH)) = Average of the 4 results from 10% TMAH L_3 (Temp.) = Average of the 4 results from 90 °C	
	L_2	89.02	85.84	87.89		
	L_3	82.08	93.29	88.78		
	L_4	92.88	84.27	87.80		
	Max-Min	11.08	9.48	4.88		
	s	8.94	8.54	3.99		

Note: Calculation for Max-Min and standard deviation s

e.g. for "c(TMAH)" column, calculate from L_1 to L_4 (93.16, 89.02, 82.08, 92.88)

$$Max - Min = 93.16 - 82.08 = 11.08$$

$$s = \sqrt{\frac{\sum \left(L_i - \bar{L}\right)^2}{n-1}} = \sqrt{\frac{(93.16 - 89.285)^2 + (89.02 - 89.285)^2 + \cdots}{4-1}} = 8.94$$

And, thus the same calculation for the "Temp. (Ex.)" and "Time (Ex.)" columns.

In this 3-factor-4-level test table, 16 experiments are needed to be completed, using the combined extraction conditions (Table 3-4) and measured by ICP-MS. Recoveries are calculated from iodine detected after extraction from the filters, divided by the original iodine added. Table 3-4 shows the results of the orthogonal test for optimisation of TMAH extraction conditions. The primary goal of the orthogonal test is to find out the most important factor that affects the extraction efficiency, high recovery in this case. “The most important factor”, which has more effect to the extraction efficiency, mathematically shows a bigger value of extreme deviation (Max-Min) or “standard deviation” (s).

As can be seen from the data analysis results, concentration of TMAH is the most important factor in this procedure, with Max-Min=11.08 and s=8.94. However, comparing the concentration of TMAH and the extraction temperature, there is no significant difference between their standard deviations (s = 8.94, 8.54). And the extraction time of 2 to 5 hours makes not much effect to the extraction efficiency comparing to the other 2 extraction conditions. Considering the determination sensitivity (all samples will be diluted to final c(TMAH) = 1%), condition of 10 % TMAH, 90°C and 3 h was selected for the iodine extraction.

3.4.3 Test results of water-soluble iodine species

100 ng iodate (as Iodine from KIO_3) and 100 ng iodide (as Iodine from KI) were mixed in a aqueous solution of 10 mL, which was used as the model sample for the separation using the anion-exchanger column method: AG1-X4 and AG2-X8 resins.

AG1-X4 resin

The test experiment using AG1-X4 resin shows unsatisfactory results for the iodate and iodide separation. Recoveries of each component could not reach 70 %, particularly for the iodide ions, regardless the concentration and volume of the HNO_3 elutant. The reason of the failure might be that the chemical bonding of iodate and iodine ions to the resin materials is too strong for the NO_3^- ions to elute the bonded ions from the active function group (R-$CH_2N^+(CH_3)_3$) of the anion exchanger. Further experiments were performed to improve the method, such as oxidation of iodide to iodate by ClO^- ions. However, these conditions made the matrix more and more complicated with negative effects for the ICP-MS measurements without a noticeable improvement of the separation performance.

AG2-X8 resin

Different volumes and concentrations of HNO_3 were applied as the elutant (i.e. 10 mL 0.008 ~ 0.025 mol·L^{-1} HNO_3 for iodate, and 3 ~ 20 mL 0.30 ~ 1.0 mol·L^{-1} HNO_3 for iodide) for the anion-exchanger column method, with the eluting flow rate of 1.0~1.5 mL/min. The results of test experiments for the separation efficiencies indicated by the recoveries of each component are shown in Figure 3-9.

As can be seen in Figure 3-9, using different concentrations and volumes of HNO_3 for the elution through the resin column, iodate and iodide could be separated successively in some experiments. For iodate elution, HNO_3 concentration of 0.008 ~ 0.025 mol·L^{-1} are suitable, but with the optimized volumes of HNO_3 (10 mL was usually applied in this case). For the iodide elution, HNO_3 concentrations higher than 0.30 mol·L^{-1} are essentially necessary due to the stronger bonding of the iodide to the resin. After the optimization, eluting conditions that

using 10 mL / 0.008 mol·L^{-1} HNO_3 for iodate and 15 mL / 0.30 mol·L^{-1} HNO_3 for iodide were selected, which obtain the recovery of both iodine species more than 93 % in the experiment.

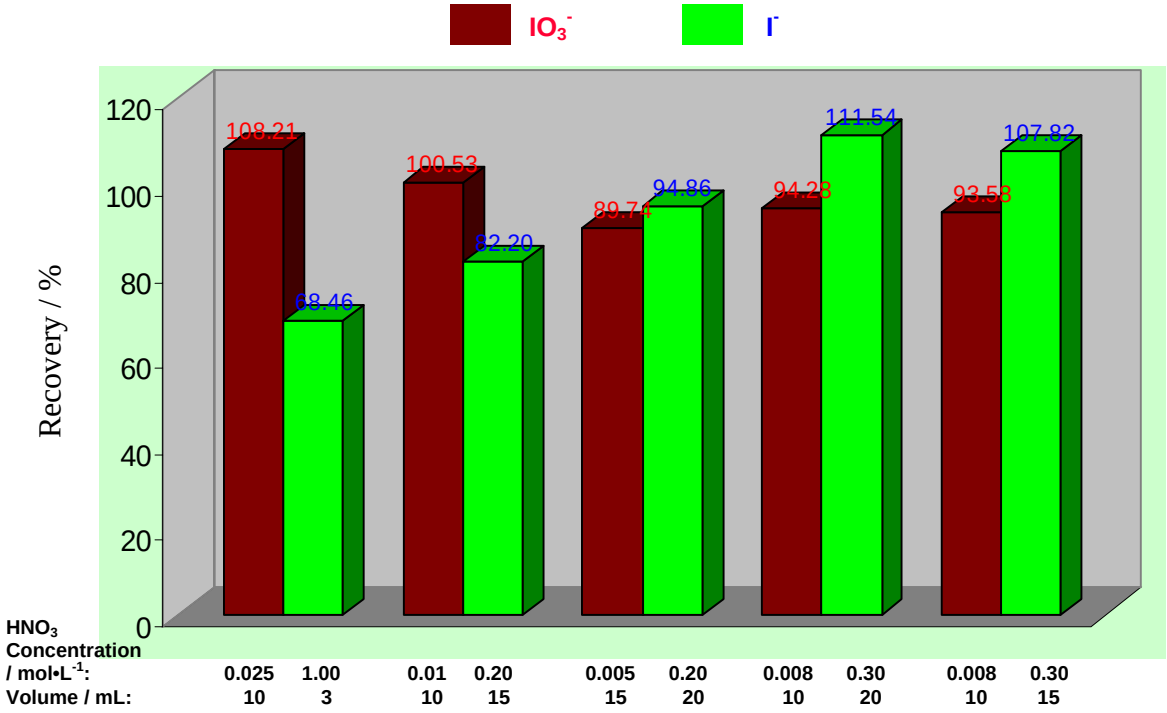

Figure 3-9 Separation results of iodate/iodide using the anion-exchanger column method of AG2-X8, 100 ng IO_3^- + 100 ng I^- in 10 mL aqueous solution used as test samples. The pH values were adjusted to 10~12 in all samples by adding about 1 % TMAH in the final measuring solutions, in order to reduce the memory effects of the iodine in the ICP-MS system. Tellurium was added as the internal standard for the measurements to reduce the deviation due to the instrumental fluctuation (also see section 3.2.2).

Additionally, there is a possibility of the water-soluble iodine species separation and analysis by using Ion Chromatrography (IC) coupling with UV-VIS spectrometry [Bichsel 1999] or ICP-MS [Leiterer 2001]. Certainly, there are at least two advantages by using this technique: (1) Quick separation and direct measuring by the coupling instrumentation; (2) The "complete" separation of the species can be seen directly by the "online" simultaneous detection, telling whether the bonded components are fully eluted from the column. Similarly, previous work done by Diemer et.al, indicated that Bromate/Bromide could be separated and measured by the IC-ICP/MS method [Diemer 1997].

Some additional experiments have been performed using the IC-ICP/MS method to separate the iodate and iodide. Iodate ions can be easily eluted from the column and detected by the mass spectrometer as a clear complete and symmetrical peak, which can accurately and easily be quantified by integration. However, iodide ions were difficult to be eluted and detected by the ICP/MS in a reasonable time. Iodide showed a very long peak tailing, which resulted in a great difficulty for the accurate quantification of iodide, especially for trace amounts (less than 100 ng absolute amount of iodide for the purpose in this work). The failure can be ascribed to the strong bonding of iodide to the column, but also to the memory effect of iodine in the ICP-MS [Al-Ammar 2001]. Therefore, based on these findings IC-ICP/MS seems not to be the ideal technique fro the iodine speciation in the particle phase.

All the developed sampling and analytical methods for the particulate iodine speciation in the marine boundary layer (MBL) have been applied to the two field measurement campaigns at the Irish west coast and in laboratory reaction-chamber experiments. All results will be presented and discussed in the following chapter.

4 Field Measurement Campaigns & Laboratory Chamber Experiments

During the project, there have been two field measurement campaigns performed at the western coast of Ireland, i.e. the QUEST campaign in late spring 2002 and the BIOFLUX campaign in autumn 2003. The developed methodologies for the iodine species in both gas and particle phase have been applied for the iodine species analysis in the campaigns. To confirm that the particle burst events are connected with biogenic iodine emission, seaweed-chamber experiments were carried out at the Mace Head Atmospheric Research Station (MHARS) during the BIOFLUX campaign. Additionally, reaction-chamber experiments in the laboratory were also conducted to identify the particle phase products that formed from the photolysis and ozonolysis of di-iodo-methane (CH_2I_2). In this chapter, all results from those field campaigns and chamber experiments will be presented and discussed.

4.1 QUEST campaign

4.1.1 Overview

The measurement campaign at the western coast of Ireland was the second part of the international EU-Project titled "Quantification of Aerosol Nucleation in the European Boundary Layer" (QUEST), in which the main objective was to quantify the number of new secondary aerosol particles formed through homogeneous nucleation in the European boundary layer and the relative contributions of natural and anthropogenic sources. The measurement campaign was considered to represent a typical undisturbed coastal area. The campaign was performed from the end of May to early June in 2002. All sampling and measurements were taken at the Mace Head Atmospheric Research Station (MHARS, 53°20'N, 9°54'W, the location shown Figure 1-3), located about 100 m from the tidal zone and surrounded by rocky area.

Previous studies done at the station have shown that aerosol particle bursts usually take place at low tide and often under sunlight [O'Dowd 1998, Grenfell 1999]. Therefore, based on the interest in the aerosol nucleation events of the MBL, it was supposed that the ideal campaign date would be the week when the tidal height are in lowest level (< 1 m at low tide and ≥ 5 m at high tide) that affected by the moon position twice a month, so called "Golden Week". Figure 4-1 shows the tidal height of the coast near MHARS during the campaign. From the tidal data, it was the last week of May 2002 (24th ~ 30th) that could be regarded as the "Golden Week" for the measurement campaign, in which the seaweeds / kelps at the coast area would be exposed to the ambient air during low tide and giving more iodine-contain emissions leading to a higher possibility for the nucleation events. The "Non-golden week", in which the tidal heights were in the range of 1.5 ~ 4.2 m, was the week after the important week for the campaign. However, besides the magnitude of precursor source, the occurrence of new particle formation depends strongly on the meteorologic conditions, such as solar strength, temperature, wind direction and speed etc. [O'Dowd 2002b, c]. Unfortunately, the weather during the campaign was not ideal for nucleation studies with frequent showers and cloudy conditions, causing only some weak aerosol nucleation events. Furthermore, these conditions gave problems and difficulties for the gas and aerosol sampling at the field site at

MHARS. For instance, the VOI measurement was almost impossible due to their extremely low concentrations and the high relative humidity (usually 60 % to 90 %) .

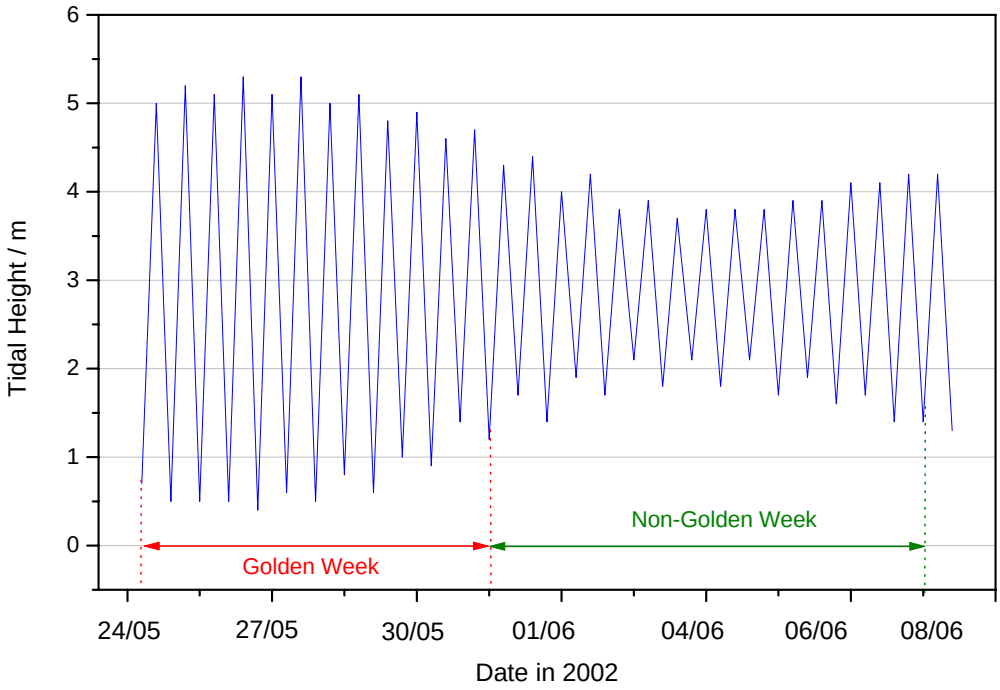

Figure 4-1 Tidal height at the coast near the MHARS during the QUEST campaign

The campaign focused on the flux of iodine species, their contribution to aerosol production, and the resultant flux of aerosols from the coastal zone. Additionally, airborne measurements spatially mapped the homogeneity of these coastal events and the relative source strength of the field station region compared to the rest of the coastline. Other quantities were measured in addition to the continuously measured variables, such as pulse height CPC (Condensation Particle Counter) -size distribution, ultrafine particle hygroscopicity, vertical aerosol fluxes, the complete aerosol size distribution and condensation sink with size distribution measurements up to 20 microns using an Aerodynamic Particle Sizer etc., performed by different research groups involved in the project. Relevant parameters including temperature, pressure, relative humidity, wind speed and direction, NO_x and O_3 concentration were also measured continuously at the station during the field campaign.

4.1.2 Total iodine in PM2.5

The concentrations of total iodine in the atmospheric particle phase (PM 2.5) from the QUEST measurement campaign was determined to be between 1.0 ng·m^{-3} and 4.0 ng·m^{-3}. All the data from the campaign are listed in Table A.II-1 in the appendix of this thesis. Figure 4-2, these data are compared with various meteorological parameters, particle number concentration (CPC data, measured simultaneously) and minimum tidal height during the campaign. As can be seen, the total iodine concentrations in the PM 2.5 samples show a high degree of variability. But in principle, the higher iodine concentrations were connected to the sampling time when the aerosol nucleation event occurred during the campaign. The typical examples were shown as 26/05 morning data (1.) and 06/06 afternoon data (3.) in Figure 4-2. In example 1, the total iodine concentration of 2.50 ng·m^{-3} was obtained during the nice weather of overhead sunlight causing the new particle formation which was detected by the nanometer-particle CPC. Similarly, 3.2 ng·m^{-3} total iodine concentration were found in

example 3, most likely caused by anther event of aerosol nucleation although it was partly cloudy. On the other hand, the lower total iodine concentrations were always observed at night-time sampling, and from those day-time measurements without new particle formation, i.e. data of 30/05 morning and afternoon (2.).

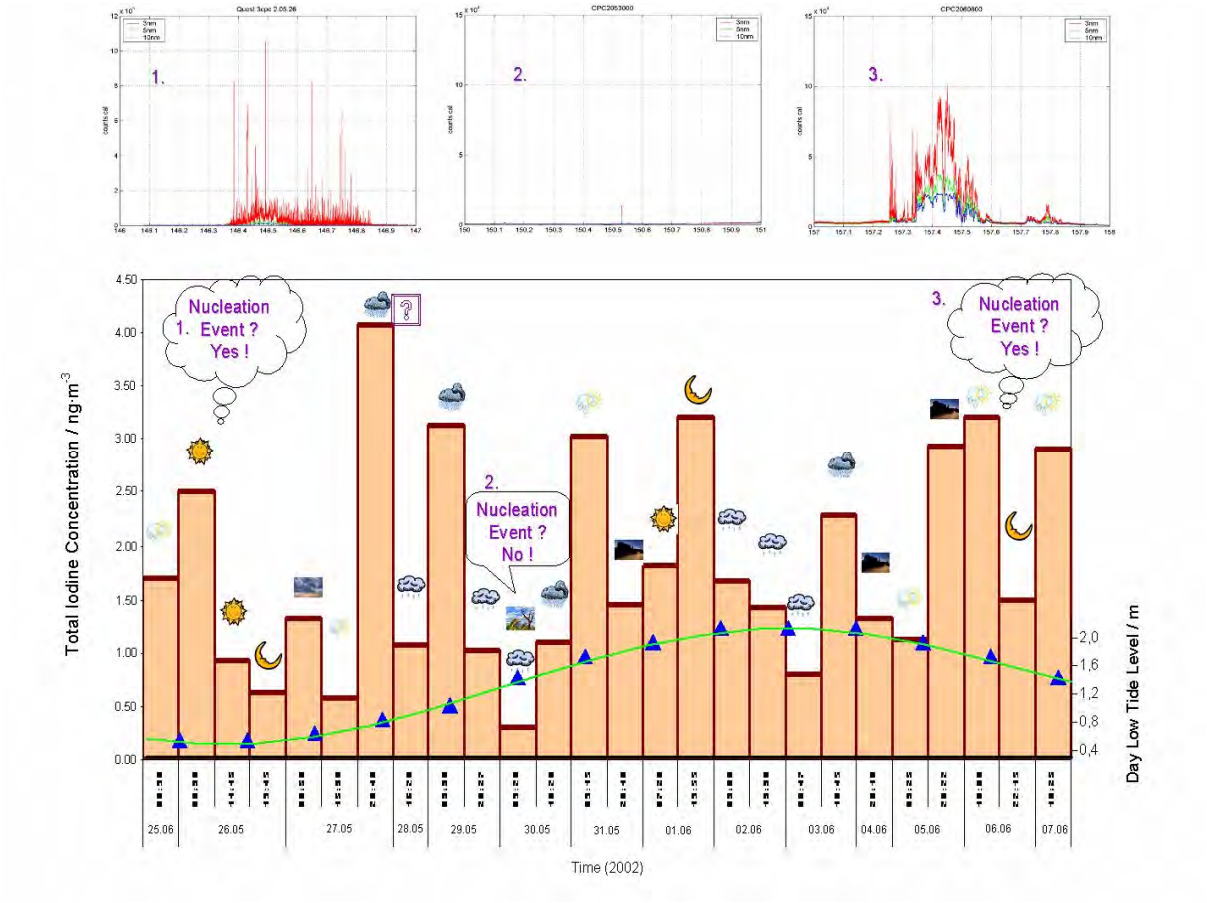

Figure 4-2 Concentration of total iodine in PM2.5 measuring in the QUEST campaign (in comparison to CPC data, low tide level and weather condition)

Moreover, it was difficult to connect the measured iodine concentration in the particle phase with the tidal height of the coast. It is supposed that more iodine is emitted at the low tide level since more seaweed is exposed to the atmosphere. However, the poor correlation might be explained by non-coastal precursor sources from sea water of the open ocean, so called sea-air transference [Huang 2001, Carpenter 2003a].

4.1.3 Total iodine in size-fractionated particle

The concentrations of total iodine in different particle size fractions of all samples are listed in Table A.II-2 and two typical examples are shown in Figure 4-3. Particles in the size region of 0.25 – 0.71 µm (Aerodynamic diameter, D_a) showed the highest concentration of total iodine, while the biggest particles (D_a > 5.9 µm) contained the lowest amount of iodine. Typically, it was found that the total iodine contents in the five stages are in this order: 0.25~0.71 µm > 0.08~0.25 µm ≥ 0.71~2.0 µm > 2.0~5.9µm> 5.9~10.0µm. As can be seen, particulate total iodine contents detected during the aerosol nucleation event (Data from June 3-4th, Figure 4-3b) were found to be 2~3 times higher than those measured in non-event sampling time (Data from June 6th, Figure 4-3a).

Although the sampling duration had been prolonged to 24 hours at a flow rate of 4.3 $m^3 \cdot h^{-1}$, some results from the impactor-samples were still below the determination limit, due to the extremely low iodine concentration in the fractionated particle phase. In addition, a relatively high iodine blank of tedlar-foils (up to 60 ng iodine per foil) was observed during the measurements. Therefore, tedlar-foil is not an ideal material for the fractionated particle sampling to measure iodine. It was proved that cellulose-nitrate filter has very low iodine blank. For the hot-spot measurement, cellulose-nitrate foil rings had been tested and used for the berner-impactor sampling procedure.

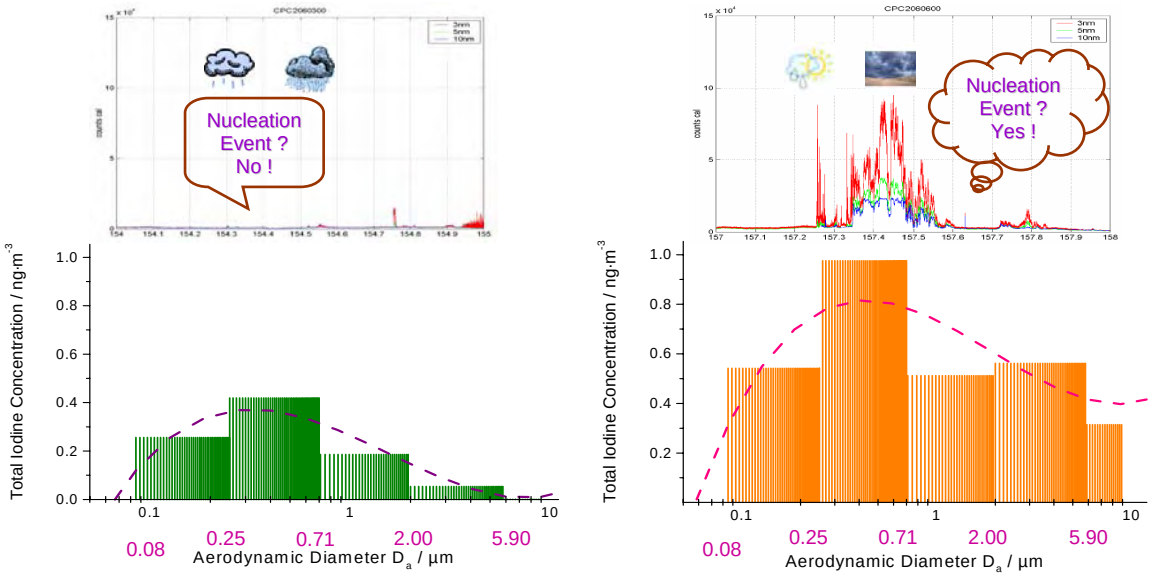

a. June 3th ~ 4th, 2002 b. June 6th, 2002

Figure 4-3 Total iodine distribution in size-fractionated particles
(In comparison to CPC data and weather conditions)

Certainly, the different environmental conditions, such as time of day, wind direction, temperature and tidal height, influence of transport as well as formation processes at the site, do have a significant effect on the particulate iodine contents. For instance, at MHARS, higher concentrations of total iodine were often found when the wind direction was primarily west and south west from the coast and the Atlantic ocean, and lower contents came with the eastern wind direction coming from the mainland of Ireland. Moreover, due to the extremely low concentration level of particulate iodine, the sampling duration of all particle samplers could not be less than 4 to 6 hours, which resulted the problem of connecting the iodine contents with the exact time of the new particle formation event. Therefore, it is difficult to establish a clear link between iodine concentration in the particle phase and nucleation events (new particle formation) observed at Mace Head.

Nevertheless, the results obtained in the first campaign (all data are listed in appendix II Table II-1 and II-2), e.g. the data shown in Figure 4-2 and 4-3, support the hypothesis that iodine compounds are involved in particle formation processes at this site, indicated by the outcome that total iodine concentrations during the nucleation event are much higher than those data in non-event at Mace Head.

4.2 BIOFLUX campaign

4.2.1 Overview

There are coastal areas around Mace Head, where sea weeds are relatively more abundant compared with the rocky area directly at Mace Head Atmospheric Research Station. As a result, it is believed that *hot spot*s nearby, such as Mweesh area, should have greater potential in terms of new particle formation. This hypothesis was proved to be true by the airborne measurements during the QUEST campaign. In May 2002, airborne particle concentration measurements using condensation particle counters (CPCs) with different size cut-offs, performed by the Group of O'Dowd from the National University of Ireland Galway, showed that nanometer-particles were formed over Mweesh and Roundstone area, Co. Galway, while the Mace Head station showed no particle formation. These *hot-spots* are likely to have a significant regional impact on the aerosol population. After the use of the research aircraft to identify *hot-spots* by the Irish research group, it was proposed to conduct a study BIOFLUX in a particularly strong *hot-spot* to examine the relationship between the flux of biogenic iodine gases into the boundary layer and the resulting flux of particles [Yoon 2004]. A field measurement campaign namely BIOFLUX was carried out in Carna, Galway Ireland, in September 2003 to identify the particle formation and biogenic gas fluxes from marine algae and seawater.

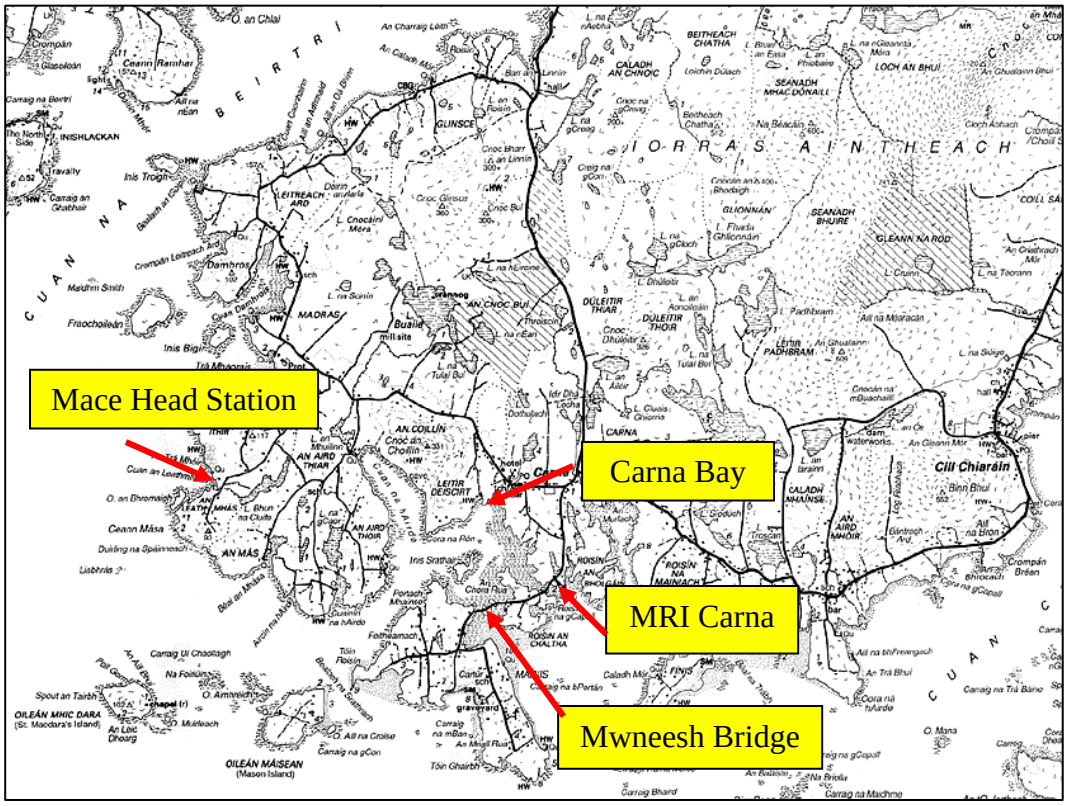

Figure 4-4 A map near and around the MHARS and MRI, Carna, Co. Galway Ireland

Similarly, the date for the campaign was fixed according to the "golden-week" and "non-golden-week" term. In this campaign, tidal height data were friendly offered by the Marine Research Institute of Ireland (also called Shellfish Lab). As shown in Figure 4-5, tidal heights at the coast area close to MRI during the last 3 weeks in September, indicates 2 golden weeks and 1 non-golden week for the measurement campaign. It was a dry summer in 2003, and a

relative dry period during the campaign in this area. Therefore, there were more probabilities for the burst of new particle formation, and providing us the convenient weather conditions to handle the sampling and measuring during the 3-week field campaign.

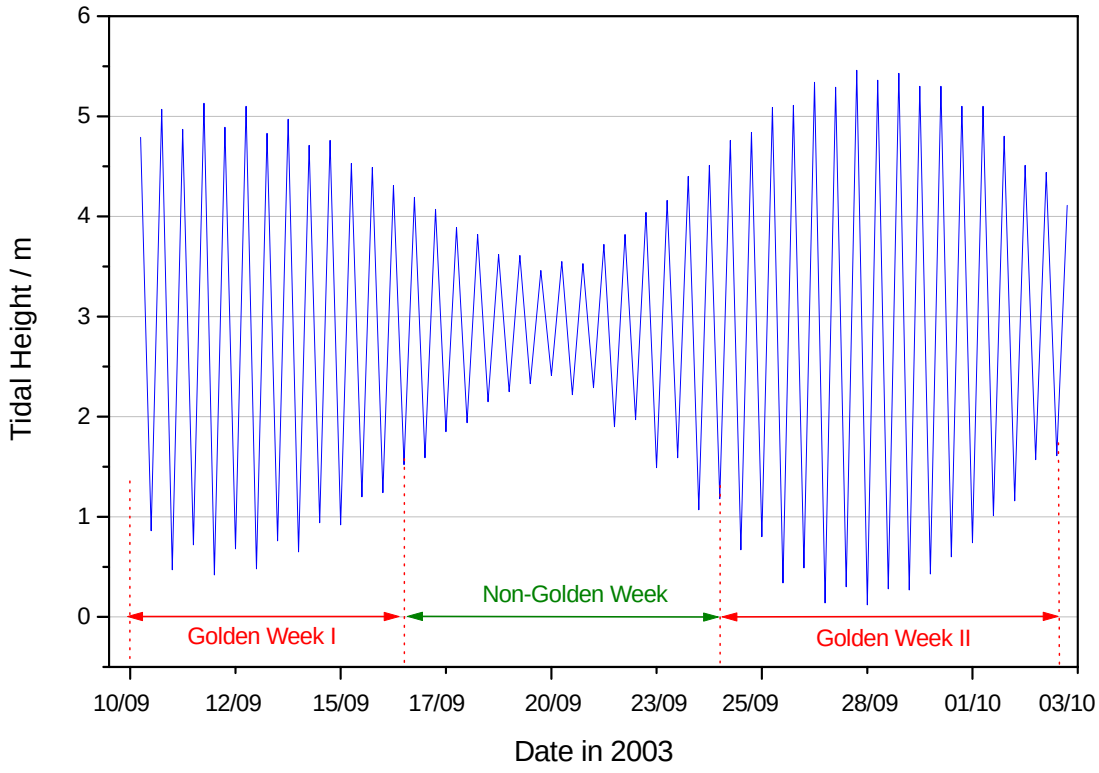

Figure 4-5 Tidal height at the coast near the MRI during the BIOFLUX campaign

For *hot-spot* particle number concentration measurements, a Scanning Mobility Particle Sizer for nano-particles (nano-SMPS) was installed into a mobile lab, which was managed and run by the group of Prof. Pirjola from Helsinki Polytechnic, Department of Technology Finland. The nano-SMPS was set to measure particle sizes from 3.5 nm to 50 nm with a time resolution of 30 seconds. The laboratory was also equipped with an Electric Low Pressure Impactor (ELPI) which measured particle size distribution from 7 nm to 10 µm. The ELPI was operated with 12 stages and a time resolution of 30 seconds.

A seaweed-chamber experiment was performed to test the hypothesis that biogenic gas emissions during low tide are connected to the new particle bursts in the coastal environment. The chamber had the dimension of 2 m×1 m×1 m and was made from Perspex (PMMA, Poly-Methyl-Meth-Acrylate), which transmits UV radiation to about 50 %. The chamber was filled with varied amounts of sea weeds collected near the Mace Head Atmospheric Research Station. Two combinations of sea weeds were tested: *Fucus Vesiculosus*, *Laminaria Digitata* and a mixture of these two species. These two species are widely found at the Mace Head tidal area. A filter was applied to the inlet and particle size distributions were measured by deploying nano-SMPS and ELPI. To identify the gaseous molecular iodine composition and VOC, chamber air was sampled and measured using the developed methods for iodine species analysis. However, only gaseous elemental iodine in the seaweed-chamber experiments was quantified using the denuder sampling technique followed by the ICP-MS detection.

4.2.2 Iodine species in the gas phase

4.2.2.1 VOI

Sampling of volatile organic iodine by Tenax-Carbotrap adsorption tubes have been taken at the *hot-spot* sites, such as MRI Carna, Mweenish Bridge and from the seaweed chamber experiment as well. However, it was failed to quantify the iodo-hydrocarbon contents in all the samples, by using the Thermo-Desorption / Cryo-Trap / GC-MS system. In most of the measurements, it was difficult even to qualify the iodo-hydrocarbons. Only three compounds could be clearly identified from some chromatograms and mass spectras of the samples concerned, i.e. 1-iodo-propane (1-C_3H_7I), Di-iodo-methane (CH_2I_2) and Tri-iodo-methane (CHI_3), although the m/z 127 of iodine were found and spread in the chromatographs of almost all the samples. Some other VOIs like Di-iodo-propane ($C_3H_6I_2$) could be detected in some samples from the site of Mweenish Bridge as well, as shown in Figure 4-6.

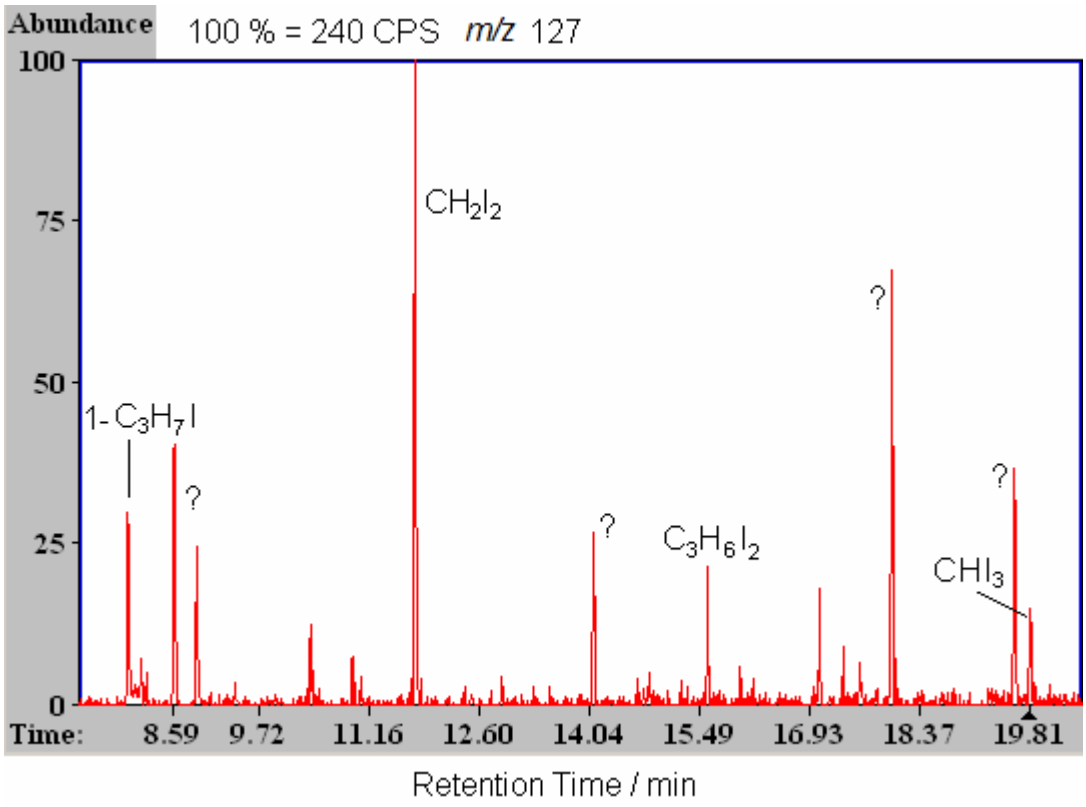

Figure 4-6 Selected Ion Current (SIC, *m/z* 127) of the air sample at the site of Mweenish Bridge on 09/30 afternoon, with 30 min sampling time

The reasons which caused the difficulties and failure in the VOI measurement could be trailed back to the following. Firstly, trace analysis of these substances in the ambient air using the developed method are relatively difficult, due to the extremely low concentrations of the VOI in the coastal atmosphere (at ppb or ppt levels as reported in literatures), although the sampling duration had been prolonged to 40~60 minutes. Secondly, relative long time of storage and transportation before the sample analysis may cause the degradation of the iodo-hydrocarbons, especially for some species such as CH_2I_2 which is very photo-sensitive to UV or visible light leading to a very short life-time in mid-day for example. Moreover, at low concentration levels, smaller molecules like CH_3I, C_2H_5I are not effectively adsorbed by the Tenax or Carbotrap in the sampling tube. Finally, like some reactive VOCs (e.g. terpenes),

iodo-hydrocarbons are prone to degradation during sampling in an ozone-rich environment (e.g. higher than 50 ppb). Ozone removal technique could help to improve the sampling methods, i.e. ozone scrubber technique. Silanized poly-1,4-phenylene sulfide (PFS), MnO_2 on copper net etc. were reported to be effective ozone scrubbers for VOC sampling and measuring, and might be potentially applied for the VOI sampling in the future measurement campaigns. KI is obviously not an ideal scrubber for VOI sampling in this case, although it appeared to be the most effective for other VOCs [Fick 2001].

4.2.2.2 Elemental iodine

Results description

Field measurements performed at the seaweed "hot-spots" at the western coast of Ireland, showed that the concentration of I_2 in the atmosphere was up to 1.6 $ng \cdot L^{-1}$ (~140 pptV), with a determination limit of 0.10 $ng \cdot L^{-1}$ at a sampling volume of 15 L (500 $mL \cdot min^{-1}$ × 30 min) All sampling details and measurement results are listed in Table A.II-3. These concentrations are higher than those from DOAS measurements (maximum level 93 ppt) [Saiz-Lopez 2004b], because of the much shorter distance between the sampling position and the kelp surface for the *in-situ* measurements. The gaseous I_2 content varied widely with the sampling site and water tidal level, the time of day and weather conditions etc.

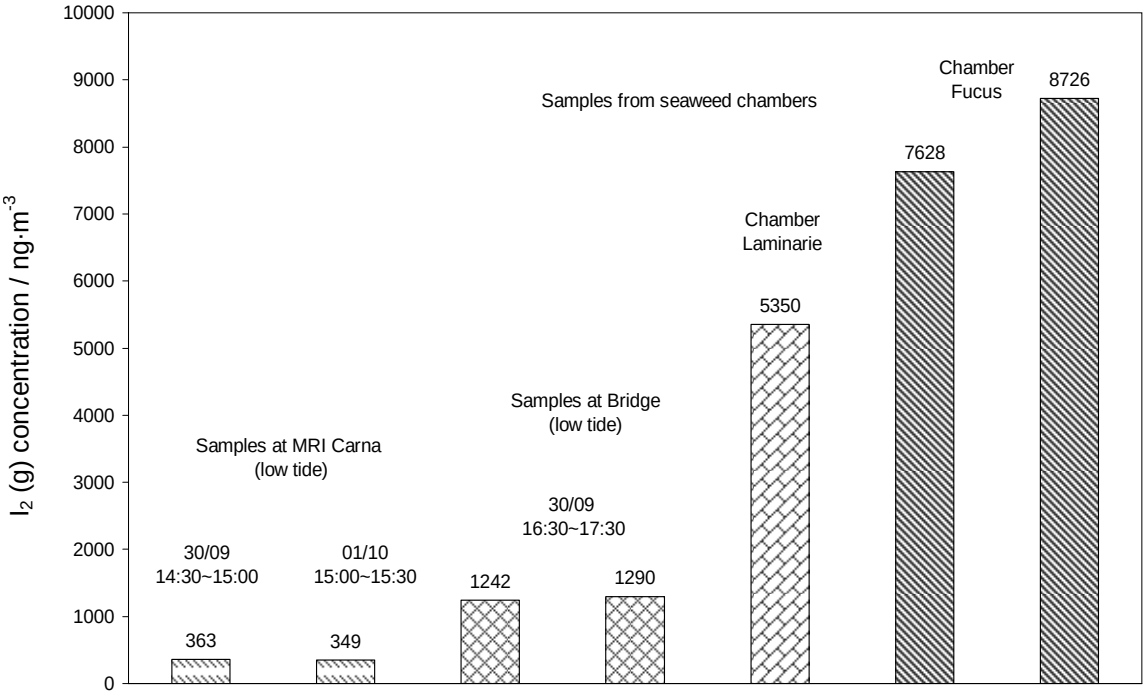

Figure 4-7 Molecular iodine concentrations measured with the denuder system; Comparison of different sampling sites and seaweed-chamber experiments.

Figure 4-7 shows the gaseous I_2 contents from different sampling sites and seaweed-chamber experiments. As can be seen, elemental iodine concentrations at "Mwneesh Bridge" were about 3 times higher than those at "MRI-Carna", obviously due to the larger amount of seaweeds at this sampling site as well as the shorter distance between the seaweeds and denuder sampler inlets. The iodine concentration measured within the seaweed chamber was

about one order of magnitude higher than the ambient concentrations (More details are described in section 4.2.4 seaweed-chamber experiments.).

It was found that the gaseous I_2 contents were not significantly related to the tide level, although it was suggested that enhanced molecular iodine emissions was linked to the significant concentration of inorganic iodine species in tidal water as the water level subsides [McFiggans 2004], in which the process was first linked to macroalgae as a source of precursor and second, and more particularly, to the concentrating effects of inorganic iodine species driven by tides that would not apply over the open ocean. At least, I_2 contents were not found to be zero when there were no kelps exposed to the atmosphere at high tidal level.

Compared to the DOAS results [Saiz-Lopez 2004b], it was found that the daytime I_2 contents were higher than those measured during the night time or evening (see Figure 4-8). It was suggested that the rapid photolysis of I_2 in the lower atmosphere (lifetime=5–10 s for an overhead sun) results from the strong absorption of visible wavelengths ($400<\lambda<700$ nm) which penetrate down to the troposphere [Saiz-Lopez 2004a]. However, if molecular iodine is directly emitted from kelps at low tide level and faded due to the photolysis process at day time, the contents might depends strongly on the tidal level and solar radiation; or if I_2 is one of the by-products of the photolysis process from other organic iodine in the presence of ozone and solar radiation [O'Dowd 2002a], it would be found that daytime contents become higher. Since the emission source of elemental iodine is not clear, and the iodine photo-chemical pathways are complicated, it is difficult to explain the observed I_2 contents so far. It seems that there might be a thermodynamic and chemical equilibrium which governs the I_2 concentration in the gas phase of the coastal atmosphere.

The Source of I_2 emission

There might be at least three potential explanations of the molecular iodine emission source in the sea-air system. One mechanism involves that iodide (I^-) is oxidized to I_2 at the surface of seaweeds and the ocean. Iodate (IO_3^-) predominates in deep sea (>250 m), while iodate is reduced to iodide by phytoplankton assumedly in near-surface seawater [Waite 2003], thus their concentrations become comparable or even more iodide in the sea-air interface [Schwehr 2002]. Then, it is suggested that I^- is oxidized by oxygen with solar radiation [Miyake 1963], ozone [Grand 1981] or hydrogen peroxide [Küpper 1998] (reaction a-c). And finally, the molecular iodine becomes saturatedly concentrated in the seaweed / seawater surface and is emitted into the atmosphere via the sea-air flux. Additionally, the photolysis pathways of iodo-hydrocarbons (such as CH_2I_2) might also produce iodine radical and form elemental iodine [O'Dowd 2002a], which might be even more difficult to be investigated quantitatively.

$$2I^- + \frac{1}{2}O_2 + H_2O \xrightarrow{h\nu} I_2 + 2OH^- \quad \text{(a)}$$

$$O_3 + 2I^- + 2H^+ \rightarrow I_2 + H_2O + O_2 \quad \text{(b)}$$

$$H_2O_2 + 2I^- + 2H^+ \rightarrow I_2 + 2H_2O \quad \text{(c)}$$

Although these pathways to yield elemental iodine are still not completely clear, ozone as an important atmospheric component to understand the iodine chemistry in the marine boundary layer. O_3 was also measured during the BIOFLUX campaign. That gave the possibility to connect the I_2 contents to the ozone concentrations in the gas phase. Figure 4-8 shows the correlation between I_2 and O_3 from the measuring data of afternoons (4-8a) and evenings (4-8b). As can be seen from the figure, ozone concentrations in the afternoon were clearly higher

than those in the evening. And obviously, it was found that higher iodine contents were observed at higher ozone mixing ratios in the ambient atmosphere, showing a one-order correlation, although the linear regression coefficients are not ideal (*R=0.817* for daytime data and *R=0.750* for evening data), and in despite of the limited data set.

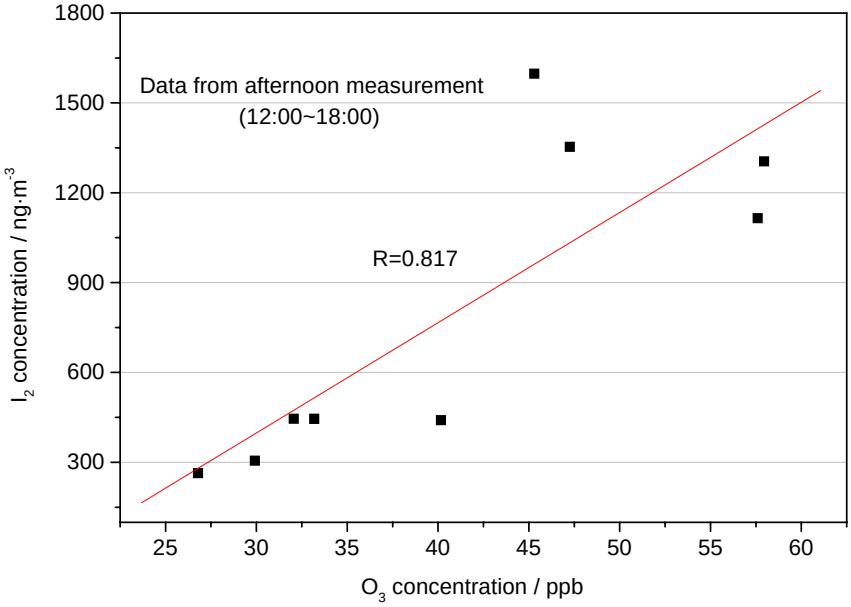

a.

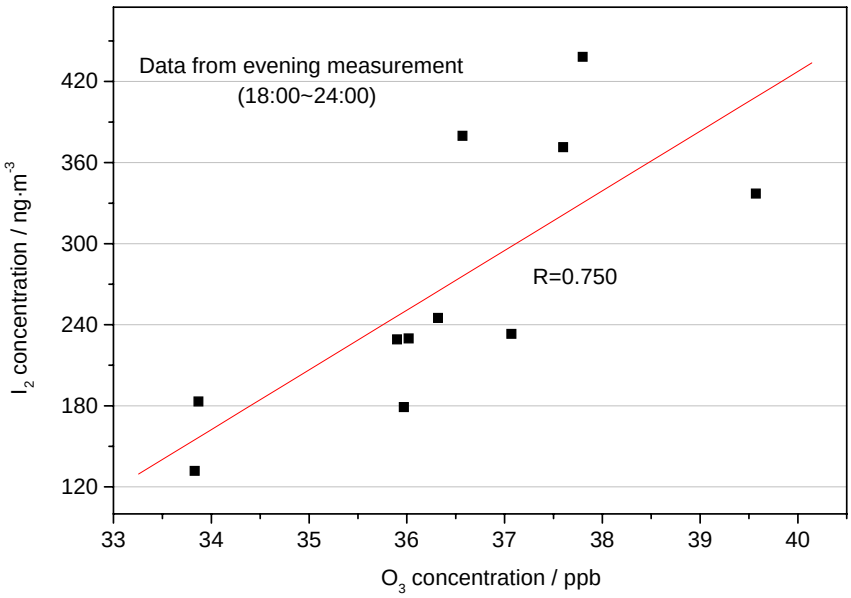

b.

Figure 4-8 One-order correlation between elemental iodine and ozone contents in the coastal troposphere (Sampling site: MRI, low tide level. a. afternoon data; b. evening data)

Actually, oxidation of iodide in the artificial seawater surface by ozone yielding gaseous elemental iodine has been confirmed in previous [Garland 1981] and recent laboratory experiments [Chen 2004], indicating that release of I_2 by O_3 will also occurs in the natural open seawater surface. It was estimated by Garland et.al. that this action of ozone at the sea surface may contribute $6\sim12\times10^{10}$ g of I_2 to the global atmosphere each year. Adding the I_2 release from UV+O_2 (4×10^{11} g, reaction a) suggested by Miyake and Tsunogai and that from H_2O_2 oxidation (amount not suggested, reaction c), the total annual atmospheric cycle of iodine may exceed 5×10^{11} g.

Unfortunately, there is no data available for the field campaign to assess and discuss how significant the release effects from UV+O_2 or from hydrogen peroxide could be. Concerning gaseous elemental iodine as the products formed from photolysis of other organic iodine species, neither the mechanism studied in the laboratory nor the actual data are available so far. Therefore, further laboratory and field measurements are necessary to understand the elemental iodine forming source in the marine boundary layer (MBL).

Gaseous iodine species as the precursors of aerosol nucleation caused by iodine emission still remains as an open question, although more and more knowledge have been gathered recently, for instance, absolute absorption cross-section and photolysis rate of I_2 has been evaluated [Saiz-Lopez 2004a]. Indeed, whether organic iodine species or inorganic species play the dominant role in the whole gas process lead to particle formation has been in deep discussion recently [Mcfiggans 2005, O'Dowd 2005]. Nevertheless, the suggestion that an additional source of iodine over the open ocean needs to be identified warrants further investigation. Actually there has been investigation for the prediction of the elemental iodine formation and its effect on ozone depletion, the role in the coastal new particle formation and the new particles' evolution to form condensation nuclei, using the *in situ* and laboratory data by a model study [Saiz-Lopez 2005].

4.2.3 Iodine species in particulate phase

4.2.3.1 PM2.5

Total iodine

From the results of total iodine measurements in PM2.5 during the BIOFLUX campaign (shown in Table 4-1 and Table A.II-4) the following can be clearly concluded. Firstly, as hotspot of seaweeds, due to the higher total amount of iodine source, the results from BIOFLUX are usually 2 to 5 times higher than those taken from Mace Head Station (1~4 $ng \cdot m^{-3}$). Secondly, the daytime iodine concentrations are higher than the night-time measurement. Thirdly, the morning concentrations are lower than those measured in the afternoon. These could be obviously because the new particle formation (Nucleation Event) always happened at daytime during the solar radiation between 9:00 to 16:00, and the stronger event was observed to occur usually around and after mid-day, according to the nano-meter particle data (SMPS – Scanning Mobility Particle Sizer was measuring at the same time.), which would show a sudden unusual high number concentration of nanometer-particle (D_a < 10 nm, $N > 10^5$ cm^{-3}) when the event occurs.

Figure 4-9 shows the iodine concentrations from event and non-event days from day time measurements, as well as from night-time measurements. The maximum iodine concentration 21.13 $ng \cdot m^{-3}$ was obtained during a strong nucleation event on 16th Sept. 2003, while the minimum was found at the night measurements. Assuming nanometer-particle as a sphere model and with the primary chemical composition of iodine oxide species (e.g. I_2O_4, with a density of about 4.0 $g \cdot cm^{-3}$ in this case) and calculating the mass of nanometer-particle during the aerosol nucleation events, then a typical total iodine concentration of about 10 $ng \cdot m^{-3}$ are estimated to equal to the number concentrations of ~ 5×10^6 cm^{-3} 1 nm-particle or ~ 6×10^5 cm^{-3} 2 nm-particle or ~ 4×10^4 cm^{-3} 5 nm-particles. These calculated data are very close to the

number concentration of nano-particles which were measured by the nano-SMPS when the new particle formation occurred during the field campaign.

Table 4-1 Comparison of total iodine concentration in different types of PM2.5 samples

Sample Types	Morning Samples (involved before mid-day)	Afternoon Samples (involved after mid-day)	Night Samples
I Concentration Range / ng·m^{-3}	3.96~6.68	6.71~21.13	1.48~4.93
Average / ng·m^{-3}	4.81 (10 samples)	11.03 (12 samples)	3.09 (15 samples)

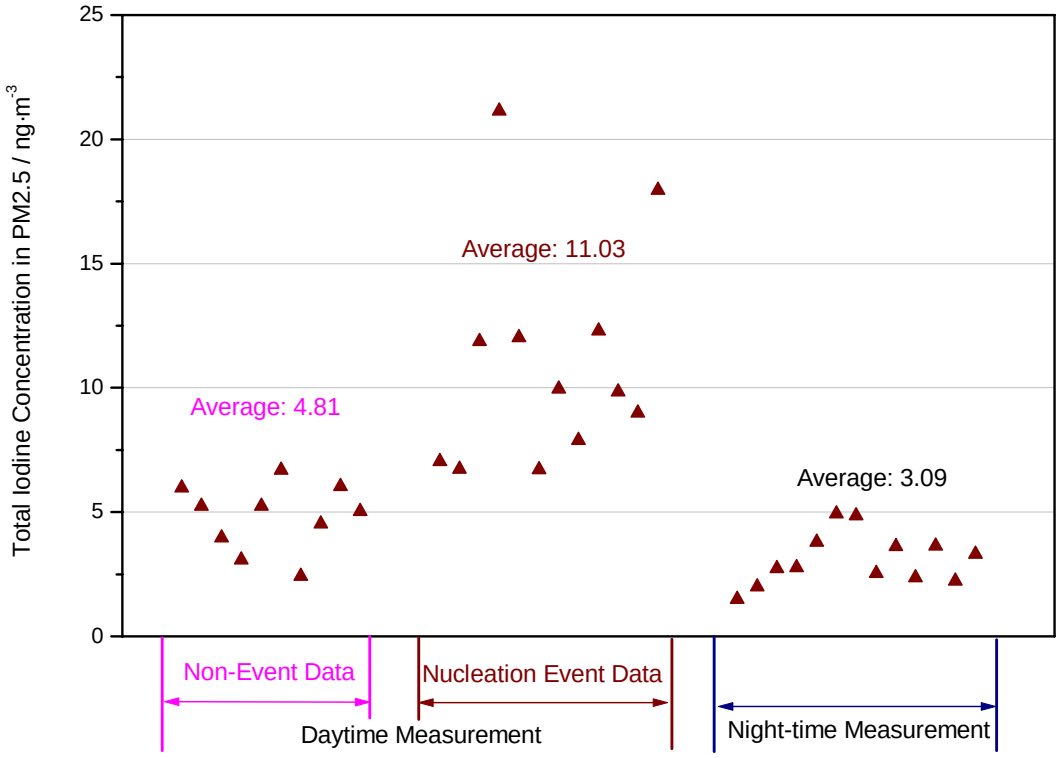

Figure 4-9 Total iodine in different types of PM2.5 samples during the BIOFLUX campaign

Iodine species

Figure 4-10 shows some typical iodine species concentrations in PM2.5 particle samples. The absolute contents of each iodine species may not be able to significantly indicate or explain the iodine emission leading to the new particle formation, while the ratio of iodate/iodide and water-soluble/-unsoluble species could be relatively important to conclude and clarify the iodine chemistry in the coastal atmosphere. As can be seen in Figure 4-10, iodide concentrations are usually higher than those of iodate in all samples with a ratio of about 2~5:1, while Iodide/Iodate ratio in seawater sample (at the interface to the air) is at a wide range of 1~4:1 [Schwehr 2002]. It looks very possible that those water-solved iodine species were transferred through the sea-air interface, and directly taken up into the particle phase. On the other hand, mechanic studies have suggested that particulate iodate can be accumulated from the iodine oxides (e.g. I_2O_2, I_2O_4 etc.) in higher oxidation state as the aerosol ages [Vogt 1999, McFiggans 2000] and iodide may be taken up into particle phase from the HI, as shown in Figure 1-2 [Carpenter 2003a].

The ratio of water soluble (iodate + iodide) and non-water soluble species (probably iodine oxide I_xO_y and organic iodine compounds) was found in the range of 1:1 to 1:2 or even up to 1:3 during the measurement campaign. It seems that higher concentrated non-water soluble species, as products which undergo gas to particle conversion, can be obtained in those samples with higher number concentration of nanometer-particles, i.e. the water-unsoluble species dominate the total iodine in the particle phase while the nucleation events occurs. In Figure 4-10, it is observed that the concentration of water-unsoluble species depended on the strength of the aerosol nucleation, e.g. 16/09 afternoon data are higher than other nucleation event data, such as 20th and 21th / 09 measurements, and the data measured during non-event period. This conclusion supports the current understanding of the iodine chemistry in the Marine Boundary Layer (MBL), in which particulate iodine species as the particle end-products is suggested to be dominated by iodine oxides.

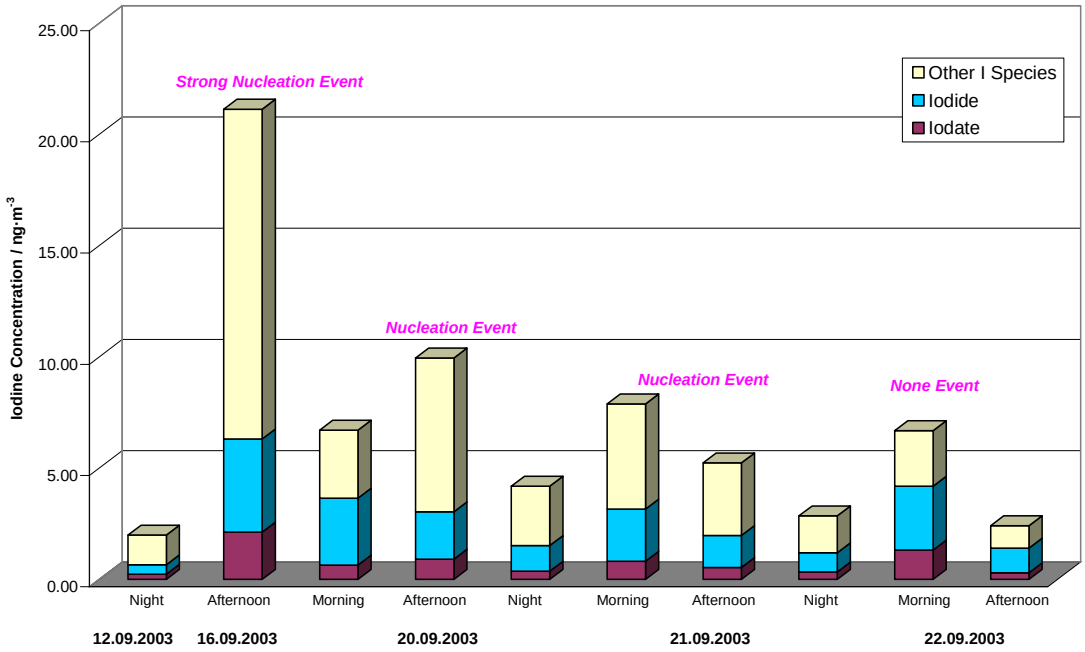

Figure 4-10 Typical concentrations of iodine species in PM2.5 during the BIOFLUX campaign

Iodate is not the only iodine species that is permanently removed to the aerosol phase. If the rate of iodate formation is fast with respect to iodine deposition fluxes, iodate would be expected to dominate iodine speciation in deposition. Recent work on the iodine speciation in both rain and aerosol implied that rates of iodate formation and iodide volatilization through reaction with hypohalous acids are relatively slow [Baker 2001]. The results presented here may support this implication as well, although the aerosol sampled here were relatively newly formed compared to those of which is deposited. More recent work, which was performed in the open ocean of the Atlantic has obtained similar results and the iodate concentration was even found to be below the detection limit in several samples from the northern hemisphere and could not be detected at all in the southern hemisphere samples. Conversely, iodide, which it has been suggested not to reach significant concentrations in seasalt or sulphate aerosol, was present at detectable levels in all samples and even at higher concentrations than iodate [Baker 2004]. These results might raise serious questions about current understanding of aerosol iodine chemistry in the marine atmosphere.

4.2.3.2 Size-fractionated particle

Some measurement results for total iodine concentrations in the particle samples from the Burner-impactor are shown in Figure 4-11 and all data listed in Table A.II-6. As indicated in Figure 4-11, total iodine concentrations of size-fractionated particles were ranging from below the detection limit to 12 ng·m^{-3}. Similar to the total iodine contents of PM2.5, it was found that total iodine contents of the size-fractionated particles during the daytime measurement (Figure4-11 a, c) were always higher than those from night time measuring data (Figure4-11 b, d), with a factor of 3 up to 10. This may again support the hypothesis of new particle formation is governed by iodine emission during daytime. Actually, it can be clearly seen in Figure 4-11 that higher total iodine contents were observed with the stronger aerosol nucleation event, when comparing the daytime measurement of 14/09 and 16/09.

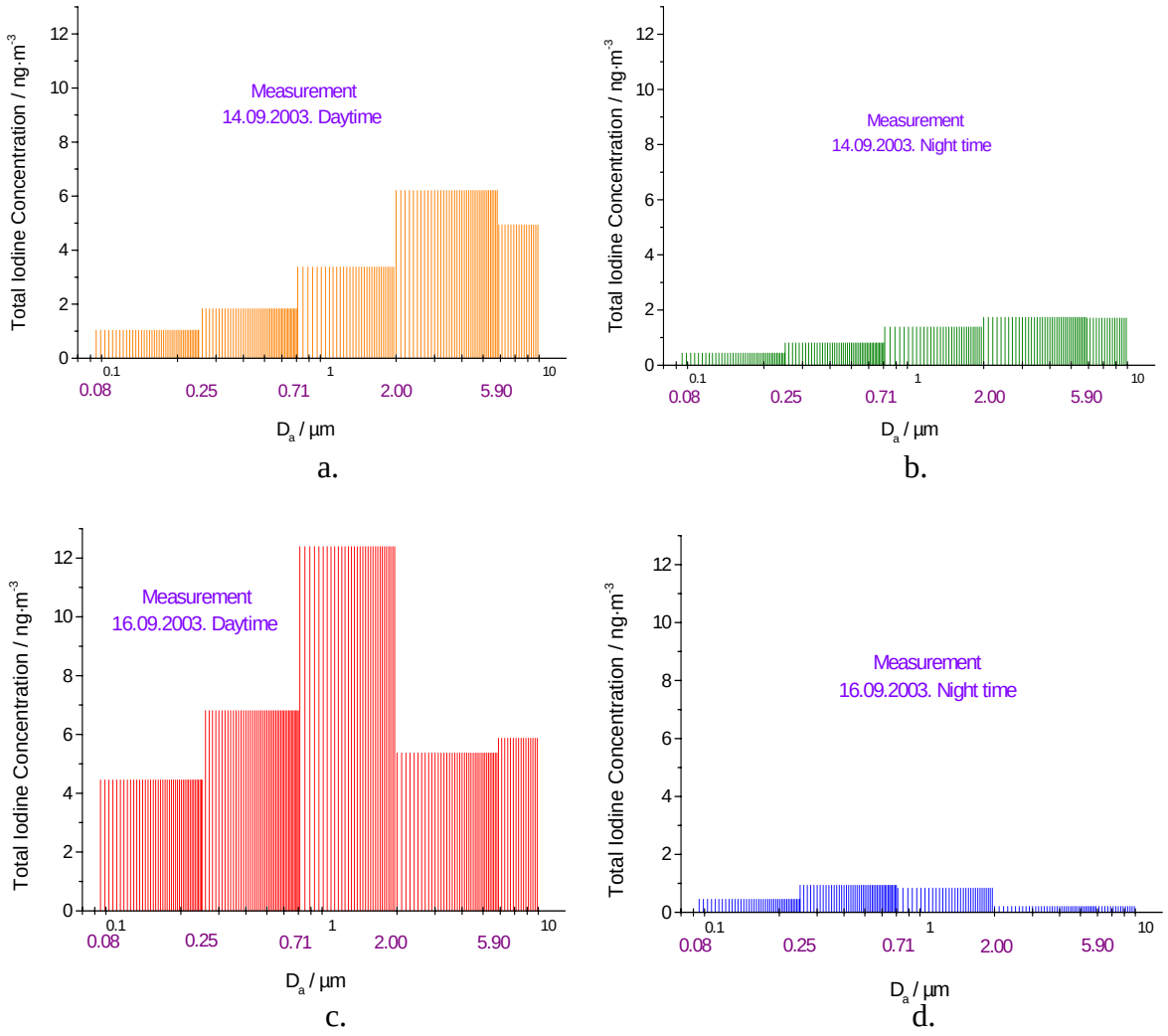

Figure 4-11 Total iodine concentration in the size-fractionated particle during the BIOFLUX campaign (Comparison for day and night time measurement)

In terms of the iodine distribution in the size-fraction according to the cutoff by the impactor-stage, it seems there is a wide variation from sample to sample, especially between the daytime and nighttime measurements. In principle, it was found that for the daytime measurement, iodine contents distribution in size-fractionated particles are in the order of

(D_a/µm): 0.71~2.00 ≥ 2.00~5.90 ≥ 0.25~0.71 ≥ 5.90~10 > 0.08~0.25, and almost no regular pattern for the nighttime measurements. Obviously, lacking of more detailed knowledge about the particle growth process and iodine transformation after the nanometer-particle formation, it is problematic to explain the observed iodine distribution in the size-fractionated particles in more detail.

However, it was difficult to compare the total iodine of the size-fractionated particles to that of the PM2.5 particles in this work, due to the difference of particle size cut off by the particle samplers, and the overlap of size range (0.08~2.5 µm) is relatively narrow so that we can not compare these two types of iodine contents exactly and reasonably. But at least the values of total iodine contents in this overlap range obtained at the same measuring day were quite the same between the two different samples.

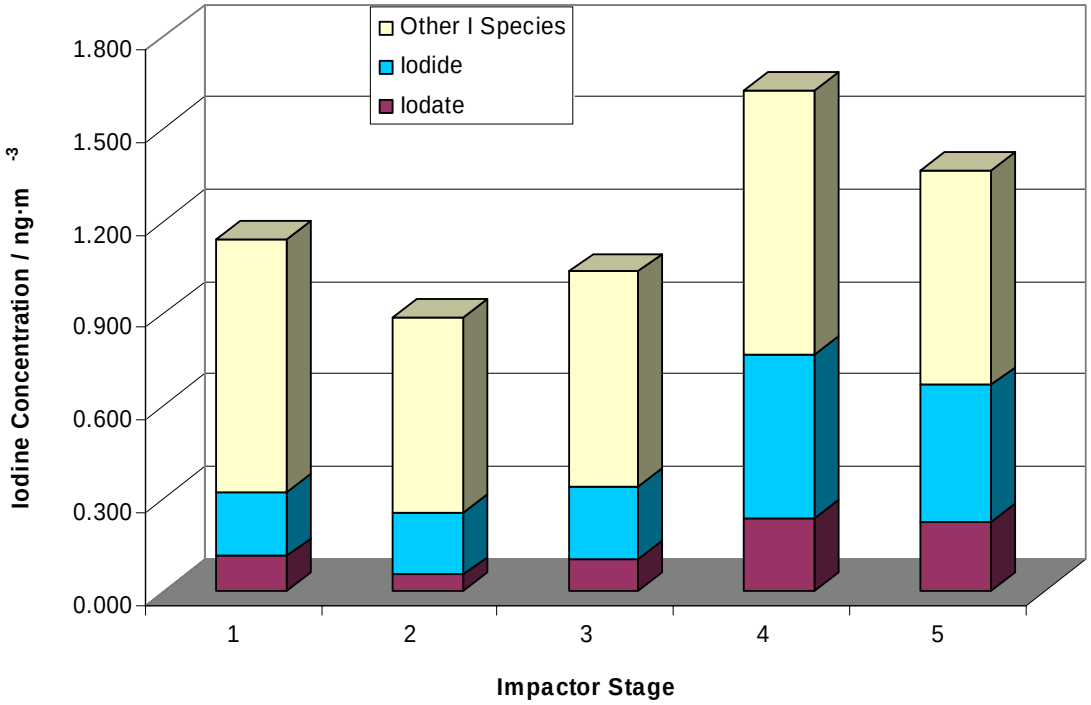

Figure 4-12 Iodine species in a size-fractionated particle sample during a medium aerosol nucleation event (taken at 12:03 27.09.2003 ~ 00:11 28.09.2003)

The results of the iodine speciation measurements in a size-fractionated particle sample during an aerosol event are shown in Figure 4-12 and in more detail in Table A.II-7. Almost the same as in the PM2.5 samples, ratios between iodide/iodate are in the range of 2~3:1 and in this event particle sample, non-water soluble iodine species contents were found to be 2 to 4 times higher than the water soluble species iodide and iodate. Former work has shown that iodate was the dominant iodine form in the size-segregated aerosol sample collected aboard ship in the tropical Atlantic [Wimschneider 1995]. Therefore again, these measurement results that iodate is not the dominant species and even less concentrated than the others, may really cause some more questions about the iodine uptake into the particle phase during the new particle formation and the particle growth process in the marine atmosphere, especially the iodide uptake source, the iodate precursor source as well as the complete identification of the non-water soluble iodine species. Detailed chamber experiments in the laboratory may help to solve those unclear questions in the future.

4.2.4 Seaweed-chamber experiments

Two representative types of macro-algae were used for the experiments, i.e. *Fucus Vesiculosus* and *Laminaria Digitata*, which are the most important macro-algae and widely spread at the western coast of Ireland [2, 3]. They can be easily collected at the tidal coast area around the MHARS. These macroalgae were then put into the PMMA-made chamber (dimension of 2 m$\times$1 m$\times$1 m) together with several liters of sea water to keep them alive. A filter was applied to the inlet of the chamber and particle size distributions were measured by deploying nano-SMPS and ELPI instrumentaton. To measure the gaseous iodine spcies, chamber air was sampled and measured using the developed methods for iodine species analysis. However, only gaseous elemental iodine in the seaweed-chamber experiments was quantified using the denuder sampling technique followed by the ICP-MS detection.

Regardless of the species of seaweeds filled in the chamber, nano-particles were formed in the chamber as soon as the chamber was covered. Size distribution measurements with nano-SMPS and ELPI from the chamber experiments showed that the concentration of these newly formed particles reached up to 4×10^6 cm^{-3}. These nanometer-particles grew very rapidly to 0.5 μm size in diameter in less than 10 minutes. As particles grew towards the larger size, nano-particles were formed again, and then followed the previous growth patterns, showing an evolution of size modes in wave types. These wave-like particle formation and growth pattern lasted until sunset, even some minutes after the sun set. No new particles were formed during night time without solar radiation. Though it was not as strong as the first day, nano-particles were formed again early in morning of the experiment day as soon as sun rose. Therefore, these seaweeds experiments clearly showed that particles can be formed quite efficiently from the nucleation of biogenically emitted gases even when there is a small amount of solar radiation are available [Yoon 2004].

Figure 4-13 shows the relation between the amount of seaweeds and the I_2 (g) concentration. Molecular iodine concentrations were found to have a 2-order polynomial correlation ($R^2 = 0.956$) with the seaweeds mass in the chamber, indicating kelps are one of the emission sources of elemental iodine (all obtained data are listed Table A.II-8). If combining the amount and exposed surface of the macroalgae and total air flow in the chamber, it was estimated that the emission rates of iodine from those kelps are: for *Laminaria digitata*, 0.019 ~ 0.022 ng/min/kg; for *Fucus vesiculosus*, 0.025 ~ 0.029 ng/min/kg. Nevertheless, as discussed above, the open ocean surface might be another source and even the primary source of gaseous I_2 at the global scale, though the detail mechanisms are not fully understood yet.

The relation between gaseous I_2 concentration and the steady state nanometer-particle concentration in the chamber is shown in Figure 4-14. As can be seen, during the pseudo-steady state particle formation, nanometer-particle concentrations (data acquired from a Scanning Mobility Particle Sizer for nano-particles at the same time) were also found to have a linear correlation ($R = 0.976$) with elemental iodine in the gas phase of the seaweed chamber, clearly indicating that gaseous I_2 is one of the important precursors of the new particle formation in the coastal atmosphere, although the data set are relatively limited. Still, due to the failure of VOIs quantification in the seaweed-chamber experiment, the effects of new particle formation by the VOIs could not be identified in the experiments. The question whether I_2 or VOIs is more important as precursors that has more significant effects on the nanometer-particle formation, can not be answered in these experiment so far. More experiments and deeper knowledge are required to fully interpret the whole chain from the gas to particle phase.

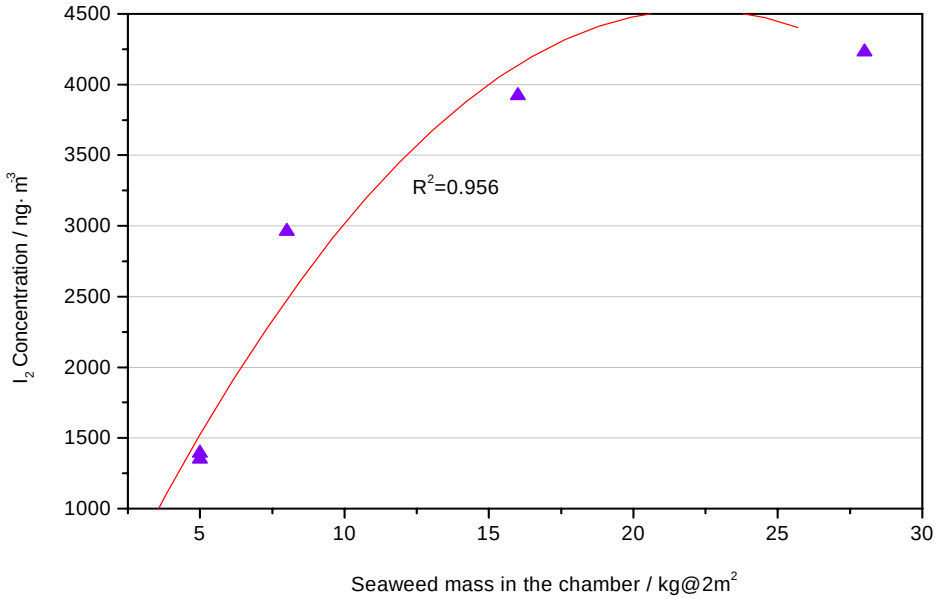

Figure 4-13 Relation between seaweed amount and gaseous I_2 concentration in the seaweed-chamber experiment

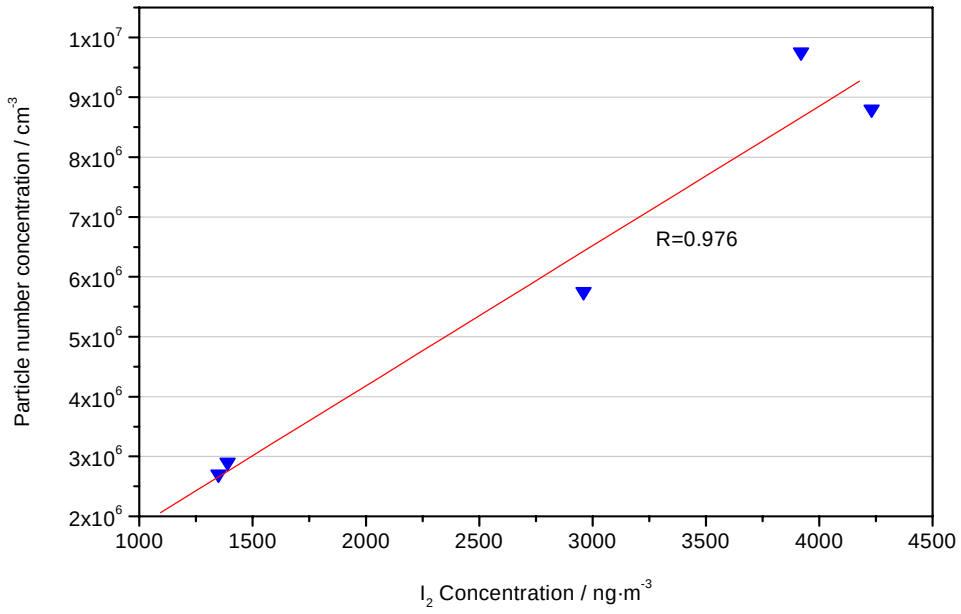

Figure 4-14 Relation between steady state nano-particle and gaseous I_2 concentration in the seaweed-chamber experiment

First results of the seaweed-chamber experiment have proved that the gaseous elemental iodine can be emitted by two types of macroalgae investigated and gaseous I_2 is one of the important precursors that lead to the new particle formation in the presence of solar light in the ambient air at the coastal tidal area. However, so far the phenomenon of particle formation linked to gaseous I_2 emission have not been observed and proved experimentally at the open ocean surface where there would not be plenty of algae exposed to the atmosphere directly. Nevertheless, even if these aerosol nucleation occur merely at the coastal area at low tide and under solar radiation, those natural new particles formed in the global scale would still be an appreciable amount, which might grow sequentially and lead to Cloud Condensation Nuclei (CCN) [Kolb 2002].

4.3 Laboratory reaction-chamber experiments

In order to identify and characterize the iodine species in the particle phase formed by nucleation from iodine emission, aerosol formation from the direct photolysis of CH_2I_2 in the presence of O_3 was investigated in a photochemical reaction-chamber. Based on the offline measurements of the CH_2I_2 degradation during the reaction in the chamber, the photolysis reaction rate as a first order kinetic were calculated from these experiments.

4.3.1 Experimental setup

The experimental setup of the photochemical reaction-chamber experiments in the laboratory is shown in Figure 4-15 and technical details of the facilities are listed as following:

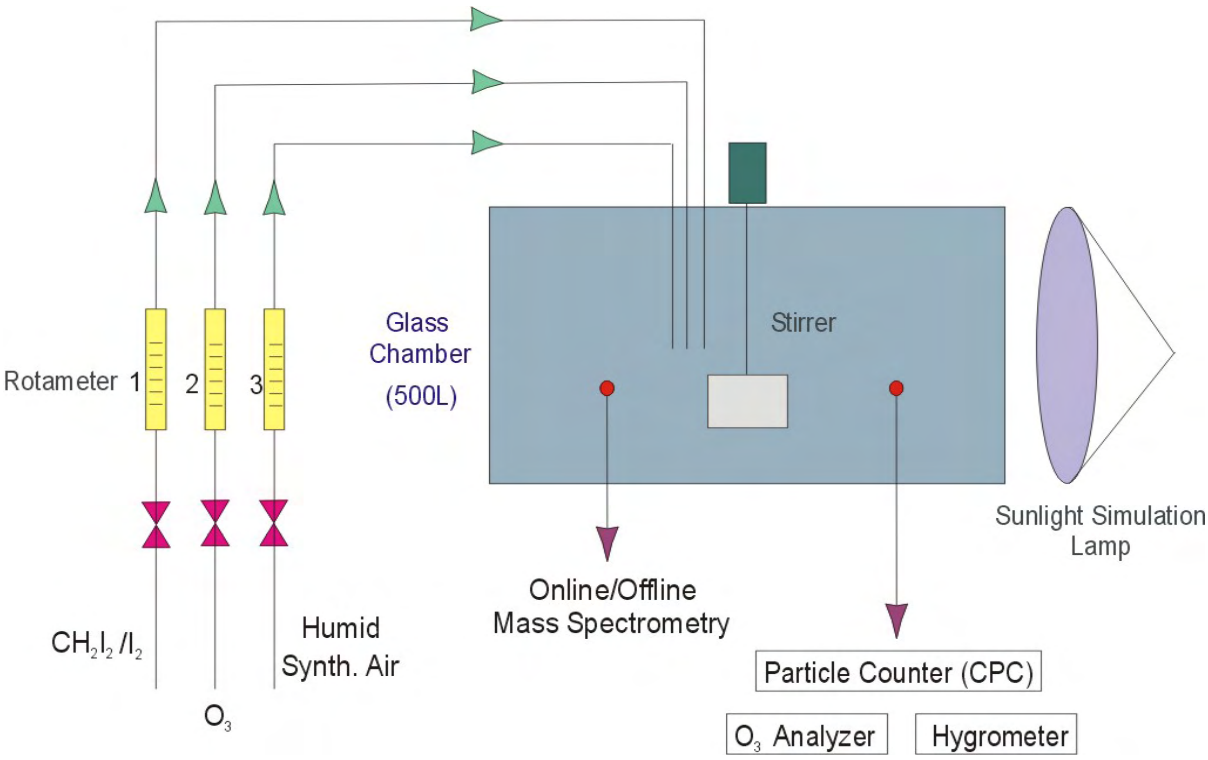

Figure 4-15 Schematic of experimental setup for the photolysis and ozonolysis of CH_2I_2 in a laboratory reaction-chamber.

- Glass Chamber: Cylindrical, 500 L, self-made in the Department of Chemical Engineering at the University of Dortmund, Germany
- Sunlight Simulation Lamp: Werzalit®, Germany
- CPC (Condensation Particle Counter): TSI Model 3010, USA
- Ozone Analyzer / Generator: Dasibi Environmental Corp., Model 1008-RS, USA
- Hygrometer: multi-function hygrolog (including temperature and pressure etc.), Endress & Hause WMY 770Z, Germany

The chamber was first cleaned by a synthetic air flow with higher ozone concentration (~ 150 ppb, ~1 L·min^{-1}) overnight, afterwards flushed by synthetic air (10 L·min^{-1}) for several hours so that the blanks of particle and ozone in the chamber are low enough before performing the experiments.

4.3.2 Photolysis and ozonolysis of CH_2I_2

Photolysis of CH_2I_2 in the absence of O_3 does not lead to particle formation; likewise, no particle form in mixtures of CH_2I_2 and O_3 [Hoffmann 2001, Jimenez 2003]. Table 4-2 summarizes the experiments carried out.

Table 4-2 Summery of the experiments performed

Experiment No.	Humidified Synthetic Air	CH_2I_2	O_3	UV-Vis Light ($h\nu$)	Particles
1.	+	–	–	–	×
2.	+	–	–	+	×
3.	+	–	+	+	×
4.	+	+	–	–	×
5.	+	+	+	–	(√)*
6.	+	+	–	+	(√)**
7.	+	+	+	+	√

Note: "+" means "switched on", "–" means "switched off";

" √ " stands for "new particle detected", "×" for "new particle not detected".

* Reaction chamber is not completed sealed to avoid any light, so that some particles were formed in experiment 5.

** O_3 can be yielded from O_2 when the UV light is strong enough in the chamber, so that some particles were formed in experiment 6.

Chamber operation parameters and conditions:

- Temperature: 22.5 °C, Relative Humidity: 17~20 %;
- CPC blank: 10 cm^{-3} Particle, O_3 blank: 13 ppb;
- Gas flow (when operated): Humidified Synthetic Air: 8 L·min^{-1};
- O_3 generation gas: 1 L·min^{-1}, concentration at 15~200 ppb for the total flow (10 L) in the reaction chamber;
- CH_2I_2 gas source: ~2.4 μg·L^{-1} CH_2I_2 in 1 L·min^{-1} N_2 flow, at 25 °C controlled by the thermostat.

CH_2I_2 was first introduced into the chamber together with the synthetic air for about 30 minutes for equilibrium. The ozone generator was then switched on to introduce an increasing O_3 content flow with the rate of about 1.5 ppb / min. Sunlight simulation light was turned on when the ozone concentration reached 40 ppb. Very rapidly new particles were formed in the chamber and detected by the CPC 3010 particle counter. Number concentration of those particles bigger than 10 nm increased to over 1.0×10^4 cm^{-3} within 4 minutes after the reaction started in the chamber.

4.3.3 Measurements and results

CH_2I_2 measurement

CH_2I_2 was sampled by the Tenax-Carbotrap sampling tube and analyzed by the Thermo-Desorption / Cryo-Trap / GC-MS method (detail described in Chapter 2). Quantification of the analyte was based on the relative peak area compared to the standard from the self-made CH_2I_2 gas calibration source. The sample was taken directly from the chamber outlet when the reaction occurred (Experiment No. 7 in Table 4-2) with sampling a flow rate of about 150 $mL \cdot min^{-1}$ and a sampling time of 2 min. It was about every 3 minutes that one sample was taken for the measurements. The measurements were continuously performed from the beginning of the photolysis until 30 minute after the beginning of the reaction. Results of the CH_2I_2 degradation measurements versus the reaction time are shown in Figure 4-16 a (see Table A.II-9).

Calculation of the photolysis rate constant based on the first order reaction kinetics and the measurement of the CH_2I_2 degradation is explained below. Upon the photolysis reaction of CH_2I_2:

$$CH_2I_2 \xrightarrow{h\nu} CH_2 + 2I^*$$

The reaction rate is defined as a first order reaction kinetics by:

$$r = -\frac{d[CH_2I_2]}{dt} = k \cdot [CH_2I_2]$$

where:

r is the reaction rate [$ng \cdot L^{-1}s^{-1}$ in this experiment];
k is the photolysis rate constant of the first order reaction [s^{-1}];
$[CH_2I_2]$ is the instantaneous concentration of CH_2I_2 in the reaction [$ng \cdot L^{-1}$];
t is the reaction time [s^{-1}].

By changing the form, one can obtain the followings:

$$\Rightarrow \quad \frac{d[CH_2I_2]}{[CH_2I_2]} = -k \cdot dt$$

$$\Rightarrow \quad \int_{[CH_2I_2]_0}^{[CH_2I_2]} \frac{1}{[CH_2I_2]} \cdot d[CH_2I_2] = -k \int_{t_0}^{t} dt \quad (t_0 = 0)$$

After integral calculus:

$$\ln \frac{[CH_2I_2]}{[CH_2I_2]_0} = -k \cdot t \quad \text{or} \quad [CH_2I_2] = [CH_2I_2]_0 \cdot e^{-kt}.$$

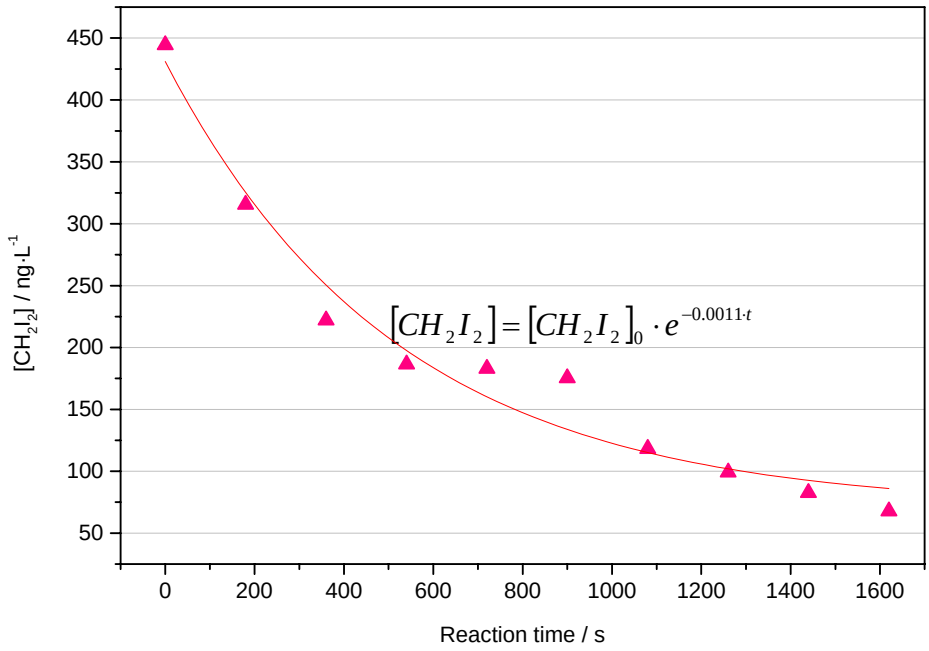

(a)

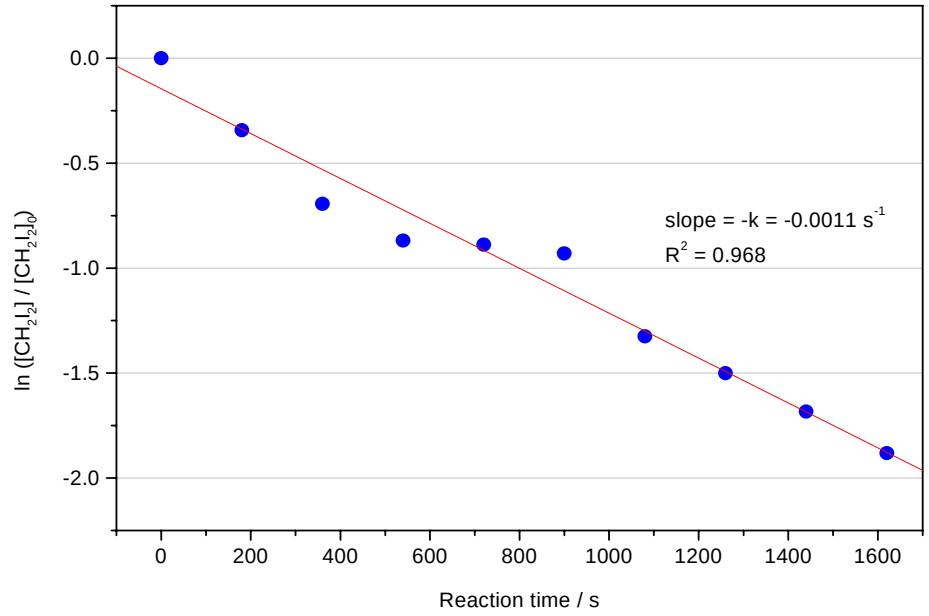

(b)

Figure 4-16 (a) The CH_2I_2 concentration in the reaction chamber as a function of reaction time; (b) The fitting line based on first order chemical reaction kinetic calculation.

Calculated from the linear regression analysis result, as shown in Figure 4-16 a and 4-16 b, the photolysis rate constant is $k = 1.10 \sim 1.30 \times 10^{-3} s^{-1}$, which is close to the value of that calculated by Jimenez et al ($k = 1.75 \times 10^{-3} s^{-1}$) [Jimenez 2003]. Perhaps, the deviation may result from the "off-line" measurements of the CH_2I_2 concentration since the measured concentrations of CH_2I_2 were the averages in the two minute duration of sampling, instead of the instantaneous concentration values.

The ozonolysis process of the active iodine atoms yielded from the photolysis has not been deeply investigated in this experiment. This may require an online monitoring which can identify and quantify all the iodine species involved in the gaseous and particulate phase. Actually, online Atmospheric Pressure Chemical Ionization Mass Spectrometry (APCI-MS) has been applied for this purpose in the previous work [Hoffmann 2001], as well as Aerosol Mass Spectrometry (AMS) [Jimenez 2003]. In these two previous works, many mechanisms have been suggested for the gaseous iodine chemistry and aerosol uptake of iodine species. Based on the AMS data of both gaseous and particulate chemical composition, model simulation had been done to compare with the data from reaction chamber experiments, in which more than 40 reactions along with the current knowledge of iodine chemistry are implied to be involved in gas and particle phase chemsitry [Jimenez 2003].

The end-products in the particulate phase

Particles were sampled by a filter sampler from the outlet of the reaction-chamber at about 30 minutes after the reactions started. Afterwards the particle samples were treated by the developed methods for the iodine species analysis (details described in Chapter 3). All the measurement results about the particulate iodine species are listed in Table A.II-10. The end-products of the particulate iodine species from the photolysis and ozonolysis of CH_2I_2 in the reaction chamber are described and discussed as following.

Some measurement results of the particle phase iodine species in relation to the ozone concentration in the reaction-chamber are shown in Figure 4-17 (absolute concentration of iodine species) and Figure 4-18 (relative composition). As can be seen in Figure 4-17, the concentration of all particulate iodine species are increasing with a longer the reaction time and an increasing ozone concentration. When the solar simulation light was switched off at 93 ppb ozone concentration, the absolute amounts of all the particulate iodine species decrease rapidly despite the continuously increasing ozone concentration in the reaction chamber. This can be explained by the lack of active iodine atoms.

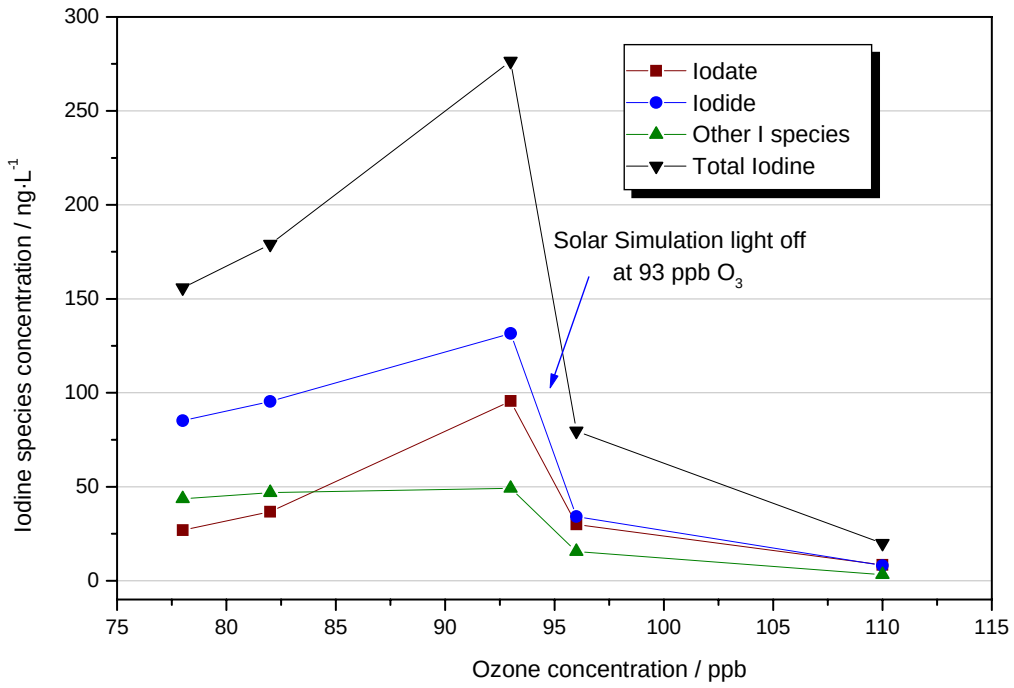

Figure 4-17 Relation between concentrations of particulate iodine species and ozone

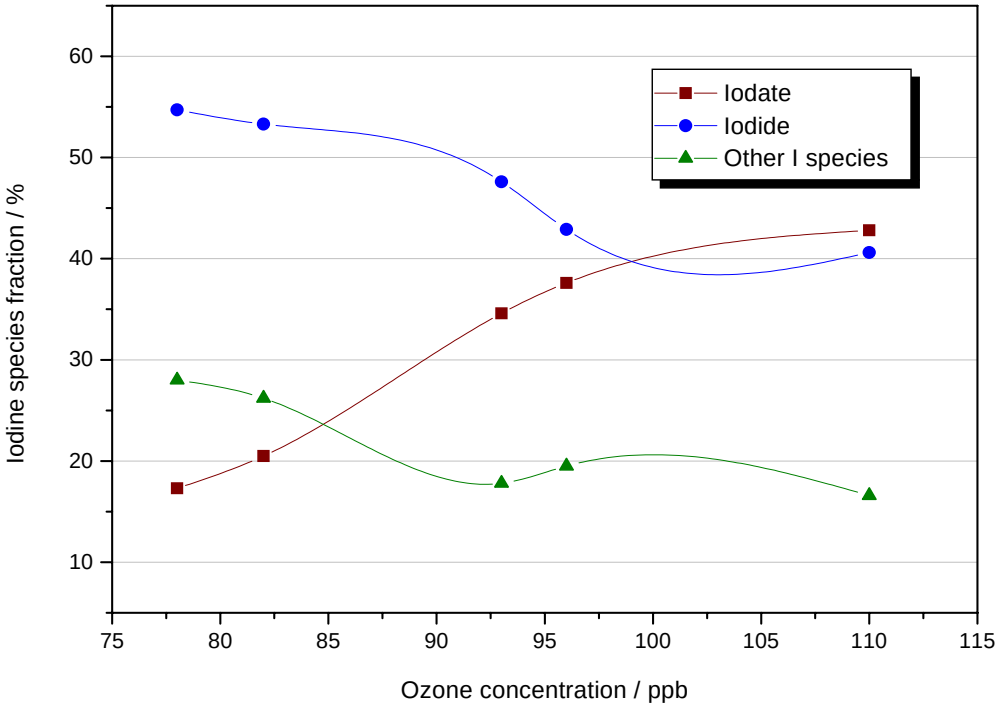

Figure 4-18 Relation between relative contribution of iodine species and ozone concentrations

As indicated in Figure 4-18, water soluble iodine forms dominate the total particulate iodine species. The ratio of iodide to iodate varied from 3:1 at the beginning of the new particle formation process to 1:1 at the end of the reaction in the chamber. Therefore, iodide dominates the primary water soluble species, probably formed from the HI products at the beginning of the reaction chain, whereas iodate dominates later in the process when ozonolysis is getting more important than the photolysis. This iodate fraction overpasses iodide and the non-water soluble species with increasing ozone concentration in spite of the fact that the solar simulation light was switched off at 93 ppb ozone concentration. These results prove again that - like in the BIOFLUX campaign -, iodate is not the dominant iodine form in the particle phase. Therefore, the transfer rate of iodide to iodate was found to be not as fast as expected, which was pointed out by Baker et al. in 2004 as well.

Unlike the measurement data during the nucleation events from the BIOFLUX campaign, non-water soluble species, occupying not more than 40 % of total iodine in the particulate phase, are not the primary iodine form in the reaction chamber experiment. This might be due to the much higher concentration of ozone (up to 120 ppb) in the chamber than the O_3 concentration in the ambient air (usually not more than 50 ppb). At higher ozone concentrations, it is supposed that more iodine oxyacids likely HIO_3 are easily formed in the ozonolysis process, which causes the iodate fractions are getting higher (see figure 4-18). As suggested by the previous work of other groups, iodine oxides may be possibly the primary iodine form in this non-water soluble species. However, knowledge about iodine oxides is still quite fragmentary at present. A number of oxides have been proposed, including I_2O, I_2O_3, I_2O_7, I_6O_{13}, $I_{10}O_{19}$ which have not been confirmed [Chase, 1996], and those known to be stable such as I_2O_4, I_2O_5, I_2O_6 and I_4O_9. Those iodine oxides have a strong tendency to form polymeric network, which may cause the growth and coagulation of the nano-particle formed from the nucleation bursts [Jimenez 2003].

In terms of the relation between the iodine species and the particle number concentration, it is difficult to link the absolute amounts or fraction ratios of iodine species to the particle counter's data, not only because of the complicated growth process of the particles involved, but also due to the fact that the number concentrations of nanometer-particle were not measured by the 3010 CPC used here. Iodine species in the newly formed particles (nanometer sized) could not be connected to their number concentrations in this case. The fraction of iodine species in the particle phase may strongly depend on the particle sizes, which could not be described and measured in the experiments performed here. More laboratory experiments in more detail are required in the future, to find out the correlation between iodine species and the particle growth process after the nanometer particle formed by nucleation.

As for the conclusions from the reaction chamber experiments, firstly, the photolysis rate constant of CH_2I_2 has been estimated based on the offline measurements of its degradation and the kinetics of the first order reaction. Secondly, it is implied that the ratio of iodide and iodate, and the ratio of water soluble and non-water soluble species in the particle phase, are probably strongly dependent on the ozone concentrations and the reaction time in the chamber. Thirdly, soluble species, iodide and iodate, are not only the direct uptake from the sea water into the particle phase during the nucleation event, but also the by- and end-products from the gas phase precursors. Finally, iodine oxides are suggested to be the primary non-water soluble species in these laboratory generated particles.

Furthermore, the photolysis and ozonlysis of elemental iodine would be another important topic in the laboratory chamber experiments to clarify new particle formation mechanisms caused by this potential precursor, although some experiments on the I_2 issue have been carried out by other research groups such as laboratory chamber study [McFiggans 2004] and model study [Saiz-Lopez 2004a, 2005].

5 Conclusions and Prospects

Summary and conclusions

An analytical methodology to identify and quantify the volatile organic iodine (VOI) species in the gas phase of the coastal atmosphere, using the Tenax / Carbotrap adsorption sampling technique and the Thermo-Desorption / Cryo-Trap / GC-MS system was developed and improved. Several iodo-hydrocarbons such as CH_3I, C_2H_5I, CH_2ICl, CH_2IBr, and CH_2I_2 etc., have been measured in the samples from a calibration test gas source (standards) and the real air samples with iodine-containing emission from seaweeds / macro-algae.

A denuder sampling technique was developed to characterize the potential precursor compounds of coastal particle formation processes, i.e. elemental molecular iodine (I_2) in the gas phase. Starch, TMAH and TBAH coated denuders have been tested in respect to their collection efficiency for I_2 at the denuder inner surface, followed by a TMAH extraction and ICP/MS determination, adding tellurium as an internal standard. The developed method has been proved to be an effective, accurate and appropriate procedure for gaseous I_2 measurement in the gas phase of the remote marine area, in which the detection limit was estimated to be ~0.10 $ng \cdot L^{-1}$ for a sampling volume of 15 L.

The H_2O/TMAH-Extraction-ICP/MS method has been developed for the sensitive and accurate determination of iodine species in tropospheric aerosol particles. The particle samples are collected on cellulose-nitrate filters using conventional filter holders or on cellulose nitrate/tedlar-foils using a 5-stage Berner-impactor for size-segregated particle analysis. The trace amounts of water soluble species as IO_3^- and I^- could be separated successfully by anion exchanging process after water extraction. Non-water soluble species including iodine oxides and organic iodine were extracted by TMAH. Afterwards the triple samples were analysed by ICP/MS. The detection limit for particulate iodine was determined to be 0.10~0.20 $ng \cdot m^{-3}$ for a sampling volume of 40~100 m^3.

During the BIOFLUX campaign in September 2003, elemental iodine as a potential aerosol precursor or/and a by-product of the iodine chemistry in the coastal atmosphere west Ireland was determined in the gas phase at certain hot-spots of seaweed population, showing that the concentrations of I_2 were in the range of 0~1.6 $ng \cdot L^{-1}$ and indicating a correlation with the actual ozone concentration. The seaweed-chamber experiments performed at the field research station showed that the I_2 emission rate from algae was in the range of 0.019 ~ 0.022 ng / min / kg at 2 m^2 exposed surface area. And during the pseudo-steady state particle formation, nanometer-particle concentrations were found to have a linear correlation with elemental iodine in the gas phase of the seaweed chamber, indicating that gaseous I_2 is one of the important precursors of the new ultrafine particle formation in the coastal atmosphere.

Iodine contents in particle phase were measured in both field campaigns at and around the Mace Head Atmospheric Research Station located in the western coast of Ireland. Total iodine concentrations were found to be in the range of 1.0 ~ 21.0 $ng \cdot m^{-3}$ in the PM2.5 samples, which had a significant correlation to the nanometer-particle number concentrations and on the strength of the aerosol nucleation events observed in the atmosphere. The particulate iodine species analysis indicates that iodide contents are usually higher than those of iodate in all samples, with a ratio of about 2~5:1. It is possible that these water-soluble iodine species are transferred through the sea-air interface into the particle phase. The ratio of water-soluble

(iodate + iodide) and non-water soluble species (probably iodine oxides and organic iodine compounds) was observed to be in the range of 1:1 to 1:2. It appears that higher concentrated water-unsoluble species, as the products of the photolysis from the gas phase into the particle phase, could be obtained in those samples taken during the nucleation events.

Furthermore, artificial aerosol particles were produced from a gaseous iodine source (i.e. CH_2I_2) in the presence of ozone and UV-Vis light in a laboratory reaction-chamber experiment. Based on the first order reaction kinetics and linear regression analysis, the photolysis reaction rate constant was calculated to be $k = 1.10 \sim 1.30 \times 10^{-3} s^{-1}$. Iodine end-products in the particle phase have been characterized as well, indicating that the ratio of iodide and iodate and the ratio of water and non-water soluble species in the particle phase are probably strongly dependent on the ozone concentration and the reaction time in the experiments. It is supposed that the origin of iodide and iodate are not only from the direct uptake from the sea water into the particle phase during the nucleation event, but also from gas to particle conversion. Iodine oxides are suggested to be primary in the non-water soluble species, though more information has to be gathered about the role of iodine compounds in the aerosol nucleation and particle growth process in the coastal atmosphere.

Prospect and outlook

Analytical methodologies for iodine species in the coastal atmosphere

To understand the entire pathways in the process of new aerosol formation and growth linked to biogenic iodine emission in the MBL, it is necessary to identify and quantify the intermediate iodine products in gas phase and end products in particle phase besides the well known precursors. Unfortunately the analytical methodologies for iodine species in the gas phase of the coastal atmosphere have not been fully developed yet. Some species which could be the potential precursors of the new coastal particle formation were not taken into account up to now. For instance, hydrogen iodide (HI) and hypoiodous acid (HOI) can be other important gaseous iodine species which might be involved in the process from the gas to particle phase in the MBL. In the iodine chemistry of the MBL, HI might be yielded from the reaction of active iodine atoms and OH radicals, while the HOI can be produced by the reaction of IO and OH radicals. As discussed in chapter 4, water soluble iodide found in the particle phase might be the aerosol uptake from HI in the gas phase (see figure 1-2). However, the challenges to determine these two species are not only the separation of the gaseous molecules from atmospheric aerosol particles, but also the separation of the iodine species in the gas phase from each other. Although some previous work has been performed, the roles of these gaseous iodine species [Gaebler 1993] are still unclear.

In terms of the characterization of end-products in the particle phase (especially the non-water soluble iodine species like iodine oxides) in detail, it will be necessary to develop a new analytical method for the purpose of particle composition measurement by *in situ* and online techniques in field campaigns. Aerosol Mass Spectrometry (AMS) could be an ideal instrumental methodology. Actually, the AMS system has been applied for the investigation of aerosol formation from iodine containing emission in laboratory chambers [Jimenez 2003], in which several particulate iodine species such as IO^+, HIO^+, IO_2^+, HIO_2^+, HIO_3^+, IO_5^+, I_2O^+ and $I_2O_3^+$ have been detected. However, the particle composition could not be identified during the nucleation and the particle growth process. Hence new online measuring methods

have to be developed in this case for future investigation of iodine species in the particle phase of the coastal troposphere.

As for the aerosol nucleation related to the reactive iodine precursors especially the emission of elemental iodine from non-coastal areas would be interesting to know. Therefore, an extension field observation above the open ocean surface should be conducted. A ship onboard measurement campaign is considered to be ideal to identify the possible iodine emission from the seawater surface and to observe new particle formation events above the open ocean.

Interaction of iodine species and other trace gases

Release of interhalogens such as ICl and IBr after interaction of HOI on salt surfaces has been verified in laboratory experiments [Holmes 2001, Mössinger 2001] and is believed to significantly increase the gas-phase halogen reservoir [Vogt 1999b]. If those interactions happen veritably in the iodine chemistry of MBL as well, more concerns upon those iodo-interhalogens have to be taken into account. Today there have not been any real observation data available for interhalogens in the remote marine atmosphere. Hence more knowledge of these interactions have to be found out and new analytical methods will be required to observe iodo-interhalogen species in future studies.

Interaction of iodine species and nitrogen oxides (NO, NO_2, or collectively NO_x) may play an very important role in the coastal atmospheric chemistry as well, for instance, the uptake and hydrolysis of $IONO_2$ on aerosol is a potentially important removal pathway for NO_x in the remote troposphere [McFiggans 2000], leading indirectly to increased rate of ozone destruction [Stutz 1999], whereas removal of atmospheric NO_x by halogens may be as important as catalytic halogen cycling in reducing boundary layer ozone concentrations. Still some uncertainties exist in the whole chain, such as formation and decomposition rate of I-N-O species, although more and more possible mechanisms have been suggested by different research groups recently [Carpenter 2003a]. “Is the NO_x chemistry involved in the new aerosol nucleation as well?” and “how and how much is its contribution compared to and together with the iodine species?” are the questions to be answered in marine aerosol research in the future.

Moreover, the issue of nucleation of iodine oxides or thermodynamically stable sulphate clusters (TSCs) is still an open question. Detailed modeling studies of TSC nucleation in the marine boundary layer predict that TSC nucleation can easily occur under ambient conditions [Pirjola 2000], but that these nuclei are rapidly scavenged by the existing aerosol before they can grow into aerosol particles or CCN [O’Dowd 2005]. The addition of condensable iodine vapors (CIVs) to the condensation process increases the survival probability of TSCs as they grow. The suggestion that iodine concentrations could be greater than previously anticipated supports the predictions. Nevertheless, given current understanding of the complex iodine-vapor system, it is not yet possible to determine whether CIV nucleation dominates over TSC nucleation. Whether or not CIVs nucleate and require sulphuric acid to grow nuclei into new aerosol particles, or vice versa, or whether a combination of both species participates in the nucleation and growth processes requires a deeper knowledge of gas-phase iodine processes and the role of iodine oxides in nucleation [O’Dowd 2005].

Modeling of the particle formation from marine iodine emission

Based on the successful modeling with satisfying agreement and using the field monitoring data, it is possible to conduct the simulation of iodine emissions and the prediction for the new particle formation in the marine boundary layer. But indeed, such a prediction has to be treated with caution due to a number of uncertainties in the mechanisms for iodine-related particle formation and growth process. Modeling studies attempting to quantify the effect of iodine chemistry on atmospheric photooxidation chemistry must explicitly include interactions with sea salt bromide and chloride, and coupling of reactive iodine with trace gases including NO_x [Carpenter 2003a]. Previous works on the model studies of particle formation linked to the iodine species emission have been performed in the laboratory, with different models and focusing on the gas-phase precursors such as I_2 [Saiz-Lopez 2005] and CH_2I_2 [Carpenter 2001], and iodine radicals like IO [McFiggans 2000], as well as other halogen species [von Glasow 2002]. However, complicacies inside the models, including the kinetic parameters, uptake coefficients and deposition rates etc. of all the known and unknown mechanisms involved, are not yet thoroughly investigated, so that a great deal of work have to be done for the full model studies in the future.

References

1. *AG® 1, AG MP-1 and AG 2 Strong Anion Exchange Resin Instruction Manual* (Bio-Rad, C.A.).

2. Introduction of Fucus Vesiculosus, in *Guide to Commercially Important Seaweeds on the Irish Coast* 27-29.

3. Introduction of Laminaria Digitata, in *Guide to Commercially Important Seaweeds on the Irish Coast* 18-20.

4. The determination of iodine species in environmental and biological samples (Technical Report). *Pure and Applied Chemistry* **70**, 1567-1584 (1998).

5. Adams, F. C. et al. Speciation of organometal and organohalogen compounds in relation to global environmental pollution. *Analyst* **123** (1998).

6. Adams, J. W. & Cox, R. A. Halogen chemistry of the marine boundary layer. *Journal De Physique Iv* **12**, 105-124 (2002).

7. Al-Ammar, A., Reitznerová, E. & Barnes, R. M. Thorium and iodine memory effects in inductively-coupled plasma mass spectrometry. *Fresenius J Anal Chem* **370**, 479-482 (2001).

8. Alicke, B., Hebestreit, K., Stutz, J. & Platt, U. Iodine oxide in the marine boundary layer. *Nature* **397**, 572-573 (1999).

9. Allan, B. J., Planc, J. M. & Mcfiggans, G. Observations of OIO in the remote marine boundary layer. *Geophysical Research Letters* **28**, 1945-1948 (2001).

10. Ashworth, S. H., Allan, B. J. & Plane, J. M. C. High resolution spectroscopy of the OIO radical: implications for the ozone-depleting potential of iodine in the marine boundary layer. *Geophysical Research Letters* **29**, 1456 (2002).

11. Baker, A. R. Inorganic iodine speciation in tropical Atlantic aerosol. *Geophysical Research Letters* **31**, L23S02 (2004).

12. Baker, A. R., Tunnicliffe, C. & Jickells, T. D. Iodine speciation and deposition fluxes from the marine atmosphere. *Journal of Geophysical Research* **106**, 28743-28749 (2001).

13. Baker, A. R., Thompson, D., Campos, M. L. A. M., Parry, S. J. & Jickells, T. D. Iodine concentration and availability in atmospheric aerosol. *Atmospheric Environment* **34**, 4331-4336 (2000).

14. Barnes, I., Becker, K. H. & Starcke, J. FTIR spectroscopic observation of gaseous HOI. *Chemical Physics Letters* **196**, 258-581 (1992).

15. Bassford, M. R. et al. The concurrent observation of methyl iodide and dimethyl sulphide in marine air; implications for sources of atmospheric methyl iodide. *Atmospheric Environment* **33**, 2373-2383 (1999).

16. Bichsel, Y. & Gunten, U. v. Determination of Iodide and Iodate by Ion Chromatography with Postcolumn Reaction and UV/Visible Detection. *Anal. Chem.* **71**, 34-38 (1999).

17. Bloss, W. J., Rowley, D. M., Cox, R. A. & Jones, R. L. Kinetics and Products of the IO Self-Reaction. *J. Phys. Chem. A* **105**, 7840-7854 (2001).

18. Bouisset, P. et al. Direct gamma-X spectrometry measurement of 129I in environmental samples using experimental self-absorption corrections. *Nuclear Instruments and Methods in Physics Research A* **437**, 114-127 (1999).

19. Brauer, F. P., Rieck, H. G., Jr. & Hooper, R. L. *Particulate and gaseous atmospheric iodine concentrations.* Physical Behaviour of Radioactive Contaminants in the Atmosphere: 351-369 (IAEA, IAEA-SM-181/6, CONF-731110, 20 p., Vienna, 1974).

20. Burkholder, J. B., Curtius1, J., Ravishankara, A. R. & Lovejoy, E. R. Laboratory studies of the homogeneous nucleation of iodine oxides. *Atmospheric Chemistry and Physics Discussions* **3**, 4943-4988 (2003).

21. Calabrese, V. T. & Khan, A. Amylose-Iodine Complex Formation without KI: Evidence for Absence of Iodine Ions within the Complex. *Journal of Polymer Science: Part A: Polymer Chemistry* **37**, 2711-2717 (1999).

22. Carpenter, L. J. Iodine in the Marine Boundary Layer. *Chemical Reviews* **103**, 4953-4962 (2003).

23. Carpenter, L. J., Liss, P. S. & Penkett, S. A. Marine organohalogens in the atmosphere over the Atlantic and Southern oceans. *Journal of Geophysical Research (Atmospheres)* **108**, ACH 1/1 - ACH 1/13 (2003).

24. Carpenter, L. J. & Lewis, A. C. Ocean-atmosphere exchange of reactive halocarbons and hydrocarbons. *Recent Research Developments in Geophysics* **4**, 45-56 (2002).

25. Carpenter, L. J., Hebestreit, K., Platt, U. & Liss, P. S. Coastal zone production of IO precursors: a 2-dimensional study. *Atmos. Chem. Phys.* **1**, 9-18 (2001).

26. Carpenter, L. J., Malin, G., Kuepper, F. & Liss, P. S. Novel biogenic iodine-containing trihalomethanes and other short-lived halocarbons in the coastal East Atlantic. *Global Biogeochem. Cycles* **14**, 1191-1204 (2000).

27. Carpenter, L. J. et al. Short-lived alkyl iodides and bromides at Mace Head, Ireland: links to biogenic sources and halogen oxide production. *Journal of Geophysical Research (Atmospheres)* **104**, 1679-1689 (1999).

28. Chase, M.W. NIST-JANAF thermochemical tables for the iodine oxides. *J. Phys. Chem. Ref. Data* **25**, 1297-1340 (1996).

29. Chen, H., Brandt, R., Jakubowski, N. & Hoffmann, T. Chemical Characterisation of coastal/marine aerosols: Contributions to understand new particle formation from biogenic iodie precursors. *Oral Presentation at the European Geosciences Union (EGU) 1st General Assembly, Atmospheric Session / Nice, France* (2004).

30. Chen, H., Brandt, R., Kuehn, T., Jakubowski, N. & Hoffmann, T. Determination of Iodine in Coastal Atmospheric Particles using Inductively Coupled Plasma Mass Spectrometry (ICP-MS). *Poster in the 2003 European Winter Conference on Plasma Spectrochemistry, Garmisch-Partenkirchen, Germany* (2003).

31. Cooper, L. W. et al. Iodine-129 and plutonium isotopes in Arctic kelp as historical indicators of transport of nuclear fuel-reprocessing wastes from mid-to-high latitudes in the Atlantic Ocean. *Marine Biology* **131**, 391-399 (1998).

32. Cotter, E. S. N., Booth, N. J., Canosa-Mas, C. E. & Wayne, R. P. Release of iodine in the atmospheric oxidation of alkyl iodides and the fates of iodinated alkoxy radicals. *Atmospheric Environment* **35**, 2169-2178 (2001).

33. Cox, R. A., Bloss, W. J., Jones, R. L. & Rowley, D. M. OIO and the atmospheric cycle of iodine. *Geophysical Research Letters* **26**, 1857-1860 (1999).

34. Davis, D. et al. Potential impact of iodine on tropospheric levels of ozone and other critical oxidants. *Journal of Geophysical Research-Atmospheres* **101**, 2135-2147 (1996).

35. Dettmer, K., Knobloch, T. & Engewald, W. Stability of reactive low boiling hydrocarbons on carbon based adsorbents typically used for adsorptive enrichment and thermal desorption. *Fresenius J Anal Chem* **366**, 70-78 (2000).

36. Diemer, J. & Heumann, K. G. Bromide/bromate speciation by NTI-IDMS and ICP-MS coupled with ion exchange chromatography. *Fresenius J. Anal. Chem.* **357**, 74-79 (1997).

37. Eiceman, G. A., Hill, J. H. H. & Gardea-Torresdey, J. Gas Chromatography. *Anal. Chem.* **70**, 321R-339R (1998).

38. Fan, B. J., Cheng, Y. S. & Yeh, H. C. Gas collection efficiency and entrance flow effect of an annular diffusion denuder. *Aerosol Science and Technology* **25**, 113-120 (1996).

39. Fecher, P. A., Goldmann, I. & Nagengast, A. Determination of iodine in food samples by inductively coupled plasma mass spectrometry after alkaline extraction. *Journal of Analytical Atomic Spectrometry* **13**, 977-982 (1998).

40. Fick, J., Pommer, L., Andersson, B. & Nilsson C. Ozone removal in the sampling of Parts per Billion Levels of Terpenoid Compounds: An Evaluation of Different Scrubber Materials. *Environ. Sci. Technol.* **35**, 1458-1462 (2001).

41. Frieß, U., Wagner, T., Pundt, I., Pfeilsticker, K. & Platt, U. Spectroscopic Measurement of Tropospheric Iodine Oxide at the Neumayer Station, Antarctica. *Geophysical Research Letters* **28**, 1941-1944 (2001).

42. Gaebler, H. E. & Heumann, K. G. Determination of atmospheric iodine species using a system of specificly prepared filters and IDMS. *Fresenius J. Anal. Chem.* **345**, 53-59 (1993).

43. Gaebler, H. E. & Heumann, K. G. Determination of particulate iodine in aerosols from different regions by size fractionating impactor sampling and IDMS. *Int. J. Environ. Anal. Chem.* **50**, 129-146 (1993).

44. Garland, J. A. & Curtis, H. Emission of iodine from the sea surface in the presence of ozone. *J. Geophys. Res.* **86**, 3183-3196 (1981).

45. Gélinas, Y., Iyengar, G. V. & Barnes, R. M. Total iodine in nutritional and biological reference materials using neutron activation analysis and inductively coupled plasma mass spectrometry. *Fresenius J Anal Chem* **362**, 483-488 (1998).

46. Giese, B., Laturnus, F., Adams, F. C. & Wiencke, C. Release of Volatile Iodinated C1-C4 Hydrocarbons by Marine Macroalgae from Various Climate Zones. *Environmental Science and Technology* **33**, 2432-2439 (1999).

47. Gormley, P. & Kennedy, M. Denuder Principle and Equation. *Proc. R. Ir. Acad.* **52A**, 163-169 (1949).

48. Grenfell, J. L. et al. An analysis of rapid increases in condensation nuclei concentration at a remote coastal site in western Ireland. *Journal of Geophysical Research* **104**, 13771-13780 (1999).

49. Gross, J. H. Chapter 5 Electron Ionization in *Mass Spectrometry* (Spinger-Verlag, Berlin, 2004).

50. Grüter, U. M., Kresimon, J. & Hirner, A. V. A new HG/LT-GC/ICP-MS multi-element speciation technique for real samples in different matrices. *Fresenius J Anal Chem* **368**, 67-72 (2000).

51. Guo, Z. X. et al. Continuous Monitoring of Sulfur Dioxide with a Gas Permeation Denuder-Based System. *Microchim. Acta* **141**, 183-189 (2003).

52. Haldimann, M., Eastgateb, A. & Zimmerli, B. Improved measurement of iodine in food samples using inductively coupled plasma isotope dilution mass spectrometry. *Analyst* **125**, 1977-1982 (2000).

53. Heumann, K. G., Gallus, S. M., Rälinger, G. & Vogl, J. Accurate determination of element species by on-line coupling of chromatographic system with ICP-MS using isotope dilution technique. *Spectrochimica Acta Part B* **53**, 273-287 (1998).

54. Hinds, W. C. Chapter 5. Straight-line Acceleration and Curvilinear Particle Motion, Chapter 7. Browniar Motion and Diffusion, Chapter 9. Filtration, in *Aerosol Technology* (ed. Hinds, W. C.) (1999).

55. Hoffmann, T., O'Dowd, C. D. & Seinfeld, J. H. Iodine oxide homogeneous nucleation: An explanation for coastal new particle production. *Geophysical Research Letters* **28**, 1949-1952 (2001).

56. Hofmann, K.A. Lehrbuch für Anorganische Chemie (1924)

57. Holleman, A. F. & Wiberg, E. Part B Main Group Elements, XII. The Halogen Group, in *Inorganic Chemistry* (ed. Wiberg, N.) 402-469 (Academic Press, Berlin, 2001).

58. Holmes, N. S., Adams, J. W. & Crowley, J. N. Uptake and reaction of HOI and on frozen and dry IONO2 NaCl/NaBr surfaces and H_2SO_4. *Phys. Chem. Chem. Phys.* **3**, 1679-1687 (2001).

59. Hon, P. K., Mak, T. C. W. & James, T. Synthesis and Structure of l-Methyl-1,3,5,7-tetraazaadamantan-l-ium Octaiodide, $[(CH_2)_6N_4CH_3]_2I_8$. A New Outstretched 2 Configuration for the Polyiodide Ion I82-. *Inorganic Chemistry* **18**, 2916-2918 (1979).

60. Hou, X., Dahlgaard, H., Rietz, B., Jacobsen, U. & Nielsen, S.P. Pre-separation neutron activation analysis of seawater urine and milk for iodide and iodate. *Journal of Radioanalytical and Nuclear Chemistry* **244**, 87-91 (2000).

61. Hou, X. et al. Determination of Chemical Species of Iodine in Seawater by Radiochemical Neutron ActivationAnalysis Combined with Ion-Exchange Preseparation. *Anal. Chem.* **71**, 2745-2750 (1999).

62. Houk, R.S. *Anal. Chem.* **58**, 97A-104A (1986).

63. Huang, S., Arimoto, R. & Rahn, K. A. Sources and source variations for aerosol at Mace Head, Ireland. *Atmospheric Environment* **35**, 1421-1437 (2001).

64. Jalkanen, L. & Manninen, P. Multivariate data analysis of aerosols collected on the Gulf of Finland. *Environmetrics* **7**, 27-38 (1996).

65. Jenkin, M. E. *The photochemistry of iodine-containing compounds in the marine boundary layer*; Environ. and Energy Rep. AEA EE-0405; AEA Harwell Lab.; Oxfordshire, England (1992)

66. Jimenez, J. L. et al. New particle formation from photooxidation of diiodomethane. *Journal of Geophysical Research* **108**, 4318 (2003).

67. Jing, H. & Amirav, A. Pesticide analysis with the pulsed-flame photometer detector and a direct sample introduction device. *Anal. Chem.* **69**, 1426-1435 (1997).

68. Katsanos, N. A. & Roubani-Kalantzopoulou, F. Denuder tubes used with gas chromatographic instrumentation to measure rate coeffients and equilibrium constants. *Journal of Chromatography A* **710**, 191-228 (1995).

69. Keppler, F., Eiden, R., Niedan, V., Pracht, J. & Schoeler, H. F. Halocarbons produced by natural oxidation processes during degradation of organic matter. *Nature* **403**, 298-301 (2000).

70. Kloskowski, A., Pilarczyk, M. & Namiesnik, J. Denudation - A convenient method of isolation and enrichment of analytes. *Critical Reviews in Analytical Chemistry* **32**, 301-335 (2002).

71. Knapp, G., Maichin, B., Fecher, P., Hasse, S. & Schramel, P. Iodine determination in biological materials Options for sample preparation and final determination. *Fresenius J Anal Chem* **362**, 508-513 (1998).

72. Kolb, C. E. Iodine's air of importance. *Nature* **417**, 597-598 (2002).

73. Komenda, M., Parusel, E., Wedel, A. & Koppmann, R. Measurements of biogenic VOC emissions: sampling, analysis and calibration. *Atmospheric Environment* **35**, 2069-2080 (2001).

74. Kritz, M. A. & Rancher, J. Circulation of Na, Cl, and Br in the tropical marine atmosphere. *J. Geophys. Res.* **85C**, 1633–1639 (1980).

75. Kulmala, M. et al. Aerosol formation during PARFORCE: Ternary nucleation of H2SO4, NH3 and H2O. *Journal of Geophysical Research* **107**, 8111 (2002).

76. Küpper, F. C., Müller, D. G., Peters, A. F., Kloareg, B. & Phillppe, P. Oligoalginate recognition and oxidative burst play a key role in natural and induced resistance of sporophytes of laminariales. *J. Chem. Ecol* **28**, 2057-2081 (2002).

77. Küpper, F. C. et al. Iodine uptake in Laminariales involves extracellular, haloperoxidase-mediated oxidation of iodine. *Planta* **207**, 163-171 (1998).

78. Laturnus, F. Marine Macroalgae in Polar Regions as Natural Sources for Volatile Organohalogens. *Environ Sci & Pollut Res* **8**, 103-108 (2001).

79. Laturnus, F., Giese, B., Wiencke, C. & Adams, F. C. Low-molecular-weight organoiodine and organobromine compounds released by polar macroalgae – The influence of abiotic factors. *Fresenius J Anal Chem* **368** (2000).

80. Leiterer, M., Truckenbrodt, D. & Franke, K. Determination of iodine species in milk using ion chromatographic separation and ICP-MS detection. *Eur Food Res Technol* **213**, 150-153 (2001).

81. Li, H. J., Yokouchi, Y. & Akimoto, H. Measurement of methyl halides in the marine atmosphere. *Atmospheric Environment* **33**, 1881-1887 (1999).

82. Lyman, W. J., Reehl, W. F. & Rosenblatt, D. H. Chapter 17: Diffusion Coefficients in Air and Water by William A. Tucker and Leslie H. in *Nelken of the "Handbook of Chemical Property Estimation Methods"* (American Chemical Society, 1990).

83. Lovelock, J. E. Natural halocarbons in the air and in the sea. *Nature* **256**, 193-194 (1975).

84. Mader, B. T., Flagan, R. C. & Seinfeld, J. H. Sampling Atmospheric Carbonaceous Aerosols Using a Particle Trap Impactor/Denuder Sampler. *Environ. Sci. Technol.* **35**, 4857-4867 (2001).

85. Mäkelä, J. M. et al. Biogenic iodine emissions and identification of end-products in coastal ultrafine particles during nucleation bursts. *Journal of Geophysical Research* **107**, 8110 (2002).

86. March, R. E. An Introduction to Quadrupole Ion Trap Mass Spectrometry. *J. Mass Spectrometry* **32**, 351-369 (1997).

87. Mcfiggans, G. Atmospheric science: Marine aerosols and iodine emissions (Arising from: O'Dowd C. et al. Nature 417, 632-636, 2002). *Nature* **433**, E13 (2005)

88. McFiggans, G. et al. Direct evidence for coastal iodine particles from Laminaria macroalgae – linkage to emissions of molecular iodine. *Atmospheric Chemistry and Physics Discussions* **4**, 939-967 (2004).

89. McFiggans, G., Cox, R. A., Mossinger, J. C., Allan, B. J. & Plane, J. M. C. Active chlorine release from marine aerosols: Roles for reactive iodine and nitrogen species. *Journal of Geophysical Research-Atmospheres* **107** (2002).

90. McFiggans, G. et al. A modeling study of iodine chemistry in the marine boundary layer. *Journal of Geophysical Research-Atmospheres* **105**, 14371-14385 (2000).

91. McLuckey, S. A. & Wells, J. M. Mass Analysis at the Advent of the 21st Century. *Chemical Reviews* **101**, 571-606 (2001).

92. Middlebrook, A. M., Murphy, D. M. & Thomson, D. S. Observations of organic material in individual marine particles at Cape Grim during the First Aerosol Characterization Experiment (ACE 1). *Journal of Geophysical Research-Atmospheres* **103**, 16475-16483 (1998).

93. Misra, A. & Marshall, P. Computational investigations of iodine oxides. *J. Phys. Chem. A* **102**, 9056-6060 (1998).

94. Miyake, Y. & Tsunogai, S. Evaporation of iodine from the ocean. *J. Geophys. Res.* **68**, 3989-3993 (1963).

95. Moore, R. M. Marine source of volatile Organohalogens, in *The Handbook of Environmental Chemistry, Vol.3, Part P* 85-101 (Springer-Verlag, Berlin, 2003).

96. Mössinger, J. C. & Cox, R. A. Heterogenous Reaction of HOI with sodium halide salts. *J. Phys. Chem. A* **105**, 5165-5177 (2001).

97. Moyers, J. L. & Duce, R. A. Gaseous and particulate iodine in the marine atmosphere. *J. Geophys. Res.* **77**, 5229-5238 (1972).

98. Murphy, D. M., Thomson, D. S. & Middlebrook, A. M. Bromine, iodine, and chlorine in single aerosol particles at Cape Grim. *Geophysical Research Letters* **24**, 3197-3200 (1997).

99. Noguchi, H. & Murata, M. Physicochemical speciation of airborne ^{131}I in Japan from Chernobyl. *J. Environ. Radioact.* **7**, 65-74 (1988).

100. O'Dowd, C. D. et al. Atmospheric science: Marine aerosols and iodine emissions (Reply). *Nature* **433**, E13-E14 (2005).

101. O'Dowd, C. D. et al. Marine aerosol formation from biogenic iodine emissions. *Nature* **417**, 632-634 (2002).

102. O'Dowd, C. D., Hämeri, K., Mäkelä, J., Väkeva, M. & Aalto, P. Coastal new particle formation: Environmental conditions and aerosol physicochemical characteristics during nucleation bursts. *Journal of Geophysical Research* **107**, 8107 (2002).

103. O'Dowd, C. D. et al. A dedicated study of New Particle Formation and Fate in the Coastal Enviroment (PARFORCE): Overview of objectives and achievements. *Journal of Geophysical Research* **107**, 8108 (2002).

104. O'Dowd, C. D. et al. On the photochemical production of new particles in the coastal boundary layer. *Geophysical Research Letters* **26**, 1707-1710 (1999).

105. O'Dowd, C. D., Geever, M., Hill, M. K., Smith, M. H. & Jennings, S. G. New Particle formation: Nucleation rates and spatial scales in the clean marine coastal environment. *Geophysical Research Letters* **25**, 1661-1664 (1998).

106. Ophardt, C. E. in *Starch - Iodine Test -- Virtual Chembook* (http://www.elmhurst.edu/~chm/vchembook/548starchiodine.html, 2003).

107. Peskova, J., Parizek, P. & Vecera, Z. Wet effluent diffusion denuder technique and determination of volatile organic compounds in air: I. Oxo compounds (alcohols and ketones). *Journal of Chromatography A* **918**, 153-158 (2001).

108. Pirjola, L, O'Dowd, C.D., Brooks, I.M. & Kulmala, M. Can new particle formation occur in the clean marine boundary layer? *J. Geophys. Res.* **105**, 26531-26546 (2000).

109. Rädlinger, G. & Heumann, K. G. Iodine Determination in Food Samples Using Inductively Coupled Plasma Isotope Dilution Mass Spectrometry. *Anal. Chem.* **70**, 2221-2224 (1998).

110. Rahn, K. A., Borys, R. D. & Duce, R. A. Determination of Inorganic and Organic Components of Gaseous Chlorine, Bromine, and Iodine in The Atmosphere. *WMO [Publ.] (Air Pollut. Meas. Tech.), Part-II.* **460**, 172-1728 (1977).

111. Rendleman, J. A. The reaction of starch with iodine vapor. Determination of iodide-ion content of starch-iodine complexes. *Carbohydrate Polymers* **51**, 191-202 (2003).

112. Richardson, S. D. Environmental Mass Spectrometry: Emerging Contaminants and Current Issues. *Anal. Chem.* **76**, 3337-3364 (2004).

113. Rosenfeld, L. Discovery and early uses of iodine. *Journal of Chemical Education* **77**, 984-987 (2000).

114. Rosman, K. et al. Laboratory and field investigations of a newand simple design for the parallel plate denuder. *Atmospheric Environment* **35**, 5301-5310 (2001).

115. Rowley, D. M., Bloss, W. J., Cox, R. A. & Jones, R. L. Kinetics and Products of the IO + BrO Reaction. *J. Phys. Chem. A* **105**, 7855-7864 (2001).

116. Saiz-Lopez, A. et al. Molecular iodine emissions in coastal marine environments: the link to new particle formation. *Atmos. Chem. Phys.* **(in press)** (2005).

117. Saiz-Lopez, A., Saunders, R. W., Joseph, D. M., Ashworth, S. H. & Plane, J. M. C. Absolute absorption cross-section and photolysis rate of I_2. *Atmos. Chem. Phys.* **4**, 1443-1450 (2004).

118. Saiz-Lopez, A. & Plane, J. M. C. Novel iodine chemistry in the marine boundary layer. *Geophysical Research Letters* **31**, L04112 (2004).

119. Schall, C., Heumann, K. G. & Kirst, G. O. Biogenic volatile organoiodine and organobromine hydrocarbons in the Atlantic Ocean from 42°N to 72°S. *Fresenius J. Anal. Chem.* **359**, 298-305 (1997).

120. Schall, C. & Heumann, K. G. GC determination of volatile organoiodine and organobromine compounds in Arctic seawater and air samples. *Fresenius J. Anal. Chem.* **346**, 717-722 (1993).

121. Schwarz, A. & Heumann, K. G. Biogenically produced halocarbons determinated by two-dimensional detection with ECD and ICP-MS after GC-separation. *Poster in AFO2000* (2000).

122. Schwehr, K. A. & Santschi, P. H. A Sensitive Determination of Iodide Species in Fresh or Saline Matrixes Using High Performance Chromatography and UV/Visible Detection. *http://loer.tamug.tamu.edu Poster* (2002).

123. Schwehr, K. A. & Santschi, P. H. Sensitive determination of iodine species, including organo-iodine, for freshwater and seawater samples using high performance liquid chromatography and spectrophotometric detection. *Analytica Chimica Acta* **482**, 59-71 (2003).

124. Seinfeld, J. H. & Spyros, N. P. Chapter 8 Brownian motion of aerosol particles, in *Atmospheric chemistry and physics: From air pollution to climate change* (John Wiley & Sons, Inc., 1998).

125. Simon, P. K. & Dasgupta, P. K. Wet Effluent Denuder Coupled Liquid/ Ion Chromatography Systems: Annular and Parallel Plate Denuders. *Anal. Chem.* **65**, 1134-1139 (1993).

126. Simon, P. K. & Dasgupta, P. K. Continuous Automated Measurment of Gaseous Nitrous and Nitric Acids and Particlate Nitrite and Nitrate. *Environ Sci. Technol.* **29**, 1534-1541 (1995).

127. Singh, H. B., Salas, L. J. & Stiles, R. E. Methyl halides in and over the eastern Pacific (40 N-32 S). *J. Geophys. Res.* **88**, 3684-3690 (1983).

128. Sioutas, C., Wang, P. Y., Ferguson, S. T. & Koutrakis, P. Laboratory and field evaluation of an improved glass honeycomb denuder/filter pack sampler. *Atmospheric Environment* **30**, 885-895 (1996).

129. Sklenska, J., Broskovicova, A. & Vecera, Z. W et effluent diffusion denuder technique and the determination of volatile organic compounds in air: II. Monoterpenes. *Journal of Chromatography A* **973**, 211-216 (2002).

130. Slanina, J. et al. The continuous analysis of nitrate and ammonium in aerosols by the steam jet aerosol collector (SJAC): extension and validation of the methodology. *Atmospheric Environment* **35**, 2319-2330 (2001).

131. Slingo, A. Sensitivity of the Earth's radiation budget to changes in the low clouds. *Nature* **343**, 49-51 (1990).

132. Spanke, J. Ph.D thesis “Beiträge zur Klärung der biogenen Partikelbildung über borealen Nadelwäldern in *Chemistry Department* 130 (University of Dortmund, Germany, 2002).

133. Stutz, J., Hebestreit, K., Alicke, B. & Platt, U. Comparison of model calculations with recent field data. *J. Atmos. Chem.* **34**, 65-85 (1999)

134. Swartz, E. & Stockburger, L. Recovery of Semivolatile Organic Compounds during Sample Preparation: Implications for Characterization of Airborne Particulate Matter. *Environ. Sci. Technol.* **37**, 597-605 (2003).

135. Taira, M. & Kanda, Y. Wet Effluent Diffusion Denuder for Sampling of Atmospheric Gaseous Nitric Acid. *Anal. Chem.* **65**, 3171-3173 (1993).

136. Thompson, A. M. & Zafiriou, O. C. Air-sea fluxes of transient atmospheric species. *J. Geophys. Res.* **88**, 6696-6708 (1983).

137. Tsunogai, S. Iodine in the deep water of the ocean. *Deep-Sea Res.* **18**, 913-919 (1971).

138. Ullman, W. J., G.W., L., G.J., d. L. & J.R.W., W. Iodine chemistry in deep anoxic basins and overlying waters of the Mediterranean Sea. *Marine Chemistry* **31**, 153-170 (1990).

139. Vestal, M. L. Methods of Ion Generation. *Chemical Reviews* **101**, 361-375 (2001).

140. Vogt, R. Iodine Compounds in the Atmosphere, in *The Handbook of Environmental Chemistry Vol. 4 Part E* 114-128 (Springer-Verlag, Berlin Heidelberg, 1999).

141. Vogt, R., Sander, R., Glasow, R. v. & Crutzen, P. J. Iodine Chemistry and its Role in Halogen Activation and Ozone Loss in the Marine Boundary Layer: A Model Study. *Journal of Atmospheric Chemistry* **32**, 375–395 (1999).

142. Voillelique, P. G. Iodine Species in Reactor Effluents and in the Environment. *EPRI-NP-1269, Electric Power Research Institute.* (1979).

143. Waite, T. J. & Truesdale, V. W. Iodate reduction by Ioschrysis galbana is relatively insensitive to de-activation of nitrate reductase activity - are phytoplankton really responsible for iodate reduction in seawater? *Marine Chemistry* **81**, 137-148 (2003).

144. Wershofen, H. & Aumann, D. C. Iodine-129 in the environment of a nuclear fuel reprocessing plant: VII. Concentrations and chemical forms of ^{129}I and ^{127}I in the atmosphere. *J. Environ. Radioact.* **10**, 141-156 (1989).

145. Wever, R., Tromp, M. G. M., Krenn, B. E., Marjani, A. & Van Tol, M. Brominating activity of the seaweed ascophyllum nodosum: impact on the biosphere. *Environ Sci. Technol.* **25**, 446-449 (1991).

146. Wimschneider, A. & Heumann, K. G. Iodine speciation in size fractionated atmospheric particles by isotope dilution mass spectrometry. *Fresenius J. Anal. Chem.* **353**, 191-196 (1995).

147. Wren, J. C., Ball, J. M. & Glowa, G. A. The chemistry of iodine in containment. *Nuclear Technology* **129**, 297-325 (1999).

148. Yokouchi, Y. et al. Distribution of methyl iodide, bromoform and dibromomethane over the ocean (east and southeast Asian Seas and the western Pacific). *J. Geophys. Res.* **102**, 8805-8809 (1997).

149. Yokouchi, Y., Barrie, L. A., Toom, D. & Akimoto, H. The seasonal variation of selected natural and anthropogenic halocarbons in the arctic troposphere. *Atmospheric Environment* **30**, 1723-1727 (1996).

150. Yoon, Y. J. et al. Biogenic Aerosol and Gas Flux study in and around Mace Head. *Proc. e 16th International Conf. Nucleation and Atmospheric Aerosols (ICNAA)/ Kyoto, Japan* (eds Kasahara, M. & Kulmala, M.) 674-677 (Kyoto University Press 2004).

151. Yoshida, S. & Muramatsu, Y. Determination of organic, inorganic and particulate iodine in the coastal atmosphere of Japan. *Journal of Radioanalytical and Nuclear Chemistry* **196**, 295-302 (1995).

Appendix I.

Mass Spectra of some Iodo-Hydrocarbons (VOIs)

[from NIST/EPA/NIH Mass Spectral Library, Version 2.0, 2001]

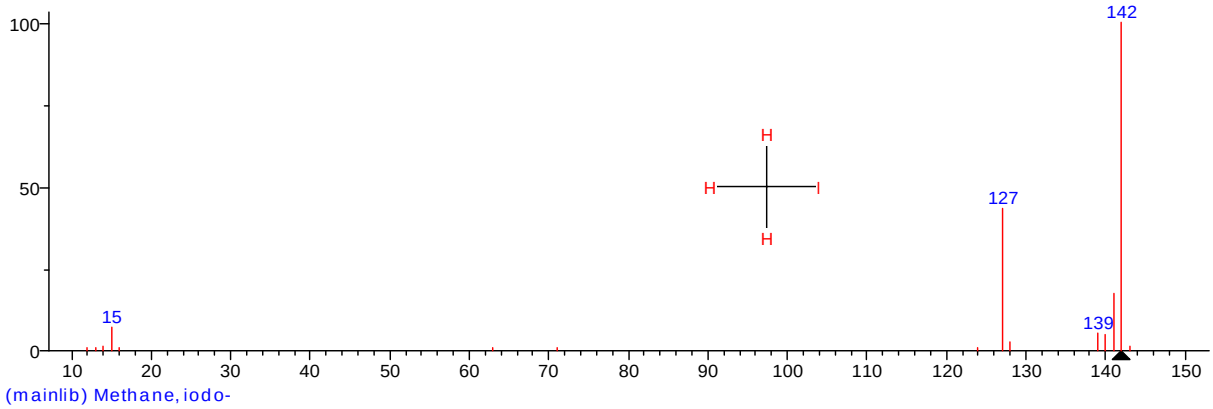

A.I-1 Mass Spectra of Iodo-Methane (CH_3I)

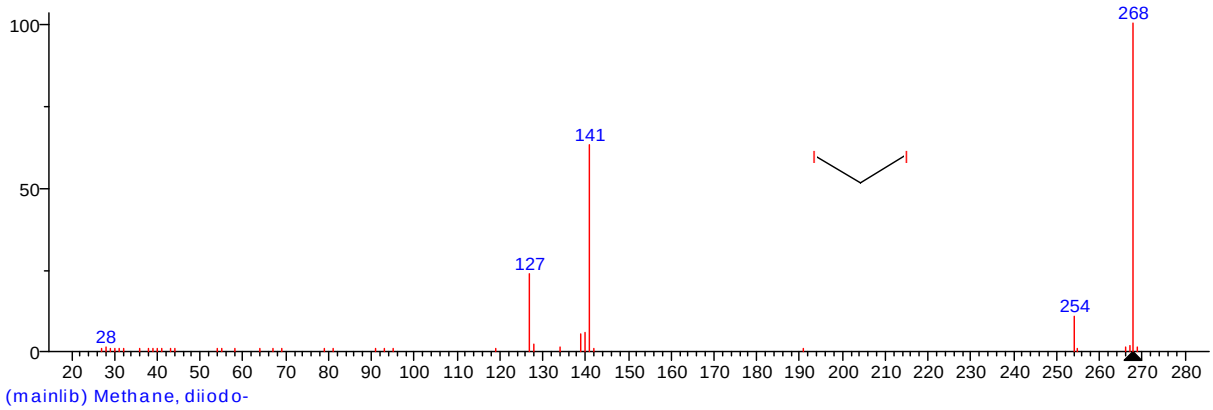

A.I-2 Mass Spectra of Diiodo-Methane (CH_2I_2)

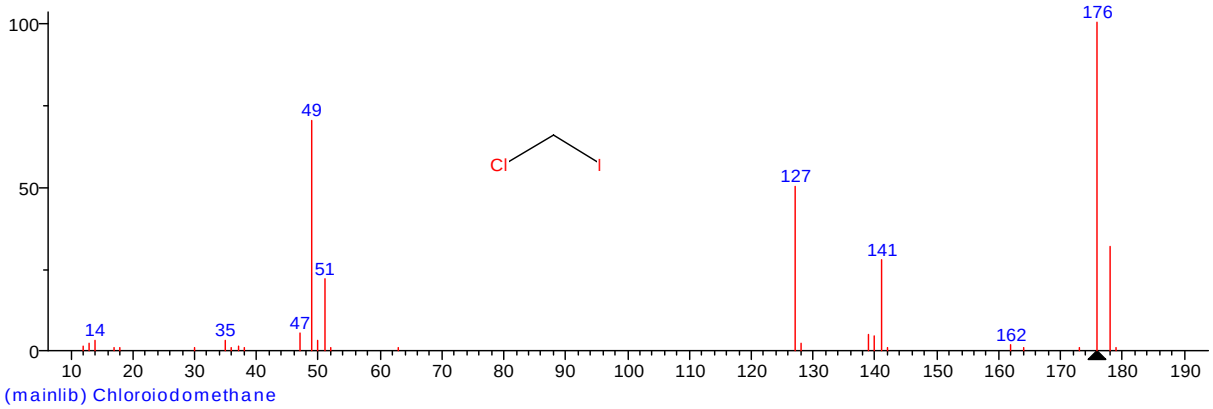

A.I-3 Mass Spectra of Chloro-Iodo-Methane (CH_2ICl)

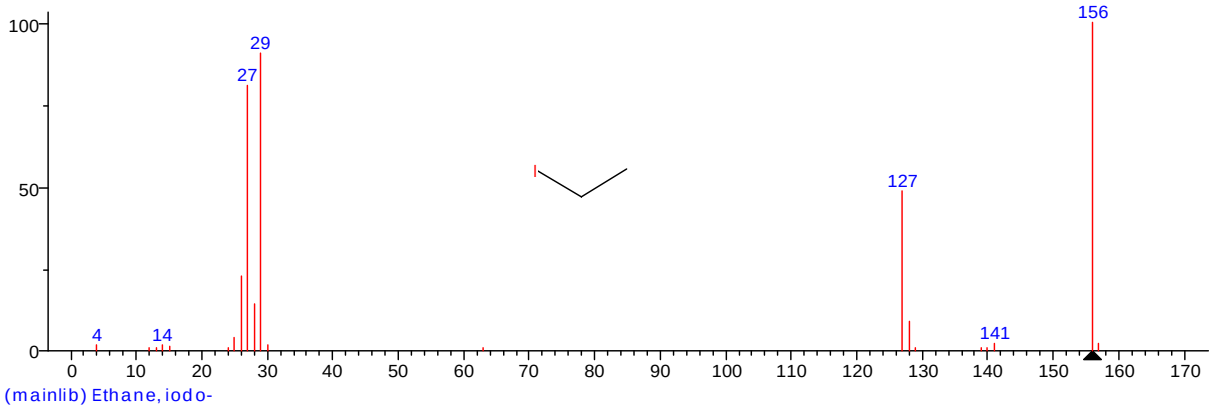

A.I-4 Mass Spectra of Iodo-Ethane (C_2H_5I)

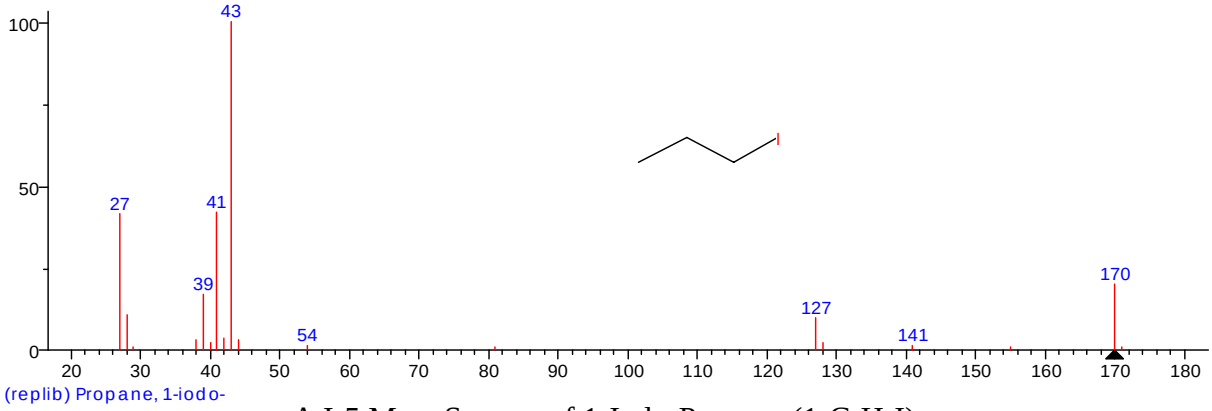

A.I-5 Mass Spectra of 1-Iodo-Propane (1-C_3H_7I)

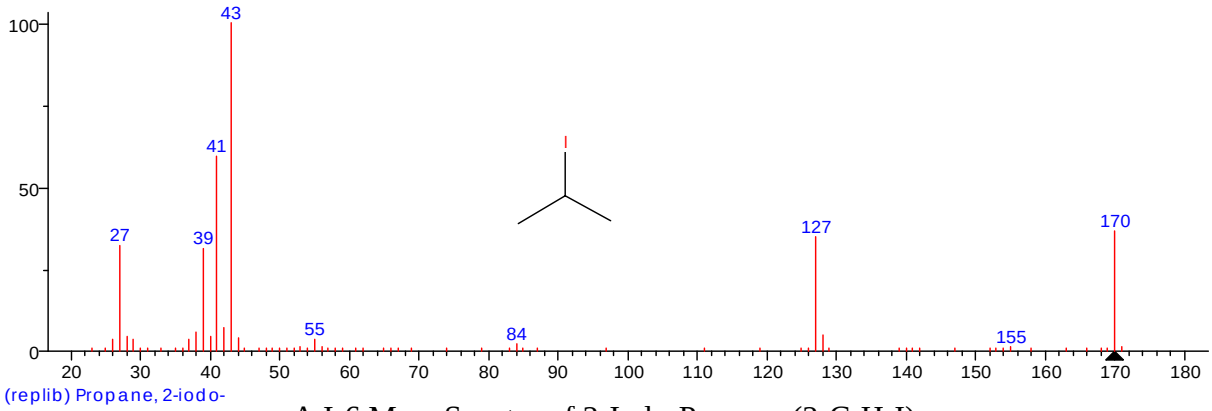

A.I-6 Mass Spectra of 2-Iodo-Propane (2-C_3H_7I)

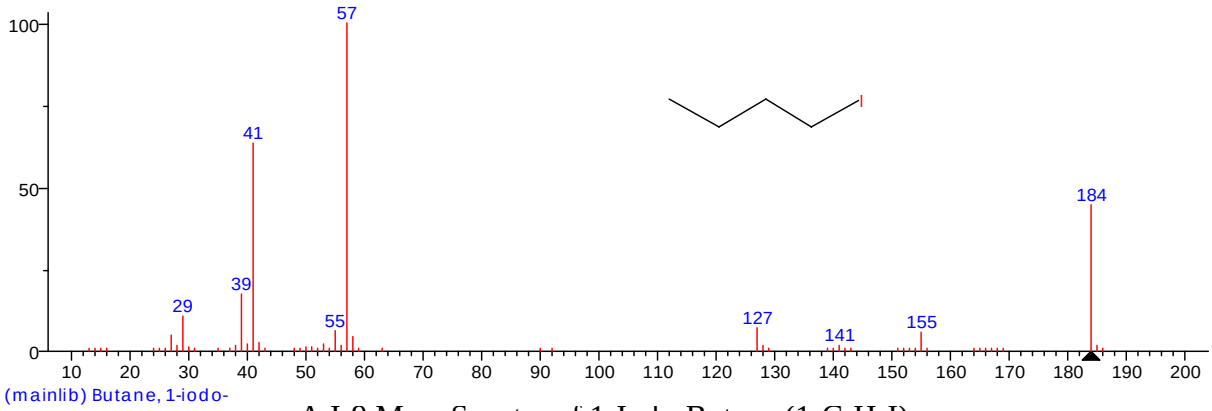

A.I-9 Mass Spectra of 1-Iodo-Butane (1-C_4H_9I)

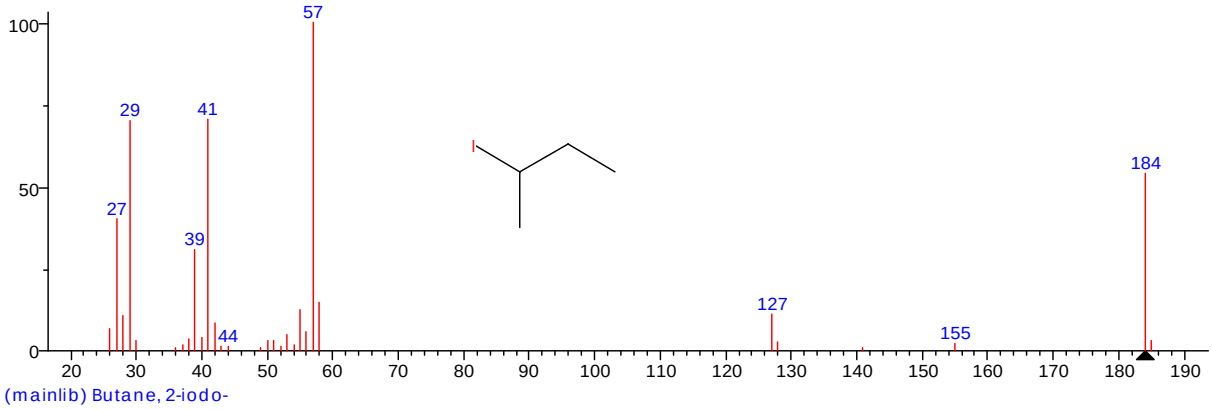

A.I-9 Mass Spectra of 2-Iodo-Butane (2-C_4H_9I)

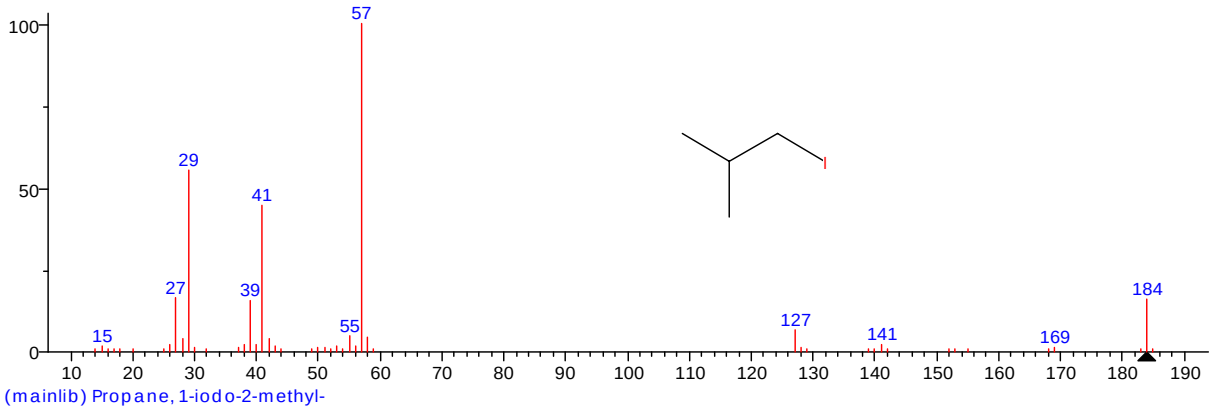

A.I-10 Mass Spectra of 1-Iodo-2-Methyl-Propane (C_4H_9I)

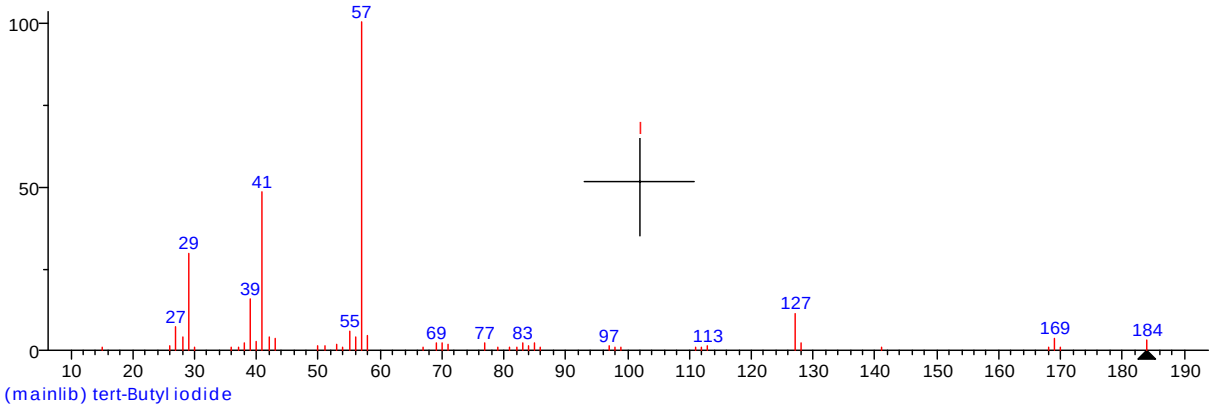

A.I-11 Mass Spectra of Tert-Butyl Iodide (C_4H_9I)

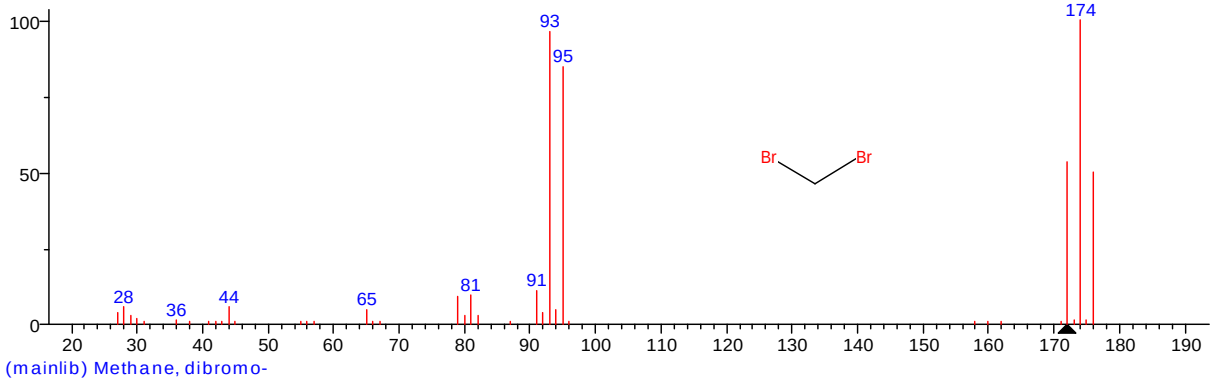

A.I-12 Mass Spectra of Di-Bromo Methane (CH_2Br_2)

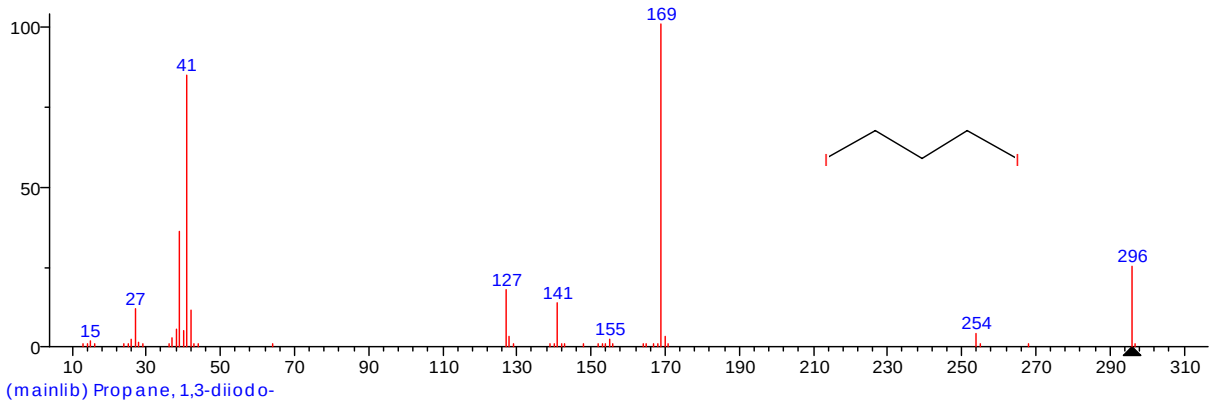

A.I-13 Mass Spectra of 1,3-Di-Iodo Methane (CHI_3)

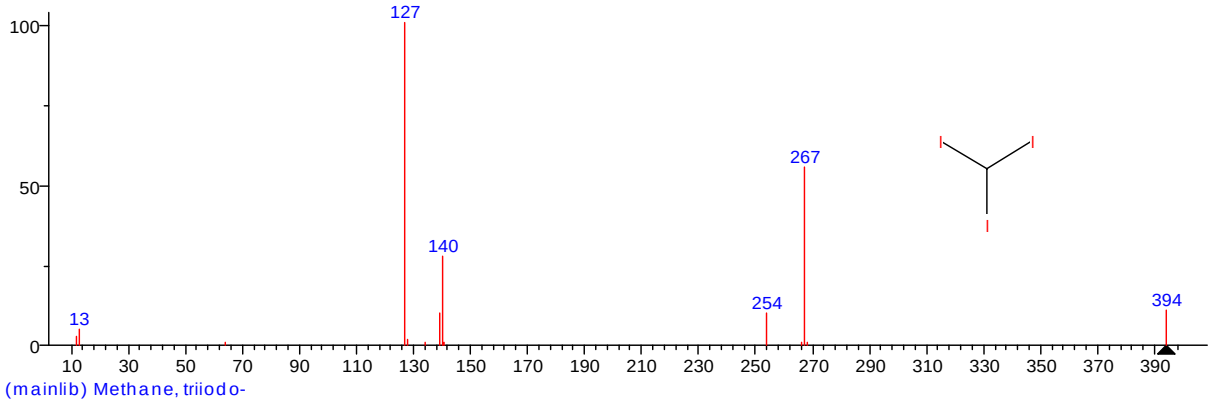

A.I-14 Mass Spectra of Tri-Iodo Methane (CHI_3)

Appendix II.

Table of Data

Table A.II-1 Total iodine measurement in the PM2.5 particles during the Quest Campaign at MHARS western coast Ireland 2002

Sample No.	Date in 2002	Sampling time	Sampling flow / $m^3 \cdot h^{-1}$	**Total iodine Con. / $ng \cdot m^{-3}$**
1.	May 25	08:30 ~ 14:00	2.67	**1.69**
2.	May 26	08:30 ~ 14:30	1.77	**2.51**
3.	May 26	14:45 ~ 19:30	1.81	**0.92**
4.	May 26 ~27	19:45 ~ 08:40	1.77	**0.61**
5.	May 27	08:50 ~ 15:20	1.73	**1.32**
6.	May 27	15:30 ~ 20:30	1.89	**0.58**
7.	May 27 ~ 28	20:40 ~ 09:20	1.61	**4.07**
8.	May 28 ~ 29	16:20 ~ 09:20	1.73	**1.06**
9.	May 29	09:30 ~ 20:20	1.29	**3.13**
10.	May 29 ~ 30	20:27 ~ 09:10	1.81	**1.02**
11.	May 30	09:20 ~ 18:00	5.66	**0.29**
12.	May 30 ~31	18:20 ~ 09:00	3.29	**1.09**
13.	May 31	09:15 ~ 19:30	3.50	**3.03**
14.	May 31~ Jun 01	20:40 ~ 07:10	3.46	**1.44**
15.	Jun 01	07:20 ~ 19:40	3.37	**1.80**
16.	Jun 01 ~ 02	19:55 ~ 08:45	3.50	**3.20**
17.	Jun 02	09:00 ~ 19:20	3.91	**1.66**
18.	Jun 02 ~ 03	19:30 ~ 08:35	3.37	**1.41**
19.	Jun 03	08:47 ~ 18:35	3.50	**0.80**
20.	Jun 03 ~ 04	18:45 ~ 09:40	4.33	**2.28**
21.	Jun 04	20:10 ~ 09:10	3.29	**1.33**
22.	Jun 05	09:25 ~ 20:14	3.67	**1.13**
23.	Jun 05 ~ 06	20:22 ~ 09:50	3.13	**2.93**
24.	Jun 06	10:00 ~ 22:00	3.37	**3.21**
25.	Jun 06 ~ 07	22:15 ~ 10:15	3.46	**1.50**
26.	Jun 07	10:25 ~ 21:55	3.46	**2.90**

Note:
All particle samples were taken by using the filteration and measured by ICP-MS after extraction (detail in section 3.1.1 and 3.2.1). Sampling was performed in the whole campaign, including golden-week and non-golden-week.

Table A.II-2 Total iodine measurement in the size-fractionated particles during the Quest Campaign at MHARS western coast Ireland 2002

Sample No.	Date in 2002	Sampling time	Impactor stage	**Total iodine Con. / ng·m^{-3}**	Σ Total iodine Con.* / ng·m^{-3}
1.	May 31 ~ Jun 01	09:40 ~ 07:20	1	**0.09**	**2.27**
			2	**0.31**	
			3	**0.60**	
			4	**0.82**	
			5	**0.45**	
2.	Jun 01 ~ 02	07:35 ~ 08:50	1	**0.12**	**1.95**
			2	**0.31**	
			3	**0.34**	
			4	**0.69**	
			5	**0.48**	
3.	Jun 02 ~ 03	09:20 ~ 08:38	1	**0.07**	**1.29**
			2	**0.12**	
			3	**0.27**	
			4	**0.50**	
			5	**0.334**	
4.	Jun 03 ~ 04	09:10 ~ 09:50	1	**0.00**	**0.92**
			2	**0.05**	
			3	**0.19**	
			4	**0.42**	
			5	**0.26**	
5.	Jun 05 ~ 06	07:35 ~ 08:50	1	**0.26**	**2.62**
			2	**0.55**	
			3	**0.67**	
			4	**0.60**	
			5	**0.54**	
6.	Jun 06	10:12 ~ 20:06	1	**0.32**	**2.91**
			2	**0.56**	
			3	**0.51**	
			4	**0.98**	
			5	**0.54**	

Continued in next page…

Continued…

Table A.II-2 Total iodine measurement in the size-fractionated particles during the Quest Campaign at MHARS western coast Ireland 2002

Sample No.	Date in 2002	Sampling time	Impactor stage	**Total iodine Con. / ng·m^{-3}**	Σ Total iodine Con.* / ng·m^{-3}
7.	Jun 06 ~ 07	20:21 ~ 08:29	1	**0.29**	**2.44**
			2	**0.53**	
			3	**0.69**	
			4	**0.48**	
			5	**0.45**	
8.	Jun 07 ~ 08	08:49 ~ 08:52	1	**0.22**	**1.96**
			2	**0.51**	
			3	**0.36**	
			4	**0.35**	
			5	**0.53**	
9.**	Jun 08	09:19 ~ 15:20	1	**5.00 ng**	**49.60 ng**
			2	**13.33 ng**	
			3	**10.99 ng**	
			4	**8.89 ng**	
			5	**11.40 ng**	

Note:
All particle samples were taken by using the berner-impaction and measured by ICP-MS after extraction (detail in section 3.1.2 and 3.2.2). Sampling flow was fixed to 4.3 $m^3 \cdot h^{-1}$ for all the samples. Sampling was performed in the second half of the campaign, the non-golden-week.

Impactor stage No. 1 ~ 5 stand for the 5 size-fractionated of $D_{50\%}$ / µm: >5.90, 2.00 ~ 5.90, 0.71 ~ 2.00, 0.25 ~ 0.71, 0.08 ~0.25.

**Σ Total Iodine Concentration stands for the total iodine in the 5 stages of the impactor.*

***Sample No.9 stood for the sampling system blank, in which the sampling materials were completely installed but without any sampling flow through the impactor, therefore the concentration column numbers were the absolute amounts of the iodine found in the system.*

Table A.II-3 Measurement of gaseous elemental iodine (I_2), during the BIOFLUX Campaign at MRI Carna, Mweenish Bridge* and MHARS**, western coast Ireland 2003

Sample No.	Date in 2003	Sampling time	**Gaseous I_2 Con. / ng·L^{-1}**	O_3 Con. /ppb	Tidal Height / m
1.	Sept. 12	12:38 ~ 12:58	**0.45**	32.1	0.68
2.		13:01 ~ 13:31	**0.29**		
3.	Sept. 13	09:48 ~ 10:18	**0.26**	26.8	--
4.		12:45 ~ 13:15	**0.52**	25.7	0.76
5.		13:18 ~ 13:48	**0.65**		
6.	Sept. 14	12:15 ~ 12:45	**0.31**	29.9	0.94
7.		12:50 ~ 13:20	**0.23**		
8..	Sept. 15	01:32 ~ 02:02	**0.17**	31.7	0.92
9.		02:07 ~ 02:37	**0.05**		
10.		14:00 ~ 14:30	**1.60**	45.3	1.2
11..		14:33 ~ 15:03	**1.35**	47.3	
12.	Sept. 16	02:22 ~ 02:52	**0.20**	38.2	1.24
13.		02:55 ~ 03:25	**0.12**		
14.		14:42 ~ 15:12	**1.30**	58.0	1.52
15.		15:15 ~ 15:45	**1.12**		
16.	Sept. 17	03:01 ~ 03:31	**0.14**	48.6	1.59
17.		03:34 ~ 04:04	**1.13**		
18.		11:20 ~ 11:40	**5.35**	Seaweed-Chamber **	
19.	Sept. 19	18:06 ~ 18:36	**0.34**	39.6	2.33
20.		18:40 ~ 19:10	**0.23**	36.0	
21.	Sept. 20	06:08 ~ 06:38	**0.36**	21.4	2.41
22.		06:40 ~ 07:10	**0.26**	21.5	
23.		12:35 ~ 13:05	**3.07**	Seaweed-Chamber **	
24.		21:13 ~ 21:43	**1.34**	20.4	2.22
25.		21:50 ~ 22:20	**0.37**	18.7	
26.	Sept. 21	20:55 ~ 21:25	**0.23**	35.9	1.9
27.		21:27 ~ 21:57	**0.23**	37.1	
28.	Sept. 22	10:03 ~ 10:33	**0.39**	34.7	1.97
29.		21:57 ~ 22:27	**0.25**	36.3	1.49
30.		22:28 ~ 22:58	**0.18**	36.0	
31.	Sept. 23	10:04 ~ 10:34	**0.50**	36.4	*
32.		10:59 ~ 11:29	**0.34**	36.6	1.59
33.		11:30 ~ 12:00	**0.48**	36.5	
34.		22:26 ~ 23:56	**0.44**	37.8	1.07
35.		22:58 ~ 23:28	**0.28**		

Continued in next page…

Continued…

Table A.II-3 Measurement of gaseous elemental iodine (I_2), during the BIOFLUX Campaign at MRI, Mweenish Bridge and MHARS, western coast Ireland 2003

Sample No.	Date in 2003	Sampling time	**Gaseous I_2 Con. / ng·L^{-1}**	O_3 Con. /ppb	Tidal Height / m
36.	Sept. 24	10:21 ~ 10:51	**0.50**	36.6	1.18
37.		23:00 ~ 23:30	**0.38**	36.6	0.67
38.		23:33 ~ 00:03	**0.37**	37.6	
39.	Sept. 25	11:12 ~ 11:18	**0.98**	46.1	0.8
40.	Sept. 26	10:47 ~ 11:17	**0.23**	--	0.49
41.		11:21 ~ 11:51	**0.13**	--	
42.		18:03 ~ 18:33	**0.18**	33.9	5.34
43.		23:47 ~ 00:17	**0.18**	25.4	0.14
44.	Sept. 27	00:18 ~ 00:48	**0.20**	25.4	0.14
45.		12:08 ~ 12:38	**0.29**	34.7	0.3
46.		18:22 ~ 18:52	**0.13**	33.8	5.46
47..	Sept. 28	00:39 ~ 01:09	**0.25**	37.7	0.12
48.		01:10 ~ 01:40	**0.41**		
49.		01:42 ~ 02:12	**0.06**		
50.		13:01 ~ 13:31	**0.44**	33.2	0.28
51.		13:32 ~ 14:02	**0.21**	34.5	
52.	Sept. 29	12:34 ~ 13:19	**0.44**	40.2	0.43
53.		13:20 ~ 13:55	**0.23**		
54.	Sept. 30	01:51 ~ 02:21	--	23.9	0.6
55.		02:23 ~ 02:53	**0.18**		
56.		02:54 ~ 03:24	**0.10**		
57.		14:31 ~ 15:01	**0.36**	33.8	0.74
58.		15:02 ~ 15:32	**0.12**		
59.		16:27 ~ 16:57	**1.24**	Mweenish Bridge*	
60.		16:59 ~ 17:29	**1.29**		
61.	Oct. 01	03:10 ~ 03:40	**0.10**	18.1	1.01
62.		03:41 ~ 04:11	**0.13**		
63.		04:12 ~ 04:42	**0.00**	20.3	--
64.		15:05 ~ 15:35	**0.35**	37.6	1.16
65.		16:38 ~ 17:08	**7.63**	Seaweed-Chamber**	
66.		17:10 ~ 17:40	**8.73**		
67.	Oct. 02	03:25 ~ 03:55	**0.03**	23.8	1.57
68.		03:58 ~ 04:28	**0.01**	22.4	
69		04:30 ~ 05:00		System Blank	

Table A.II-4 Total iodine measurement in the PM2.5 particles during the BIOFLUX Campaign at MRI Carna, western coast Ireland 2003

Sample No.	Date in 2003	Sampling time	**Total iodine Con. / ng·m^{-3}**	O_3 Con. /ppb
1.	Sept. 11 ~ 12	18:30 ~ 08:30	**1.48**	32.8
2.	Sept. 12	09:20 ~ 13:35	**7.03**	30.1
3.	Sept. 12 ~ 13	19:50 ~ 09:10	**1.99**	32.6
4.	Sept. 13	09:40 ~ 13:53	**6.72**	26.1
5.	Sept. 13 ~ 14	18:45 ~ 11:38	**2.73**	27.5
6.	Sept. 14	12:08 ~ 18:25	**5.97**	31.7
7.	Sept. 14~ 15	18:55 ~ 09:13	**2.76**	31.4
8..	Sept. 15	09:41 ~ 13:31	**11.87**	45.7
9.	Sept. 15 ~ 16	21:51 ~ 09:35	**3.79**	41.12
10.	Sept. 16	10:05 ~ 14:52	**21.13**	44.0
11..	Sept. 16	15:01 ~ 19:00	**12.02**	59.3
12.	Sept. 16 ~ 17	19:52 ~ 10:05	**4.93**	53.1
13.	Sept. 17	10:32 ~ 16:05	**5.24**	49.0
14.	Sept. 17 ~ 19	16:30 ~ 08:50	**System Blank**	--
15.	Sept. 19	10:12 ~ 13:21	**3.96**	38.4
16.	Sept. 19	13:26 ~ 18:06	**3.07**	39.3
17.	Sept. 19 ~ 20	18:20 ~ 06:36	**4.85**	30.3
18.	Sept. 20	06:51 ~ 13:43	**6.71**	28.8
19.	Sept. 20	13:47 ~ 21:02	**9.95**	28.6
20.	Sept. 20 ~ 21	21:13 ~ 08:49	**4.19**	26.0
21.	Sept. 21	08:57 ~ 13:01	**7.89**	31.7
22.	Sept. 21	13:15 ~ 18:40	**5.23**	34.0
23.	Sept. 21 ~ 22	18:46 ~ 09:25	**2.85**	37.0
24.	Sept. 22	09:30 ~ 13:36	**6.68**	33.9
25.	Sept. 22	13:39 ~ 18:10	**2.41**	34.2
26.	Sept. 23 ~ 24	18:50 ~ 09:18	**2.54**	37.5
27.	Sept. 24	09:30 ~ 15:16	**12.28**	37.3
28.	Sept. 24	15:21 ~ 22:21	**4.53**	38.1
29.	Sept. 24 ~ 25	22:47 ~ 10:13	**3.62**	42.5
30.	Sept. 25	10:18 ~ 16:04	**9.84**	45.7
31.	Sept. 25 ~ 26	16:06 ~ 10:23	**2.36**	39.9
32.	Sept. 26	10:26 ~ 14:46	**8.99**	34.6
33.	Sept. 26	14:50 ~ 18:50	**6.02**	33.7
34.	Sept. 26	18:50 ~ 23:09	**3.64**	28.1
35.	Sept. 26 ~ 27	23:22 ~ 11:42	**2.23**	31.51

Continued in next page…

Continued…

Table A.II-4 Total iodine measurement in the PM2.5 particles during the BIOFLUX Campaign at MRI Carna, western coast Ireland 2003

Sample No.	Date in 2003	Sampling time	**Total iodine Con. / ng·m^{-3}**	O_3 Con. /ppb
36	Sept. 27	11:45 ~ 18:12	**17.95**	31.5
37	Oct. 01	02:40 ~ 10:35	**3.30**	22.1
38	Oct. 01	10:37 ~ 14:37	**5.03**	36.6
39	Oct. 01 ~ 02	14:41 ~ 03:30	**System Blank**	--

Note:
All particle samples were taken by using the filteration and measured by ICP-MS after extraction (detail in section 3.1.1 and 3.2.1). The sampling flow was fixed to 3.43 m^3·h^{-1}. Sampling was performed in the whole campaign, including golden-week and non-golden-week.

Table A.II-5 Iodine species measurement in the PM2.5 particles during the BIOFLUX Campaign at MRI Carna, western coast Ireland 2003

Sample No.	Date in 2003	Sampling time	**Iodine species Con. / ng·m^{-3}**			**Total iodine Con. / ng·m^{-3}**
			Iodate	**Iodide**	**Other I**	
1	Sept. 12 ~ 13	19:50 ~ 09:10	**0.23**	**0.43**	**1.34**	**1.99**
2	Sept. 16	10:05 ~ 14:52	**2.12**	**4.18**	**14.83**	**21.13**
3	Sept. 20	06:51 ~ 13:43	**0.63**	**3.01**	**3.06**	**6.71**
4	Sept. 20	13:47 ~ 21:02	**0.91**	**2.13**	**6.91**	**9.95**
5	Sept. 20 ~ 21	21:13 ~ 08:49	**0.36**	**1.15**	**2.67**	**4.19**
6	Sept. 21	08:57 ~ 13:01	**0.81**	**2.34**	**4.73**	**7.89**
7	Sept. 21	13:15 ~ 18:40	**0.53**	**1.44**	**3.26**	**5.23**
8	Sept. 21 ~ 22	18:46 ~ 09:25	**0.33**	**0.87**	**1.65**	**2.85**
9	Sept. 22	09:30 ~ 13:36	**1.32**	**2.87**	**2.49**	**6.68**
10	Sept. 22	13:39 ~ 18:10	**0.30**	**1.11**	**1.00**	**2.41**

Note:
All particle samples were taken by using the filteration and measured by ICP-MS after extraction (detail in section 3.1.1 and 3.2.2). The sampling flow was fixed to 3.43 m^3·h^{-1}. Sampling was performed in golden-week during the campaign

Table A.II-6 Total iodine measurement in the size-fractionated particles during the BIOFLUX Campaign at MRI Carna, western coast Ireland 2003

Sample No.	Date in 2003	Sampling time	Impactor stage	**Total iodine Con. / ng·m^{-3}**	**Σ Total iodine Con.* / ng·m^{-3}**
1.	Sept. 12 ~ 13	19:50 ~ 09:10	1	**0.24**	**6.43**
			2	**0.41**	
			3	**0.98**	
			4	**3.10**	
			5	**1.69**	
2.	Sept. 13	09:40 ~ 18:15	1	**0.79**	**21.26**
			2	**1.59**	
			3	**4.31**	
			4	**7.63**	
			5	**6.94**	
3.	Sept. 13 ~ 14	18:45 ~ 11:38	1	**0.21**	**8.56**
			2	**0.44**	
			3	**1.01**	
			4	**3.09**	
			5	**3.81**	
4.	Sept. 14	12:08 ~ 18:25	1	**1.04**	**17.39**
			2	**1.83**	
			3	**3.37**	
			4	**6.21**	
			5	**4.94**	
5.	Sept. 14 ~ 15	18:55 ~ 09:13	1	**0.44**	**6.06**
			2	**0.80**	
			3	**1.38**	
			4	**1.73**	
			5	**1.71**	
6.	Sept. 15	09:41 ~ 21:23	1	**1.28**	**7.81**
			2	**2.65**	
			3	**2.30**	
			4	**0.71**	
			5	**0.87**	

Continued in next page…

Continued…

Table A.II-6 Total iodine measurement in the size-fractionated particles during the BIOFLUX Campaign at MRI Carna, western coast Ireland 2003

Sample No.	Date in 2003	Sampling time	Impactor stage	**Total iodine Con. / ng·m^{-3}**	**Σ Total iodine Con.* / ng·m^{-3}**
7.	Sept. 15 ~ 16	21:51 ~ 09:35	1	**0.14**	**2.22**
			2	**0.61**	
			3	**1.01**	
			4	**0.24**	
			5	**0.22**	
8.	Sept. 16	10:33 ~ 19:00	1	**4.45**	**34.89**
			2	**6.81**	
			3	**12.39**	
			4	**5.37**	
			5	**5.87**	
9.	Sept. 16 ~ 17	19:33 ~ 10:05	1	**0.45**	**2.64**
			2	**0.94**	
			3	**0.84**	
			4	**0.21**	
			5	**0.21**	
10.	Sept. 17	10:31 ~ 16:34	1	**0.16**	**2.22**
			2	**0.42**	
			3	**0.67**	
			4	**0.51**	
			5	**0.46**	
11.	Sept. 19	09:30 ~ 19:05	1	**0.18**	**3.06**
			2	**0.37**	
			3	**0.30**	
			4	**1.83**	
			5	**0.39**	
12.	Sept. 21	08:57 ~ 18:40	1	**0.37**	**1.95**
			2	**0.37**	
			3	**0.51**	
			4	**0.51**	
			5	**0.20**	

Continued in next page…

Continued…

Table A.II-6 Total iodine measurement in the size-fractionated particles during the BIOFLUX Campaign at MRI Carna, western coast Ireland 2003

Sample No.	Date in 2003	Sampling time	Impactor stage	**Total iodine Con. / ng·m^{-3}**	**Σ Total iodine Con.* / ng·m^{-3}**
13.	Sept. 23 ~ 24	19:10 ~ 09:18	1	**0.26**	**4.78**
			2	**0.48**	
			3	**1.11**	
			4	**1.89**	
			5	**1.05**	
14.	Sept. 24	09:42 ~ 22:21	1	**1.08**	**16.62**
			2	**1.69**	
			3	**3.46**	
			4	**5.15**	
			5	**5.24**	
15.	Sept. 24 ~ 25	22:54 ~ 10:13	1	**0.76**	**6.38**
			2	**1.40**	
			3	**1.64**	
			4	**1.36**	
			5	**1.22**	
16.	Sept. 25 ~ 26	10:51 ~ 10:23	1	**0.47**	**6.36**
			2	**0.81**	
			3	**1.18**	
			4	**2.07**	
			5	**1.84**	
17.	Sept. 26	10:34 ~ 23:09	1	**0.59**	**6.13**
			2	**0.66**	
			3	**1.43**	
			4	**2.12**	
			5	**1.33**	
18.	Sept. 26 ~ 27	23:37 ~ 11:42	1	**0.24**	**3.33**
			2	**0.31**	
			3	**0.67**	
			4	**1.28**	
			5	**0.84**	

Continued in next page…

Continued…

Table A.II-6 Total iodine measurement in the size-fractionated particles during the BIOFLUX Campaign at MRI Carna, western coast Ireland 2003

Sample No.	Date in 2003	Sampling time	Impactor stage	**Total iodine Con. / ng·m^{-3}**	**Σ Total iodine Con.* / ng·m^{-3}**
19.	Sept. 27 ~ 28	12:03 ~ 00:11	1	**1.14**	**6.05**
			2	**0.89**	
			3	**1.04**	
			4	**1.62**	
			5	**1.36**	
20.	Oct. 01	03:03 ~ 14:37	1	**0.26**	**2.44**
			2	**0.75**	
			3	**1.04**	
			4	**0.21**	
			5	**0.17**	
21.	Sept. 17 ~ 19	16:56 ~ 08:50	1	**System**	**Blank 1**
			2		
			3		
			4		
			5		
22.	Oct. 01 ~ 02	14:56 ~ 03:30	1	**System**	**Blank 2**
			2		
			3		
			4		
			5		

Note:
All particle samples were taken by using the berner-impaction and measured by ICP-MS after extraction (detail in section 3.1.2 and 3.2.2). Sampling flow was fixed to 4.8 $m^3 \cdot h^{-1}$ for all the samples. Sampling was performed in the second half of the campaign, the non-golden-week.

Impactor stage No. 1 ~ 5 stand for the 5 size-fractionated of $D_{50\%}$ / µm: >5.90, 2.00 ~ 5.90, 0.71 ~ 2.00, 0.25 ~ 0.71, 0.08 ~0.25.

**Σ Total Iodine Concentration stands for the total iodine in the 5 stages of the impactor.*

Table A.II-7 Iodine species measurement in the size-fractionated particles during the BIOFLUX Campaign at MRI Carna, western coast Ireland 2003

Sample No.	Date in 2003	Sampling time	Impactor Stage	**Iodine species Con. / ng·m^{-3}**			**Total iodine Con. / ng·m^{-3}**	**Σ Total iodine Con.* / ng·m^{-3}**
				Iodate	**Iodide**	**Other I**		
1	Sept. 21	08:57 ~ 18:40	1	**0.06**	**0.22**	**0.09**	**0.37**	**1.95**
			2	**0.05**	**0.13**	**0.18**	**0.37**	
			3	**0.07**	**0.23**	**0.21**	**0.51**	
			4	**0.05**	**0.15**	**0.31**	**0.51**	
			5	**0.03**	**0.09**	**0.08**	**0.20**	
2	Sept. 27 ~ 28	12:03 ~ 00:11	1	**0.11**	**0.21**	**0.82**	**1.14**	**6.05**
			2	**0.05**	**0.20**	**0.64**	**0.89**	
			3	**0.10**	**0.24**	**0.70**	**1.04**	
			4	**0.24**	**0.53**	**0.86**	**1.62**	
			5	**0.22**	**0.44**	**0.70**	**1.36**	

Note:
All particle samples were taken by using the filteration and measured by ICP-MS after extraction (detail in section 3.1.1 and 3.2.2). The sampling flow was fixed to 4.8 $m^3 \cdot h^{-1}$. Sampling was performed in a non-golden-week (No.1) and golden-week (No.2) during the campaign.

**Σ Total Iodine Concentration stands for the total iodine in the 5 stages of the impactor.*

Table A.II-8 The gaseous I_2 measurement in the seaweed-experiment at Mace Head Atmospheric Research Station (MHARS)

Experiment No.	Denuder Sample No.	Sampling Parameter: Flow rate / mL·min^{-1}	Sampling Parameter: Time / min	**I_2 concentration / ng·L^{-1}**	Seaweed amount (depth in chamber)	Chamber Flow / L·min^{-1}	Particle Number Conctration / cm^{-3}
1.	1.	530	26	**0.00**	-- empty chamber	0.0	--
2.	2.	530	11	**6.14**	21 kg (5-7cm)	700	5×10^6
	3.	530	10	**7.63**			
3.	4.	530	15	**N.D.**	Ambient air sampling	N/A	6000 (atmosphere)
	5.	530	13	**N.D.**			
4.	6.	530	12	**14.37**	25 kg (6-7cm)	700	$8\sim11\times10^6$
5.	7.	530	12	**14.43**	25 kg (6-7cm)	700	18×10^6
6.	8.	530	10	**10.81**	25 kg (6-7cm)	>800	22×10^6
7.	9.	530	12	**24.18**	25 kg (6-7cm)	0.0	$9\sim10\times10^6$
	10.	530	10	**26.92**			
8.	11.	530	10	**11.36**	38 kg (8-9cm)	0.0	0.5×10^6 (but no nano-particle)
	12.	530	15	**10.39**			
9.	13.	530	15	**4.23**	28 kg (8-9cm)	800	10×10^6 (3 nm mode)
10.	14.	530	12	**3.92**	16 kg (5-6cm)	800	$7\sim8\times10^6$ (3 nm)
11.	15.	530	10	**2.96**	8 kg (3-4cm)	800	5×10^6 (3 nm mode)
12.	16.	530	13	**1.39**	5 kg (2-3cm)	800	$2\sim3\times10^6$
	17.	530	13	**1.35**			
13.	18.	110	26	**0.78**	5 kg (2-3cm)	800	$2\sim3\times10^6$, 0.3×10^6

Note:
Those experiments were performed at the MHARS, 24~25 June, 2004. Seaweeds (Fucus Vesiculosus and Laminaria Digitata) were collected at the tidal coast area nearby. Particle number concentration was measured by CPC, and the size distribution of aerosol was measured by nano-SMPS, at the same time when sampling by denuder. "N.D."= "Not Detected"

Table A.II-9 Online-monitoring of CH_2I_2 during the photolysis and ozonolysis of CH_2I_2 in the reaction-chamber experiment

Sample No.	Reaction Time / min	**CH_2I_2 Concentration / ng·L^{-1}**	Ozone Con. / ppb	Particle number Con. / cm^{-3}
1.	0	**417.90**	12	90
2.	3	**444.41**	12	90
3.	6	**315.43**	56	26,000
4.	9	**221.98**	56	40,800
5.	12	**186.38**	58	42,500
6.	15	**182.84**	58	42,200
7.	18*	**175.28**	60	41,900
8.	21	**118.14**	63	42,800
9.	24	**99.13**	62	43,800
10.	27	**82.53**	65	45,600
11.	30	**67.71**	68	46,300

Note:
CH_2I_2 were sampled by the Tenax/Carbotrap adsorption tube, during the photolysis and ozonolysis in the reaction-chamber, and measured by the TD/GC-MS. Sample No. 1 and 2 were taken before the reactions started.
Particle number concentrations were measured by the CPC (TSI 3010).
**CH_2I_2 source was shut off at reaction time of 18 min.*

Table A.II-10 Measurement of iodine species in the particle products from the photolysis and ozonolysis of CH_2I_2 in the reaction-chamber experiment

Sample No.	**Iodine species concentration / ng·L^{-1}**				Ozone Con./ ppb	Particle number Con./cm^{-3}
	Iodate	**Iodide**	**Other I**	**Total Iodine**		
1. and 2. Blank samples	**N.D.**	**N.D.**	**N.D.**	**N.D.**	12 13	27 27
3.	**26.95**	**85.23**	**43.63**	**155.8**	78	50,000
4.	**36.69**	**95.39**	**46.89**	**179.0**	82	52,100
5.	**95.62**	**131.55**	**49.19**	**276.4**	93	45,100
6.*	**29.94**	**34.16**	**15.53**	**79.6**	96	39,900
7.*	**8.50**	**8.07**	**3.30**	**19.9**	110	32,600

Note:
Particle samples were taken by filters after the CH_2I_2 source switched off, but with solar simulation lamp (UV-Vis light)on and the increasing O_3 concentrations in the chamber.
Particle number concentrations were measured by the CPC(TSI 3010).
** Sample No.6 and7 were taken after the UV-Vis light was off.*

Abbreviation Index

AI	Amylose-Iodine Complex
AMS	Aerosol Mass Spectrometry
ATOFMS	Aerosol Time-Of-Flight Mass Spectrometry
BVOC	Biogenic Volatile Organic Compound
BIOFLUX	the campaign of BIO-genic iodine gaseous FLUX
CCN	Cloud Condensation Nuclei
CIV	Condensation Iodine Vapor
CPC	Condensation Particle Counter
DOAS	Differential Optical Absorption Spectrometry
ECD	Electron Capture Detector
EFID	Electrolyzer-power Flame Ionization Detector
EI	Electron (Impact) Ionization
ELPI	Electric Low Pressure Impactor
EU	European Union
FID	Flame Ionization Detector
FTIR	Fourier Transform Infrared Spectroscopy
GC	Gas Chromatography
ICP	Inductively Coupled Plasma
IDMS	Isotope Dilution Mass Spectrometry
ITDS	Ion Trap Detection System
QUEST	the international EU-Project of “Quantification of Aerosol Nucleation in the European Boundary Layer”
MBL	Marine Boundary Layer
MHARS	Mace Head Atmospheric Research Station, at Carna, Co. Galway, Ireland
MRI	Marine Research Institute of Ireland, at Carna, Co. Galway, Ireland
MS	Mass Spectrometry / Mass Spectrometer
NAA	Neutron Activation Analysis
NIST	National Institute of Standards and Technology, USA
PFPD	Pulsed-Flame Photometer Detector
PM2.5	Particulate Matter, smaller than 2.5 µm in diameter
PMMA	Poly-Methyl-Meth-Acrylate

PTFE	Poly-Tetra-Fluoro-Ethylene (Teflon®)
PVF	Poly-Vinyl-Fluoride (Tedlar®)
RF	Radio Frequency
SERS	Surface Enhanced Raman Spectrometry
SI	Starch-Iodine Complex
SIC	Selected Ion Chromatograph
SMPS	Scanning Mobility Particle Sizer
TBAH	Tetra-Butyl-Ammonium Hydroxide
TD	Thermo Desorption
TIC	Total Ion Chromatograph
TMAH	Tetra-Methyl-Ammonium Hydroxide
TSC	Thermodynamically stable Sulphate Cluster
UV	Ultra-Violet
VOC	Volatile Organic Compound
VOI	Volatile Organic Iodide/Iodine Compound

Acknowledgements (deleted for e-version)